EXPERIMENTAL STUDY ON NEGATIVE SKIN FRICTION ON PILES IN COLLAPSIBLE SOILS DUE TO INUNDATION

Ibrahim Mashhour

A Thesis in the

Department

of

Building, Civil and Environmental Engineering

Presented in Partial Fulfillment of the Requirements

For the Degree of

Doctor of Philosophy (Civil Engineering) at

Concordia University

Montreal, Quebec, Canada

February 2016

© Ibrahim Mashhour, 2016

CONCORDIA UNIVERSITY

School of Graduate Studies

This is to certify that the thesis prepared

By: **Ibrahim Mashhour**

Entitled**:**   **Experimental Study on Negative Skin Friction on Piles in Collapsible Soils Due to Inundation**

and Submitted in Partial Fulfillment of the Requirements for the degree of

Doctor of Philosophy (Civil Engineering)

complies with the regulations of the University and meets with the accepted standards with respect to originality and quality.

Signed by the final examining committee:

_____ Chair
Dr. M. Y. Chen

_____ External Examiner
Dr. S.K. Vanapalli

_____ External to program
Dr. A. Hammad

_____ Examiner
Dr. O. Pekau

_____ Examiner
Dr. A. Zsaki

_____ Supervisor
Dr. A. Hanna

Approved by _____
            Dr. M. Zaheeruddin, Chair, Department of Building, Civil & Environmental Engineering

_____ 2016   _____
                        Dr. C. Trueman
                        Dean, Faculty of Engineering and Computer Science

ABSTRACT

Experimental Study on Negative Skin Friction on Piles in Collapsible Soils due to Inundation

Ibrahim Mashhour, Ph.D.

Concordia University, 2016

Collapsible soil is a special type of soil, classified as problematic soil. It possesses a high strength in the unsaturated phase and loses its strength and exhibits substantial settlement when inundated. Many foundation failures occur around the world, many of which involve loss of lives, caused by problems associated with collapsible soils. One of the most commonly used type of foundation in collapsible soils is end-bearing piles resting on firm soil strata. However, these piles will be subjected to negative skin friction during wetting of the collapsible soil, inducing additional loads. Various case studies have reported foundation failures and excessive settlements upon the wetting of collapsible soil.

Researchers are facing serious challenges in dealing with piles in collapsible soils due to the complexity of the problem and the difficulties associated with modeling this behaviour numerically and experimentally. Relatively few investigations pertinent to pile foundations in collapsible soils subjected to inundation are available in the literature.

An experimental investigation was carried out to simulate the complex interaction between collapsible soil and a single end-bearing pile under various wetting and loading conditions. The experimental prototype setup was developed and calibrated in the laboratory in order to measure the drag load and accordingly the negative skin friction acting on the pile's shaft for given soil/wetting/loading conditions. Collapsible soils with different collapse potential values were

created in the laboratory by mixing kaolin clay with fine sand at predetermined ratios. A two-dimensional axi-symmetrical numerical model was generated in order to conduct a parametric study by extending the data for a wider range. The numerical model was validated by experimental results obtained from this study. Based on the results obtained from the experimental and numerical models, a design theory capable of taking into account the effect of soil collapse under different wetting schemed was developed and recommended for use in practice.

ACKNOWLEDGEMENTS

TABLE OF CONTENTS

LIST OF TABLES

LIST OF FIGURES

LIST OF SYMBOLS

β = negative skin friction coefficient

$\bar{\beta}$ = negative skin friction coefficient for collapsible soils

C_p = Collapse potential

C = Calibration Factor

c = Cohesion

c´ = Effective cohesion (saturated condition)

D = Diameter of pile

D_W = Degree of wetting

H_o= is the initial height of the soil specimen

H_s = Depth of collapsing soil

h = Radius of wetting

ΔH = Collapse settlement

$\Delta H/H_0$ = Collapse strain

Δe or ΔV/Vs = Change in void ratio

e_o = Natural (initial) void ratio

e_u = initial void ratio of a soil specimen under a given net confining stress

e_f = final void ratio (after complete saturation)

f_n= Unit Negative Shaft Resistance

FS: Factor of Safety

f_s= Unit Shaft Resistance

G_s = Soil specific gravity

H_o = Initial height of the specimen

V_0 = Total volume

E_p = Young's modulus

K_0 = Coefficient of earth pressure at rest

$K_{0(OC)}$ = Coefficient of earth pressure at-rest at over-consolidated state

NSF = Negative skin friction

P = Percentage of full collapse experienced during partial inundation

P = Stress applied on soil sample in odoemeter test

Q_u = Ultimate pile capacity

Q_s = Positive skin friction

Q_b = Tip resistance

Q_a = Design Load

Q_a = Dead Load

Q_l= Live Load

Q_n = Drag Load

Q_u = Ultimate pile capacity

Q_n = Indirect load due to negative skin friction

$Q_n/\pi D$ = Unit negative skin friction

f_n = Average negative shear stress

R_a: arithmetic average of absolute values

R_s"= Positive Shaft Resistance

R_s = Shaft Resistance

R_s'= Negative Shaft Resistance

R_t= Toe Resistance

R_p: maximum peak height

R_v: maximum valley depth

R_t: maximum height of the profile

R_q: root mean squared

S_r = Degree of saturation = 1 (after full saturation)

S_b = Initial degree of saturation before major collapse

S_f = Final degree of saturation after major collapse

SWCC = Soil-water characteristic curve

$(u_a - u_w)$ = Matric suction

u_a = Pore air pressure

u_w = Pore water pressure

w_0 = Initial water content

w_n = Soil moisture content at natural condition

w_{sat} = Soil moisture content at saturated condition

φ = Angle of internal friction

υ_{inter} = Interface friction angle

γ_c = Unit weight of concrete

γ_{sat} = Soil unit weight at saturated condition

γ_{bulk} = Bulk unit weight

γ_{dry} = Dry unit weight

ρ_d = Initial Dry Density

I_p = Plasticity index

σ = Normal stress acting on soil

θ = Volumetric water content

θ_s = Saturated volumetric water content

θ_r = Residual volumetric water content

Θ = Normalized volumetric water content

κ = Fitting parameter

υ_p = Poisson's ratio

ψ = Matric suction

CHAPTER 1

INTRODUCTION

1.1 General

Unsaturated collapsible soils experience sudden and substantial reduction in volume upon wetting with or without additional loading (Clemence and Finbarr 1981). Many problems resulting in foundations built on collapsible soils have been reported in the literature, and therefore collapsible soils are classified as problematic soils. Various sources of wetting due to human activities or natural causes can induce uncontrolled wetting causing sudden collapse of these soils, leading to foundation failure. Catastrophic damages in terms of economic and human loss can result in such soils, as reported by Ayadat and Hanna (2008).

Different measures can be taken to avoid foundation failure due to the reduction of the volume and strength of collapsible soil upon inundation. These measures have been studied by many researchers including (Clemence and Finbarr, 1981, Houston and Houston, 1989, Rollins and Rogers, 1994, Beckwith, 1995; Evstatiev, 1995, Houston and Houston, 1997, and Pengelly, et al., 1997). Most of these mitigation measures fall under the following categories: removal and replacement of the collapsible soil layer, pile or pier foundations, avoidance of wetting, pre-wetting, controlled wetting, chemical stabilization or grouting, dynamic compaction and differential settlement resistant foundations. Some of these measures such as removal and displacement of the collapsible soil layer underneath new structure foundations, can only be feasible for shallow collapsible layers.

The utilisation of end-bearing pile foundations is one of the most effective and commonly used type of foundation in collapsible soils. For these piles, bearing capacity is governed mainly by the tip resistance of the strata underlying the collapsible soil layer. However, during the inundation process of the collapsible soil layer, piles experience substantial negative skin friction causing additional loads on the pile, sometimes leading to failure. The problem of negative skin friction is one of the most common problems for the design of pile foundations in soft ground (Lee et al. 2001; Hanna and Sharif 2006).

For pile foundations subjected to external loads, the load transfer mechanism depends on many factors including the relative movement between soil and pile. Figure 1.1 demonstrates the load transfer mechanism for floating piles, where the load acting on the pile is resisted by the friction along the pile's shaft. Figure 1.2 presents the load transfer mechanism for an end-bearing pile, where the load acting on the pile is carried by the pile's tip.
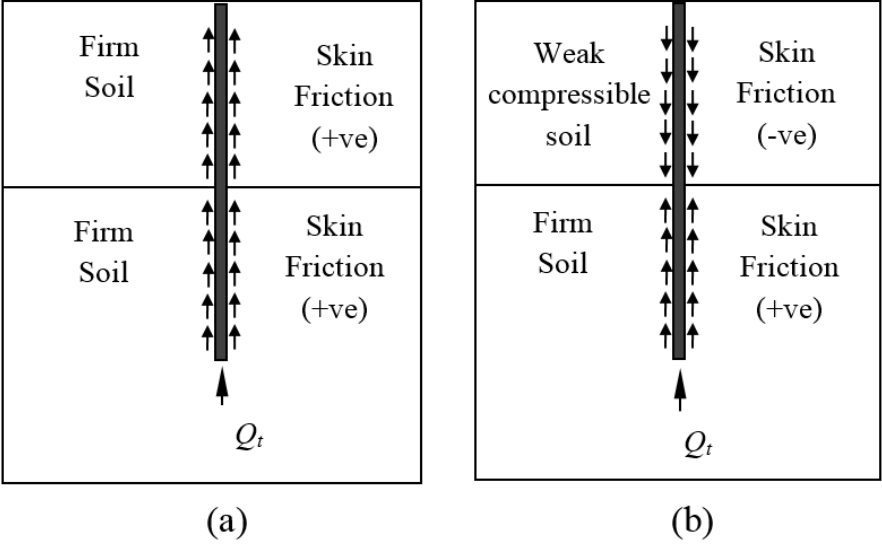
Figure 1.1 Load transfer mechanism for floating piles
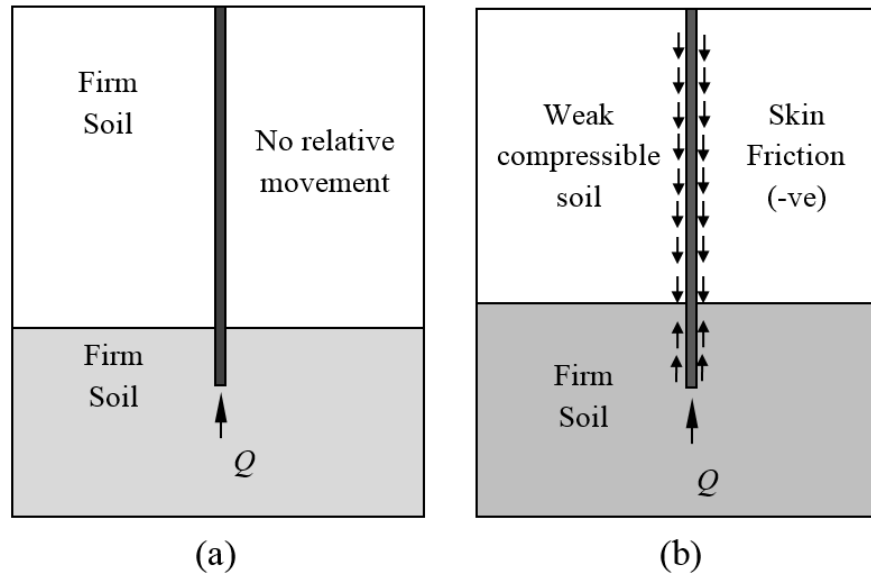
Figure 1.2 Load transfer mechanisms for end-bearing piles

1.2 Problem Statement

Collapsible soils exhibit sudden and substantial settlement upon inundation, inducing significant

negative skin friction (NSF) stresses on the pile's shaft. The magnitude of soil settlement, is one of

the factors that affects the magnitude of NSF, where the larger the soil settlement, the greater the

negative skin friction as suggested by Poulos (1997) and Lee et al., (2001). Furthermore, the rate

of inundation and hence the rate of settlement are important factors that affect the development of

NSF on piles in collapsible soils Grigoryan (2005). Case studies have indicated that the magnitudes

of the negative skin friction developed due to the settlement of collapsible soil upon inundation,

were much higher than the values computed using theories developed for consolidation settlement

in saturated clays (Hepworth 1993; Li et al. 1994; Grigorian 1997; Krutov 2003; Chen et al. 2008;

and Ma et al. 2009).

Significant contributions and well established conventional theories have been introduced for

estimating negative skin friction on piles in soft ground, with an emphasis on saturated clays subject

to consolidation settlement. However, most of these conventional theories fail to provide an adequate prediction for the NSF induced on piles in collapsible soils due to inundation. To date there is a lack of design procedures to account for the soil-pile interaction upon inundation of collapsible soil due to the complexity of modeling collapsible soil, especially during inundation.

1.3 Research Objectives

The main goal of this study is to provide a better understanding of the development of negative skin friction on piles in collapsible soil and to develop experimental based methods for estimating these stresses. Therefore, the objectives of this thesis are listed as follows:

1. To conduct an experimental investigation simulating piles in collapsible soils for different soil/pile conditions subjected to various wetting schemes.

2. To develop a numerical model to perform a parametric study showing the effect of key parameters on the negative skin friction as a result of soil settlement upon inundation.

3. To introduce an analytical model for predicting negative skin friction for various collapsible soils under different loading and wetting conditions. This model take into account the effect of parameters such as: the rate of inundation from the bottom (simulating a rise in the groundwater table) and degrees of wetting from the top (simulating partial wetting due to rainfall and pipe leakage).

4. To postulate a new design procedure and design charts that can be used by practicing engineers for estimating pile capacity in collapsible soils. The equations postulated by this study were compared to field tests reported in the literature to validate the proposed model.

1.4 Thesis Outline

This thesis is presented in seven chapters. This Chapter presents an introduction, explaining the load transfer mechanism in a soil-pile system. A comprehensive literature review is reported in Chapter two, providing a brief review on key aspects of collapsible soils and negative skin friction in soft ground, and highlighting the previous work pertinent to negative skin friction acting on piles in collapsible soils.

Chapter three explains the experimental setup, materials and testing procedures utilised in this study. The tests results are presented in the fourth Chapter, expressed in figures providing the relationship between soil settlement and drag load for a range of load/soil/wetting conditions. Analyses of these results are presented at the end of the Chapter, highlighting the effect of critical parameters on the developed drag loads. A numerical model is presented in the fifth Chapter, extending the data obtained from the experimental investigation in order to present a parametric study.

Chapter six presents analytical and empirical models and suggests a design procedure for estimating negative skin friction on piles due to collapsible soil settlement upon inundation. Finally, the conclusions obtained from experimental and numerical data are summarized and recommendations for further research are suggested in chapter seven.

CHAPTER 2

LITERATURE REVIEW

2.1 General

In this chapter the literature review is presented, with emphasis on negative skin friction on piles in collapsible soils. A brief introduction pertinent to collapsible soil was essential to provide a better understanding of the collapsible soils behaviour. Discussion of previous work is presented at the end of the chapter.

2.2 Collapsible Soil Behaviour

Collapsible soils are known as unsaturated soils that exhibits a sudden and substantial volume reduction upon wetting under a constant stress. A wide range of soils can be categorized as collapsible soils, including wind-blown deposit sands and silts (loess), alluvial flood plains, fans, mud flows, residual soils, colluvial deposits, mud flows and volcanic tuffs (Clemence and Finbarr 1981). Recently different types of clayey soils are being included in the collapsible category (Houston et, al. 1993). Fredlund and Gan (1995) divided collapsible soils into two main groups: dry collapsible soils, and wet collapsible soils, where the category of wet collapsible soils includes quick clays in eastern part of Canada and Scandinavia. Figure 2.1 presents classification of different types of collapsible soils after Rogers (1995).
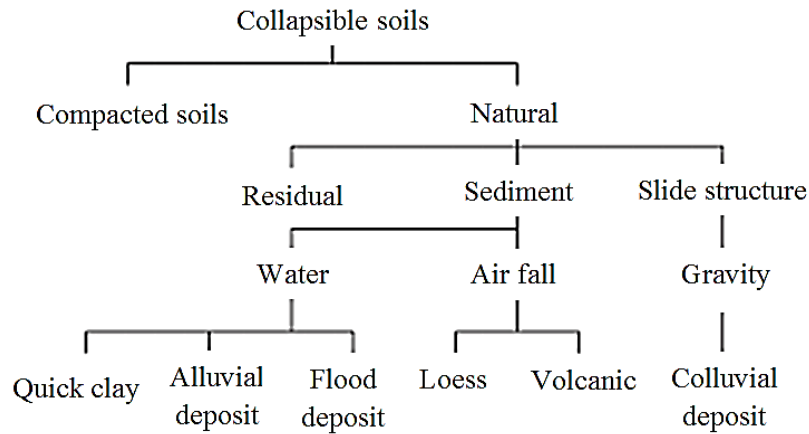
Figure 2.1. Types of collapsible soils (Rogers 1995)

Unsaturated collapsible soils can be found in different arid and semi-arid regions, and they are located in many parts of the world including: Asia (China and Central Asia), Europe (Russia, Serbia, Hungary, Bulgaria, Northern France and different regions in Eastern Europe), North America (Midwestern and western United states), Africa (Egyptian western desert, northern and southern Africa,), South America (Argentina and Uruguay) and New Zealand (Kezdi 1974, Clemence and Finbarr 1981; Evstatiev 1995; Evans et al., 2004; Delage et al., 2005; Abdrabbo et al., 2006). Collapsible soils can also be divided into two main types based on their behaviour under loading, where some types of soils undergo collapse upon wetting under existing overburden stresses while for other types this collapse only takes place under additional stresses (Grigoryan 1997). Barden et al. (1973) list that the development of the collapse mechanism requires three essential conditions: a potentially unstable open partly saturated structure, stress acting on the soil, and a sufficient soil bonding resulting from soil suction or other cementing agent.

There are different types of inter-particle bonds for collapsible soils, as shown in figure 2.2 as presented by (Clemence and Finbarr, 1981). These inter-particle bonds stabilize the contacts

between granular particles, and they break immediately upon inundation with water, causing substantial reduction in strength and volume.
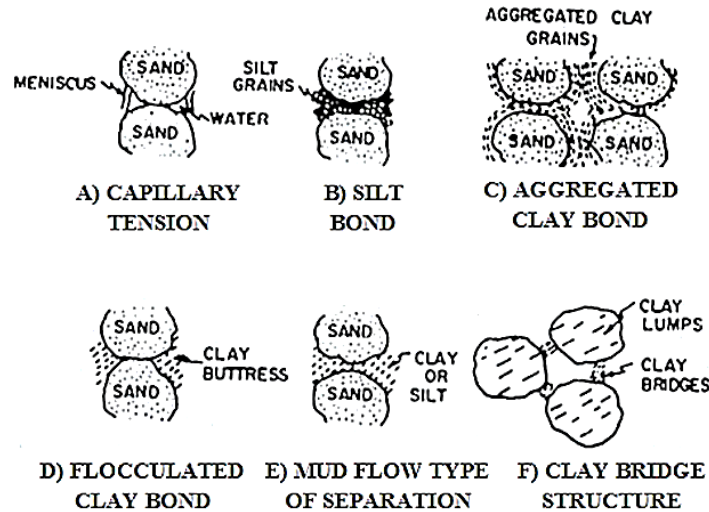
Figure 2.2 Typical collapsible soil structures (Clemence and Finbarr 1981)

2.2.1 Identification and Classification of Collapsible Soils

Knight (1963) has introduced a factor known as the collapse potential C_P, that determined through a simple procedure using the oedometer test. To determine the collapse potential C_P, the soil sample is placed in the oedometer at the natural moisture content, and load is applied on increments up to a maximum pressure of 200 kPa (inundation pressure) at which the soil is being fully inundated with water. The inundation pressure 200 kPa is applied on the soil sample for 24 hours. By plotting the e-log$p$ curve from the oedometer test results, the change in void ratio upon wetting Δe_c, can be determined from the curve as shown in figure 2.3. The collapse is equal to the deformation of soil due to the addition of water, divided by the initial height of the specimen, expressed in percent, as expressed in Equation [2.1], where Δe_o is void ratio of soil at the natural state, ΔH_c is the change in height of the soil upon wetting and H_o is the initial height of the soil specimen.

$$C_p = \frac{\Delta e_c}{1 + e_o} = \frac{\Delta H_c}{H_o} \text{............................} \quad [2.1]$$
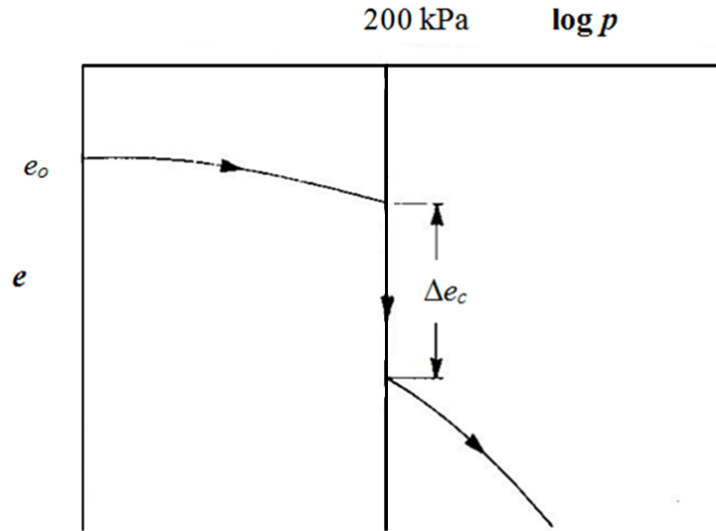
Figure 2.3 Typical collapse potential results (Clemence and Finbarr 1981)

Jennings and Knight (1975), has introduced a classification criteria that enables engineers to judge the severity of the problem based on the collapse potential obtained from oedometer test C_p, as shown in the Table 2.1.

Table 2.1 Severity of foundation problems with respect to C_p (Jennings and Knight 1975)

C_p (%)	Severity of problem
0-1	No problem
1-5	Moderate trouble
5-10	Trouble
10-20	Severe trouble
>20	Very severe trouble

2.2.2 Factors Governing the Behaviour of Collapsible Soils

Experimental and field testing have manifested that there are many different factors that affect the collapse potential of soils such as: soil type, compaction effort, stress-level at inundation, clay percent and initial water content, (Ho and Fredlund 1982, Houston and Houston, 1997, Ayadat and

Hanna 2007). Lawton et al. (1992) listed that the most important factors that determine the collapse potential are initial water condition and dry density. Tadepalli and Fredlund (1991) have carried out a study on a compacted silty-sand specimen, and it was found that the percent of collapse decreases with an increase in the dry density and water content, prior to wetting. Lommler and Bandini (2015) noticed from test results that sample disturbance may cause reduction in collapse potential of in situ soils while it might increase the collapse potential of compacted soils.

Another important factor that has a significant effect on the magnitude of collapse is the stress level at wetting (inundation pressure). The effect of inundation pressure on collapse potential has been studied by various researchers, and the values of inundation pressure, ranging from 50 kPa to 600 kPa have been studied by various researchers. Kezdi (1974) indicated that the collapse potential of loess increases linearly with increasing inundation pressure up to 400 kPa and then it remains constant. These findings are with agreement with the results obtained by Lawton et al. (1992), who carried out oedometer testing, indicating that the collapse potential reaches the maximum value at a critical inundation pressure value, beyond which the collapse potential remains constant with increasing vertical stress. These studies show that the collapse settlement increases with an increase in inundation pressure, up to a limiting value of stress. This limiting stress value depends on the packing and arrangement of soil particles.

The percent of fines has a significant effect on collapse potential, since the clay acts as a cementing agent in a clay-sand mixture. Ho et al. (1988) indicated from experimental testing, that as the percentage of fines increases, the amount of maximum collapse increases. These findings were similar to these obtained by Alwail et al. (1994). The collapse potential magnitude is directly proportional to the increase in the clay percentage in the collapsible soil mixture, until it reaches a specific clay content value, where soils are expected to swell rather than to collapse beyond that

limit as reported by (Adnan and Edril 1992). This limiting value is observed when the clay content reaches approximately 18% for kaolin clay as found by (Miller et al., 1998).

Several studies indicated that the wetting of unsaturated soil due to water infiltration does not cause fully saturation of soil, different studies show that the degree of saturation for such case can only increase up to 50 percent (El-Ehwany and Houston, 1990). El-Ehwany and Houston (1990) performed a series of laboratory tests on sandy silt, to investigate the effect of partial wetting on the collapse potential. These tests indicated that the partial wetting causes only partial collapse, where a substantial collapse took place at degree of saturation between 60 and 75 percent as shown in figure 2.4.
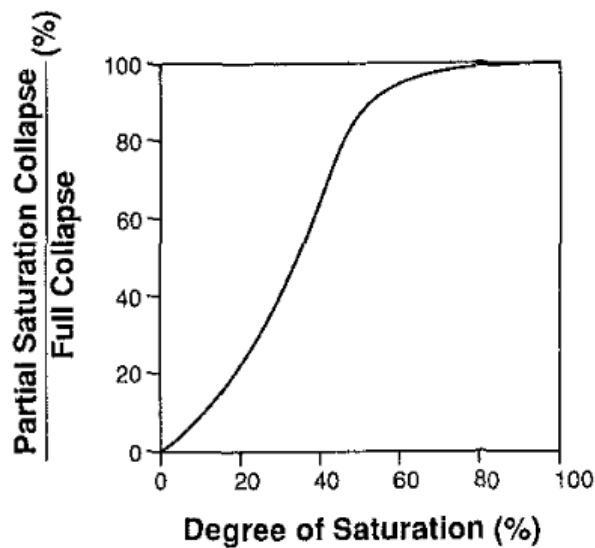
Figure 2.4 Partial collapse due to partial wetting after (El-Ehwany and Houston 1990)

It can be noted fully saturation due to wetting, can overestimate the collapse settlement in many cases in the field such as water infiltration, where only a partial saturation takes place. It is very important therefore to consider the effect of partial saturation in laboratory tests to simulate different cases in field.

There any various causes of soil wetting that have been reported as a result of urbanization or natural causes, such as: rising in groundwater level, landscape irrigation, intentional and unintentional groundwater recharge, broken water pipelines or sewer lines, poor surface drainage, damming due to cut/fill construction, and moisture increase due to capillary rise. The wetting scheme has an effect on degree of saturation and hence on the collapse mechanism.

Generally for unsaturated soils, the shear strength is governed by the net normal stress and matric suction. Therefore the relationship between partial collapse and the increase in the degree of saturation, is receiving attention of researchers. Figure 2.5 shows the variation of matric suction and partial collapse with respect to degree of saturation after (Houston et al., 1993).
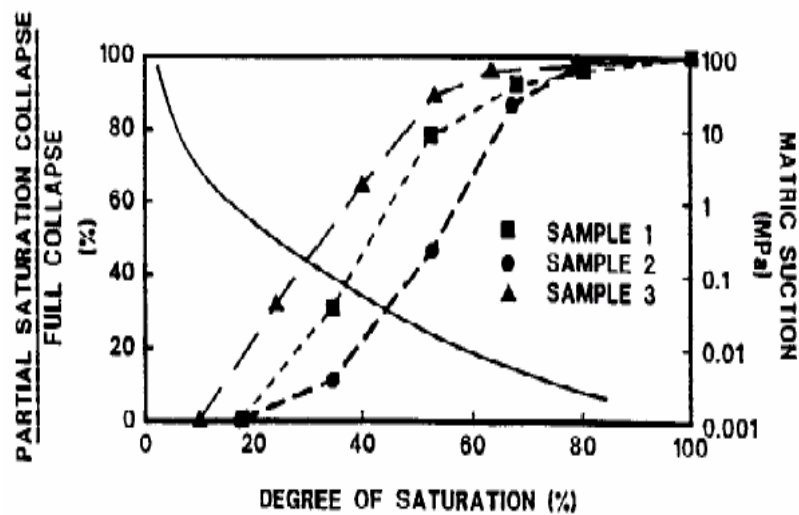
Figure 2.5 Partial collapse due to partial wetting after (Houston et al., 1993)

The net normal stress in this case can be calculated from Equation [2.2]

$$\sigma'_v = \sigma - u_a \text{ ... . } [2.2]$$

While the matric suction (ψ) is the difference between pore air (u_a) pressure and pore water pressure (u_w) as shown in Equation [2.3], where for saturated soils for saturated soils $u_a = u_{w.}$.

$$\psi = u_a - u_w \ldots \ldots \ldots \ldots \quad [2.3]$$

Pereira and Fredlund (2000) suggested the following equation, providing a relationship that links the change in void ratio to the matric suction as shown below in Equation [2.4].

$$e = e_u + \frac{e_f - e_u}{\left[1 + \left(\frac{(u_a - u_w)}{c}\right)^b\right]^a} \ldots \ldots \quad [2.4]$$

where:

e = void ratio

e_u = initial void ratio of a soil specimen under a given net confining stress

e_f = final void ratio (after complete saturation)

c = matric suction value at the inflection point (i.e., middle point of collapse phase);

b = slope parameter (i.e., slope of the collapse phase); and

a = symmetry parameter that makes the logistic function asymmetric.

In this case the shear strength can be calculated using Equation [2.5] as following:

$$\tau_f = c' + (\sigma - u_a)\tan\phi' + (u_a - u_w)\tan\phi^b \ldots \ldots \ldots \ldots \ldots \ldots \ldots \ldots \quad [2.5]$$

The saturation water characteristic curves SWCC is one of the most important relationships for interpreting unsaturated soil behaviour. Where the SWCC can be defined as the relationship between water content of soil and soil matric suction (Zapata et al., 2000 and Fredlund, 2006). Different unsaturated soil parameters can be estimated from the SWCC such as volumetric water content (θ) and unsaturated coefficient of permeability (k_o). Numerous experiments have been

introduced for estimating SWCC. Many limitations associated with SWCC laboratory equipment have been highlighted by researchers (Zapata et al, 2000; Fredlund and Houston 2009; Fredlund and Houston 2013).

Several satisfactory methods were introduced for estimating the SWCC based on soil properties such as grain size distribution (GSD) and atterberg limits (Fredlund and Houston 2013, Fredlund and Houston 2009; Fredlund 2006; Aubertin et al. 2003; Zapata et al. 2000; Chen et al., 2014; Mihalache and Buscarnera 2015). Figure 2.6 presents different methods for estimating SWCC, using experimentally or based on soil properties as suggested by Fredlund and Houston (2009).
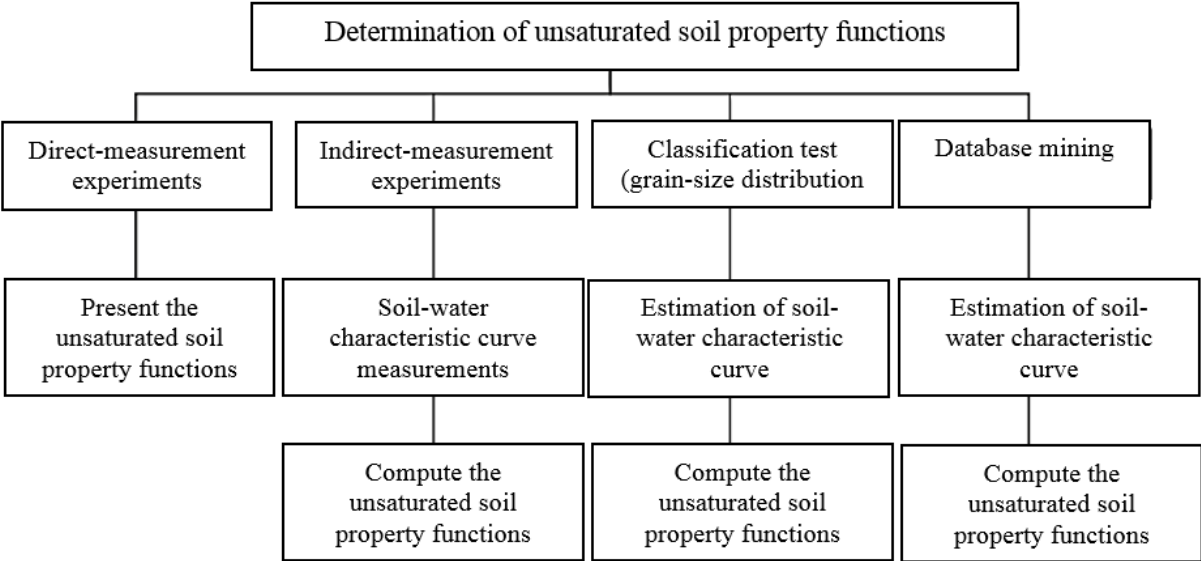
Figure 2.6 Approaches for estimating SWCC (Fredlund and Houston 2009)

Figures 2.7 and 2.8 present relationships between degree of saturation and matric suction for different soil types after (Walsh et al, 1993) and (after Zapata et al, 2000) respectively. Such relationships can be useful for determining SWCC based on soil parameters. Zapata et al, (2000) suggested that these models (based on GSD or soil index properties) in many cases can result in error less than that associated with operator measurements.
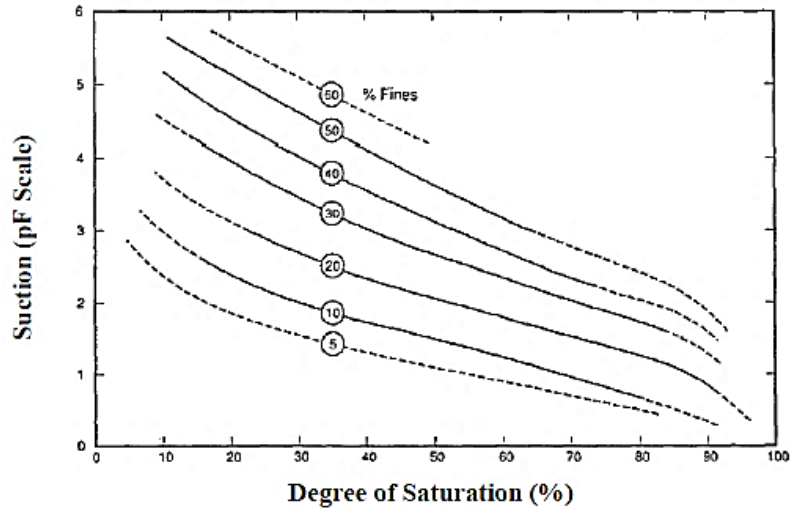
Figure 2.7 SWCC for soils having different percent of fines after (**Walsh et al, 1993**)
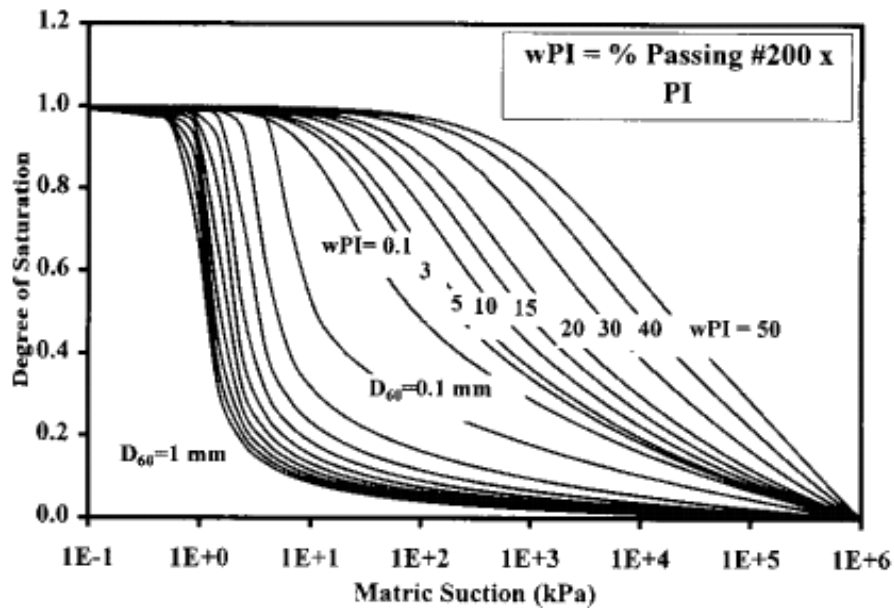
Figure 2.8 Predicted SWCC based on D60 and wPI after (**Zapata et al, 2000**)

Since the direct measurements of unsaturated soil properties can be time consuming. Houston (2014) therefore suggested a simple and economic approach for determining unsaturated soil properties, without measuring soil suction directly. This approach is based on measuring saturated

soil parameters and performing response to wetting tests. Figure 2.9 presents a hierarchical level approach for determining unsaturated soil properties when dealing with different unsaturated soils problems after (Houston 2014).
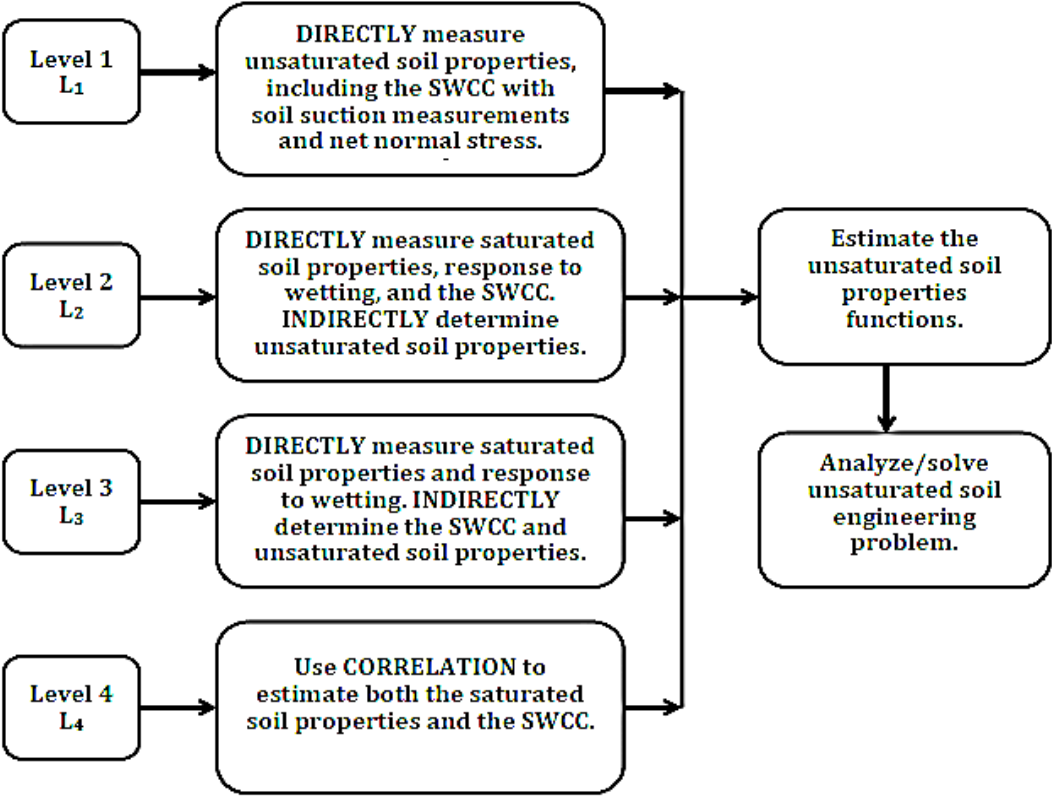
Figure 2.9 Hierarchical level approach for unsaturated soils (Houston 2014)

Various numerical models have been presented in literature for modeling unsaturated soil behaviour (Fredlund and Gan 1995; Costa et al., 2007; Kakoli et al. 2011, Noor et al. 2013).

2.2.3 Mitigation Measures for Foundations on Collapsible Soils

There are many different measures that can be taken to avoid foundation failure, due to the reduction of volume and strength of collapsible soil upon inundation. These measures have been studied by many researchers (Clemence and Finbarr, 1981, Houston and Houston, 1989, Rollins and Rogers,

16

1994, Beckwith, 1995; Evstatiev, 1995, Houston and Houston, 1997, and Pengelly, et al., 1997).

Most of these mitigation measures fall under the following categories: removal and replacement of the collapsible soil layer, pile or pier foundations, avoidance of wetting, pre-wetting, controlled wetting, chemical stabilization or grouting, dynamic compaction and differential settlement resistant foundations. Some of these measures such as removal and displacement of the collapsible soil layer underneath the new structure foundations can be a very economic measure for shallow collapsible layers only. Pile foundations therefore are commonly used for building on deep collapsible soils.

2.3 Piles in Collapsible Soil Subjected to NSF

Additional force known as drag loads is applied on the pile's shaft during the settlement of the surrounding soils. Therefore piles installed in deformable soils are susceptible to negative skin friction that can cause serious damages, as reported in the history. The accounting of the negative skin friction in the design of pile foundation is important. Negative skin friction is considered to be a common problem in the design of pile foundations in soft ground, and yet there is a lack of reliable methods, as both empirical and elastic methods overestimate the NSF values in many cases (Lee et al., 2001).

Fellenius (1989) stated that observations for end-bearing piles have shown that negative skin friction force can reach very high values for end-bearing piles. Such high values of NSF can exceed the structural capacity of the piles and result in pile failure. Fellenius also stated that the field investigations reported in literature show that extremely small movements (as small as 1mm) are large enough to generate negative skin friction force and to reverse the shear-force direction. Therefore all piles might be subjected to negative skin friction forces since it's very common to have small relative movements between the soil and the pile.

Depending on the relative movement of the pile and the surrounding soils, the stress along the pile's shaft may change from positive to negative. As a result a neutral plane is developed at a section on the pile, where there is no relative movement between the soil and the pile (Fellenius, 1989 and Hanna and Sharif 2006).

Fellenius (1989) reported that the neutral plane for end-bearing piles is at the soil-bedrock interface, where there is no pile movement at the tip of the pile. While for floating piles resting on less firm soils, the neutral plane is located below the midpoint of the pile. He suggested that the depth of the neutral plane varies with respect to the strength of the soil at the pile tip and the magnitude of the dead load, where the firmer the soil at the pile tip, the lower the depth of the neutral plane, and the higher the dead load, the higher the depth of the neutral plane as shown in figure 2.10. Fellenius (1989) listed that the location of the neutral plane was located at the lower third of the pile in case of floating pile where the applied load is one third the bearing capacity of the pile. These findings are with agreement with the concept of the equivalent-footing, proposed by (Terzaghi and Peck 1948), as he suggests the equivalent footing to be located at the lower third of the pile.
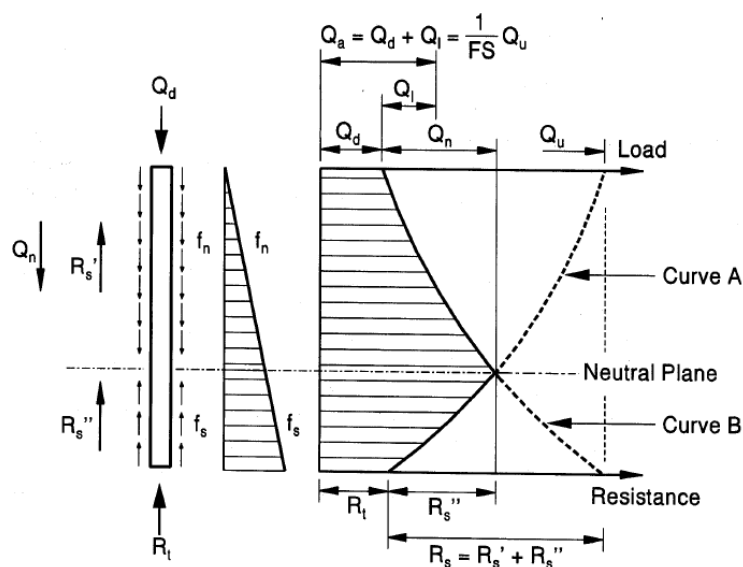
Figure 2.10 Definition and construction of the neutral plane (Fellenius 1989)

where:

Q_a : Design Load R_s : Shaft Resistance

Q_d : Dead Load $R_{s'}$: Negative Shaft Resistance

Q_l : Live Load $R_{s''}$: Positive Shaft Resistance

Q_n : Drag Load R_t : Toe Resistance

Q_u : Ultimate Pile Capacity f_n : Unit Negative Shaft Resistance

FS : Factor of Safety f_s : Unit Shaft Resistance

2.3.1 NSF on Piles in Soft Ground

Johannessen and Bjerrum (1965) were the first to indicate that the negative skin friction in clay depends on the effective earth pressure. These findings were based on full-scale tests of instrumented end-bearing steel piles subjected to negative skin friction caused by the consolidation of the surrounding soil. The effect of the effective stress was noticed by measuring the excess pore water and determining the effective stress after full dissipation of excess pore-water pressure. These findings were confirmed later on by many researchers (Endo et al. 1969, Burland 1973, Konrad and Roy 1987, Bond and Jardine 1995, Fellenius 2008 and others).

Based on the effective stress concept, the ultimate negative skin friction f_s can be calculated from Equation [2.6], where f_s is the negative skin friction at any point along the pile length, σ'_v is the effective vertical stress, K is the coefficient of earth pressure and φ' is the effective angle of internal friction. This method is widely used and known as the beta method, where β can be calculated from Equation [2.7] such that f_s can be calculated from Equation [2.8]

$$f_s = \sigma'_v K \tan \varphi' \dots \dots \dots \dots \dots \dots \dots \dots \quad [2.6]$$

$$\beta = K \tan \varphi' \dots \dots \dots \dots \dots . \dots \dots \quad [2.7]$$

$$f_s = \sigma'_v \beta \dots \dots \dots \dots \dots \dots \dots \dots \dots \quad [2.8]$$

Meyerhof (1976) suggested that the negative skin friction coefficient β decreases as the pile length increases, and that the ultimate skin friction is only mobilized due when a sufficient soil movement takes place. According to this study, the experimental results have shown that the value of K_s for bored piles in over-consolidated clay, can range from 0.7 K_o to 1.2 K_o, and β can vary from 0.7 to 1.4, while for driven piles K_s can range from K_o to more than $2K_o$ and β can vary from 1 to more than 2 . Where K_o is the coefficient of earth pressure at rest can be calculated from Equations [2.9] and [2.10] where R_o is the over consolidation ratio of clay.

$$K_o = 1 - \sin \varphi' \dots \dots \dots \dots \dots \dots \dots \dots \dots \quad [2.9]$$

$$K_o = (1 - \sin \varphi')\sqrt{Ro} \dots \dots \dots \quad [2.10]$$

Therefore it can be noted from this study that the skin friction factor β can vary for over consolidated clays in a wide range with respect to degree of over-consolidation, pile shape, pile installation and other factors. It can be noted also that considering $K_s=K_o$ result in underestimating the skin friction for driven piles and overestimating it for bored piles. Meyerhof noted also that the problem of negative skin friction is more critical for end-bearing piles rather than floating piles.

The variation of the skin friction coefficient β has been reported in many researches, based on field tests piles. Table 2.2 suggested by Burland and Strake (1994), compares between values of β as reported in literature.

Table 2.2 Different values of β from published field data (Burland and Strake, 1994)

Type of Soil	Range of β	Pile Material	Reference
Low plasticity marine	0.15-0.25	Steel	Johanneson and Bjerrum (1965)
Silty Clay	0.26	Steel	Bjerrum et al. (1969)
Silty Clay	0.2-0.4	Steel	Endo et al. (1969)
Low plasticity marine	0.12-0.2	Steel	Bozozuk (1972)
Silty Clay	0.51	Steel	Walker and Darvall (1973)
Soft Clay	0.2-0.25	Steel	Garlanger (1974)
Highly plastic clay	0.26-0.38	Steel	Auvinet and Hanell (1981)
Clayey Silt	0.25-0.4	Steel	Keenan and Bozozuk (1985)
Singapore marine clay	0.35	Concrete	Leung et al. (1991)

Hanna and Sharif (2006) proposed a procedure based on a numerical model using finite element method to predict the pile capacity. This procedure takes into consideration, the effect of the location of the neutral plane location and the effect of pile coating on the negative skin friction on piles embedded in clay subjected to surcharge. Equations [2.11], [2.12] and [2.13] were suggested to predict the negative skin friction acting on a pile's shaft in soft clay due to surcharge. A reduction factor R_N was introduced for floating pile, to take into consideration the effect of neutral depth, where R_N is the ratio between the existing or the mobilized negative skin friction force Q_n acting on the pile till the depth of the neutral plane, and the maximum negative skin friction force $Q_{n(max)}$ acting on the entire length of the pile. The reduction factor R_N can be calculated from Equation [2.14]. For piles coated with bitumen, the value of the coefficient of friction β is reduced, and replaced by β_c therefore the correction factor R_N can be calculated from Equation [2.15]. For calculating the allowable bearing capacity for pile Q_a Equation [2.16] was proposed.

$$Q_{n(max)} = \int_0^L \beta (\pi D) (\gamma' Z + S)\, dz \dots\dots\dots\dots\dots\dots\quad [2.11]$$

$$Q_n = \int_0^{LNP} \beta \, (\pi \, D) \, (\gamma' Z + S) \, dz \dots\dots\dots\dots\dots\dots\dots\ \text{[2.12]}$$

$$\beta = Ks \tan \delta' \dots\dots\dots\dots\dots\dots\dots\dots\dots\dots\dots\dots\dots\ \text{[2.13]}$$

$$R_N = \frac{Q_n}{Q_{n(max)}} = \left(\frac{L_{NP}}{L}\right)^2 \dots\dots\dots\dots\dots\dots\dots\dots\dots\ \text{[2.14]}$$

$$R_N = \frac{\beta_c}{\beta} \left(\frac{L_{NP}}{L}\right)^2 \dots\dots\dots\dots\dots\dots\dots\dots\dots\dots\ \text{[2.15]}$$

$$Q_a = \left[\frac{Q_t + Q_s}{FS} - Q_n\right] = \left[\frac{Q_t + Q_s}{FS} - R_N Q_{n(max)}\right] \dots\ \text{[2.16]}$$

where:

$Q_{n(max)}$: Maximum negative skin friction force

L: Length of pile penetrating settling soil

β =coefficient of friction

L_{NP}: Depth of the neutral plane

Ks: coefficient of earth pressure

Q_t: Ultimate tip resistance of the pile

Z: Height of fill

Q_s: Ultimate shaft resistance of the pile

S: surcharge pressure

Q_a: Allowable bearing capacity of the pile

D: Diameter of pile

β_c: Coeff. of friction for bitumen-coated pile

δ': angle of friction between soil and pile shaft

In the literature several methods were reported based on theory of elasticity to predict the negative skin friction acting on pile's shaft due to consolidation settlement in clays (Poulos and Davis 1980; Chow et al. 1990; Lee 1993; Teh and Wong 1995). Lee et al. (2002) studied the distribution of negative skin friction forces on single piles and pile groups, by carrying out numerical analyses using the finite element package ABAQUS. The case of single piles were modeled in a 2D axisymmetrical conditions and the pile groups in were modeled in 3D. To simulate the behaviour at the pile-soil interface, the ABAQUS interface modeling technique was used, where coulomb

frictional law was applied to represent the interface frictional behaviour between soil and pile surfaces. The study noted the importance of considering the soil slip at the pile-soil interface for predicting the NSF. The study indicated also that the methods based on elasticity theory are over estimating the negative skin friction acting on piles. Figure 2.11 compares between field measurements, numerical analysis and calculations using beta method for the development of drag load with depth.
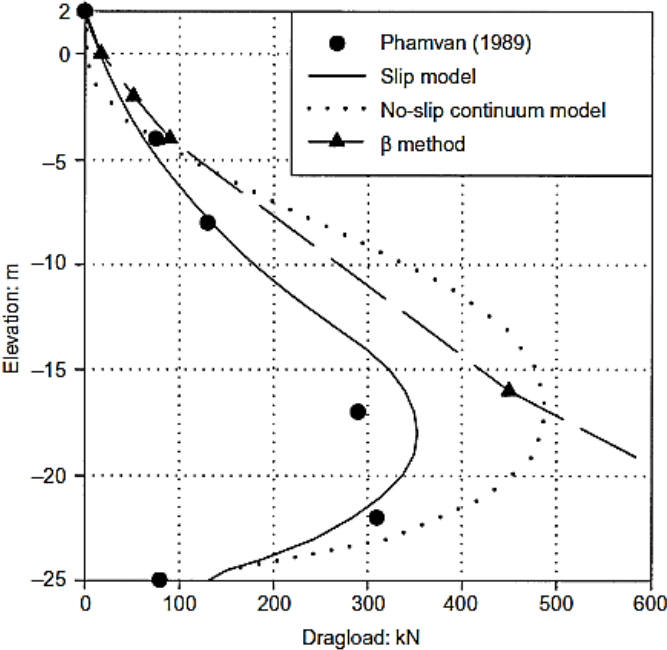
Figure 2.11 Development of dragload (Lee et al. 2002)

Weiping et al., (2014) introduced a load transfer hyperbolic model for pile-soil interface that estimates negative skin friction on single piles, based on field measurements reported in literature. Figure 2.12 presents a comparison between the negative skin friction presented by Poorooshasb et al., (1996) and these obtained by the model presented by Weiping et al., (2014).
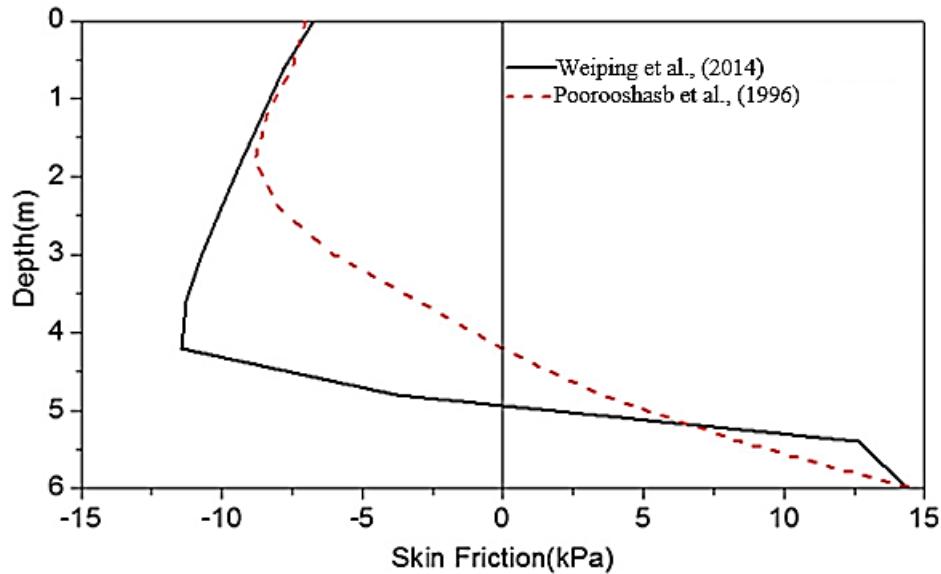
Figure 2.12 Comparison of skin friction on pile shaft after Weiping et al., (2014)

Various measures were proposed in literature to reduce negative skin friction, and many studies have been carried out to consider the effect of these measures. The use of bitumen coating for pile subjected to negative skin friction has been recommended by many researchers as an effective solution for reducing negative skin friction (Fellenius 1972; Walker et al. 1973; Clemente 1981; Briaud 1997; Hanna and Sharif 2006). Pile coating however isn't desirable in all cases as it reduces both negative and positive skin friction.

The consolidation settlement takes place over time, depending on different soil parameters, applied loading and drainage conditions. Therefore NSF is time dependent as well, and many different studies have noted the effect of time and rate of settlement on NSF (Fellenius and Broms, 1969; Fellenius 1972; Walker et al. 1973, Grigoryan 2005).

The shaft resistance and negative skin friction can be mobilized at a very low displacement as stated by many researchers based on measurements. Where settlement in the range of $(0.005 - 0.02)$ D_p was enough to mobilize skin friction as indicated by researchers (Fellenius 1989; Fleming et al.

2009; Guo 2013, Zhang and Wang 2015). The magnitude of soil settlement also has a great effect on negative skin friction forces, so the larger the soil settlement, the greater the negative skin friction force that develop on pile (Poulos 1997; Lee et al., 2001).

Vanapalli and Taylan (2012) introduced the modified beta method, taking into consideration the effect of matric suction in unsaturated soils on the frictional stresses acting on pile as presented in Equations 2.17 through 2.20.

$$Q_{f(US)} = Q_{f(sat)} + Q_{f(Ua-Uw)} \; .... \; [2.17]$$

$$Q_{f_{(sat)}} = [\sigma'_v \beta)] \, \pi.d.L \; .... \; [2.18]$$

$$Q_{f_{(Ua-Uw)}} = [(Ua - Uw)(S^K)(tan\,\delta')] \, \pi.d.L \; .... \; [2.19]$$

$$Q_{f(US)} = [(\sigma'_v \beta) + (Ua - Uw)(S^K)(tan\,\delta')] \, \pi.d.L \; .... \; [2.20]$$

where:

$Q_{f(US)}$: Ultimate shaft capacity $\qquad$ K : Fitting parameter

$Q_{f(sat)}$: Shaft capacity in the saturated zone $\qquad$ S: Degree of saturation

$Q_{f(Ua-Uw)}$: Shaft capacity in the unsaturated zone

Figure 2.13 presents the measured ultimate shaft bearing capacity compared to the values estimated using α, β, and λ methods for compacted Indian head till samples after Vanapalli and Taylan (2012).
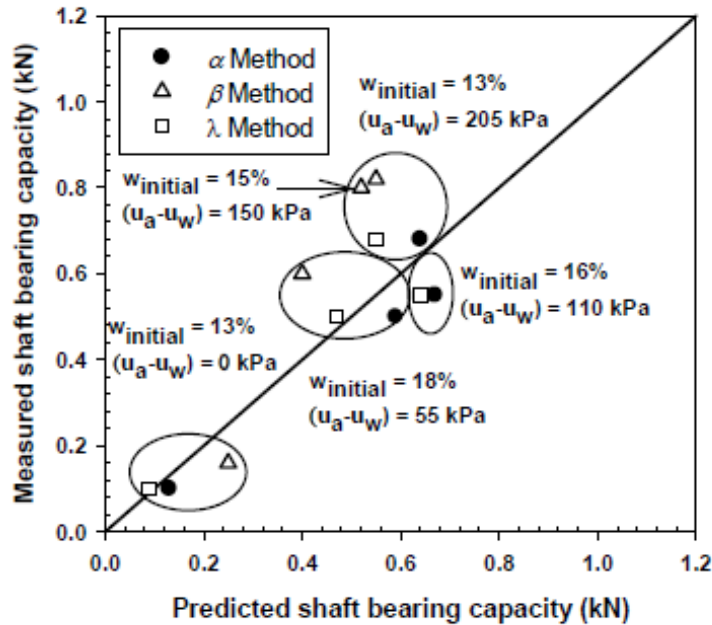
Figure 2.13 Measured and estimated ultimate shaft bearing capacities for compacted Indian head till samples (Vanapalli and Taylan, 2012)

Chuang and Yang (2014) studied the loading behaviour of a small scale single pile in unsaturated clay, by conducting laboratory tests and numerical analysis using PLAXIS finite element software. In order to simulate the reduced friction along pile shaft in the axisymmetric model, the interface strength reduction factor ($R_{interface}$). The dilatancy angle (ψ) was used in the FEM to take into account the swelling clay behaviour, where the dilatancy angle increases with decreasing the water content. The authors concluded from the experimental results that the ultimate bearing capacity decreased by 52.5% due to the increase in the soil water content from 15 to 21%.

It can be concluded from this section that that there are many factors that affect the NSF acting on pile's shaft, including the magnitude and rate of soil settlement, friction on the soil-pile interface, the stiffness of soil at the pile tip and the surcharge load acting on top of soil.

2.3.2 NSF on Piles in Collapsible Soils

The performance of piles in collapsible soils is affected by the substantial loss of strength and collapse settlement of collapsible soil upon inundation. The soil strength is reduced instantly and the collapse settlement will take place instantaneously, unlike the consolidation settlement in clays that takes place over a longer period of time. The behaviour of piles in collapsible soils are therefore different than that in clays, and the developed NSF forces due to the sudden soil collapse upon wetting, are expected to be much higher than the NSF forces developed due to consolidation settlement.

Many researchers in Russia have been studying the behaviour of piles in collapsible soils, and only a few field tests carried out on floating piles embedded in collapsible soils were reported (Grigoryan and Grigoryan 1975; Kalashnikova 1976; Grigoryan and Yushube 1986; Grigoryan and Chinenkov 1990 and Krutov 2003).

Grigoryan and Grigoryan (1975) have carried out field tests on floating piles in collapsible soils, to study the effect of collapsible soil on piles upon soils collapse under the soil own weight upon wetting with water, so that this effect can be take in to consideration when designing piles in similar conditions. In order to measure the negative skin friction forces, bored cast-in-situ piles (NI and NII) were constructed, 16 and 22 m deep and 600 and 500 mm in diameter respectively, as shown in figure 2.14. The piles were equipped with strain gauges to measure pile settlement and dynamometers (N1 to N6) were installed at different depths to measure the forces acting on the piles' shafts.
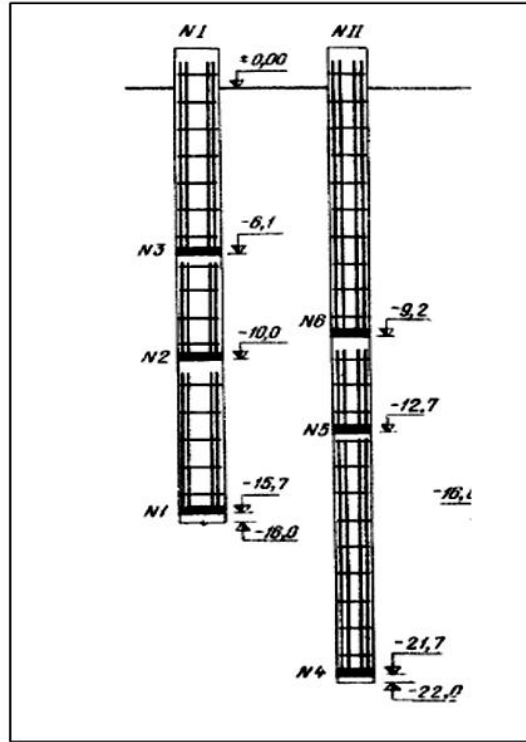
Figure 2.14 Locations of dynamometers along the pile length (Grigoryan and Grigoryan, 1975)

Four piles (NIII to NVI) were installed, to attain the reaction of the loading jack during the testing. Depth markers (D1 to D6) were used to record the settlement of soil, as shown in figure 2.15. A constant static load has been applied to the piles throughout the test, and in order to introduce water for soil wetting, trenches have been constructed to be filled with water during the test.
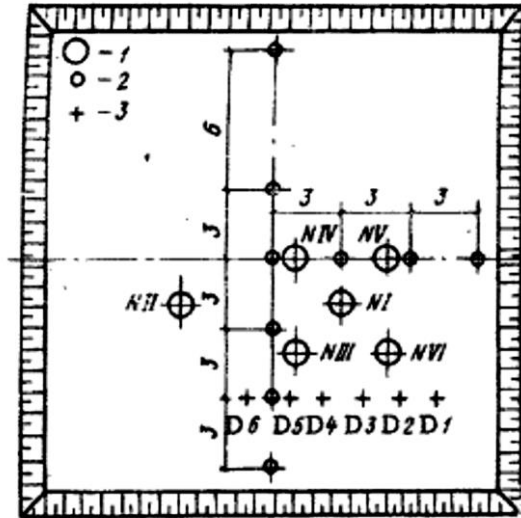
Figure 2.15 Plan for piles and depth markers (Grigoryan and Grigoryan 1975)

It was noted from these measurements that the settlement of floating piles was observed as a result of soil settlement upon wetting with water. Soil and pile settlements were recorded and a relationship between the rate of soil settlement and the rate of pile settlement with respect to time established. This relationship was useful for analysing the development of NSF with respect to relative movement between soil and pile. Since the NSF will only develop when there is a relative movement between the soil and the pile therefore, negative skin friction measurements occurred only when soil settlement rate exceeded that of the pile. It can be noted also from these findings that the negative skin friction forces increase with the increase of relative movement between soil and pile, and the maximum value of negative skin friction force that was recorded during the test was 282 kN.

Grigoryan (1991) has postulated three analytical schemes for pile-soil interaction for floating piles penetrating a large layer of collapsible soil depending on: soaking direction, soil settlement due to soil wetting, the depth of collapsible layer, source of wetting and neutral plane. He stated that in the late 80s a large number of problems in pile foundations have been reported, due to the effect of

29

negative skin friction on reducing the piles' bearing capacity and causing pile foundation settlement due to the rise in groundwater level. The study has proposed some measures for eliminating settlement of pile foundations in collapsible soils such as: the construction of deep end-bearing piles resting on a firm strata and eliminating the possibility of soaking soils entirely. Both measures however, provide uneconomical solutions in many cases as Grigoryan (1991) noted.

Hepworth (1993) reported a case study where negative skin friction due to settlement of collapsible soil due to sub-soil accidental wetting, resulted in larger than expected settlements reaching several inches causing failure, and also it was considered that a pile has parted at one of the splices. Underpinning using pile foundation was carried out as a remedial measure with a cost of about 21 Million us dollars failure however occurred again due to wetting and a new underpinning was performed using casing, and the former pile was cut free from the cap to avoid additional load due to NSF. Piles design criteria allowed an ultimate bearing capacity of 200 tons for each pile. Allowing a working load of 60 tons, a safety factor of two and 100 tons allowed for negative skin friction. Hepworth (1993) reported that the failure could have been prevented by considering: full depth wetting, higher skin friction values or using higher capacity piles with sleeves. These test result showed that, negative skin friction is a significant force and can be easily underestimated.

Li et al. (1994) reported field measurement for four large diameter cast in place belled piles penetrating collapsible soils where the effect of wetting on negative skin friction was studied. The neutral plane depth was found between 17.5 to 25 m and the measured negative skin friction due to wetting reached high values, between 27.3 and 44.9 kPa. The pile were subjected to static load after inundation took place, and it was noticed that the neutral plane moves upwards as the load acting on the pile increases and accordingly pile settlement develops until the relative movement between

30

soil and pile no longer exists and negative skin friction disappeared. The wetting process took place over almost two months until full saturation.

Grigoryan (2005) has noted that the consideration of the time factor is very important, and he suggests that the study carried out by (Krutov 2003), to consider the effect of GWT rising on piles in collapsible soil, didn't consider the critical case, as the soil settlement took place over months, since the rate of rise in GWT didn't exceed 0.5-1.5 m/year.

Gao et al., (2007) investigate the load transfer mechanism on a special type of pile (squeezed branch and plate pile) in collapsible soil, and compared the performance of this pile to conventional piles. The study was conducted on piles in pre-wetted collapsible soils, therefore negative skin friction didn't develop. The authors highlighted the importance of examining negative skin friction that act on piles in collapsible soils due to inundation in further studies.

Chen et al. (2008) reported field measurements for piles in collapsible soil in different locations in China, where negative skin friction occurred due to inundation. The maximum values of negative skin friction reached 57.6 kPa and the average values reached 44 kPa, while the soil settlement due to inundation reached 55 cm. The frictional resistance distribution for one of the piles in the saturated state is shown in figure 2.16.
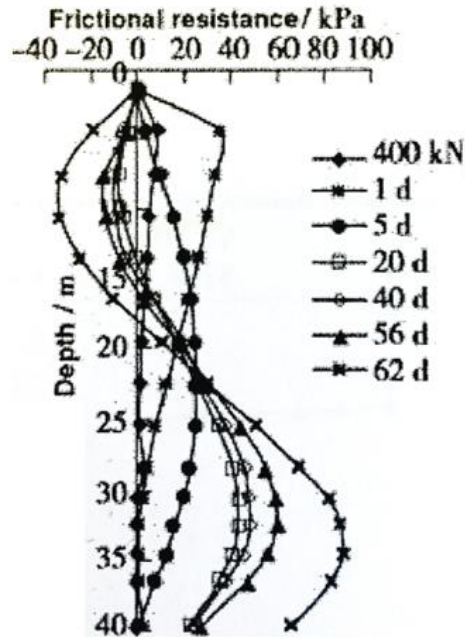
Figure 2.16 Frictional resistance for pile ZH4 in saturated state after (Chen et al. 2008)

Mashhour (2009) has carried out tests to study the negative skin friction resulting on end-bearing piles. The research has postulated a new procedure for measuring negative skin friction on piles in collapsible soils; and the test results showed that negative skin friction is directly proportional to collapse potential and inundation pressure as shown in Table 2.3, where $Q'_{n(max)}$ is the drag load measured after inundation. The study was limited to a narrow range of parameters, and did not consider the effect of inundation rate and partial inundation.

Table 2.3 Experimental results (Mashhour 2009)

Test	C_p (%)	φ'	γ (kN/m³)	σ (kPa)	$Q'_{n(max)}$ (kg)
Test 1	12.5	35	16.20	40	34
Test 2	12.5	35	16.20	60	60
Test 3	12.5	35	16.20	80	89
Test 4	9	38.5	16.25	80	62
Test 5	4.2	40	16.28	80	56

Ma et al. (2009) reported field results comparing between skin friction before and after wetting of collapsible soil. The study included five test piles subjected to static load, and the wetting process took place over 53 days, where the volume of water used for wetting was about 50,000 m^3 and the maximum ground settlement recorded was equal to 358 mm. Piles used in this study are 60 m in length and 800 mm in diameter, and the collapsible soil layer extended up to a depth of 33 m, where the maximum collapsibility was at a depth of 16 to 17 m below ground surface. The results show the development of negative skin friction after wetting, where it reached values of 44 kPa in some cases where pile was subjected to a static load of 3000 kN while the pile settlement after wetting reached 11.7 mm under the same load. Figures 2.17 and 2.18 show the friction stress distribution along pile depth before and after wetting for different loading cases. Figure 2.18 show how NSF disappear with pile loading.
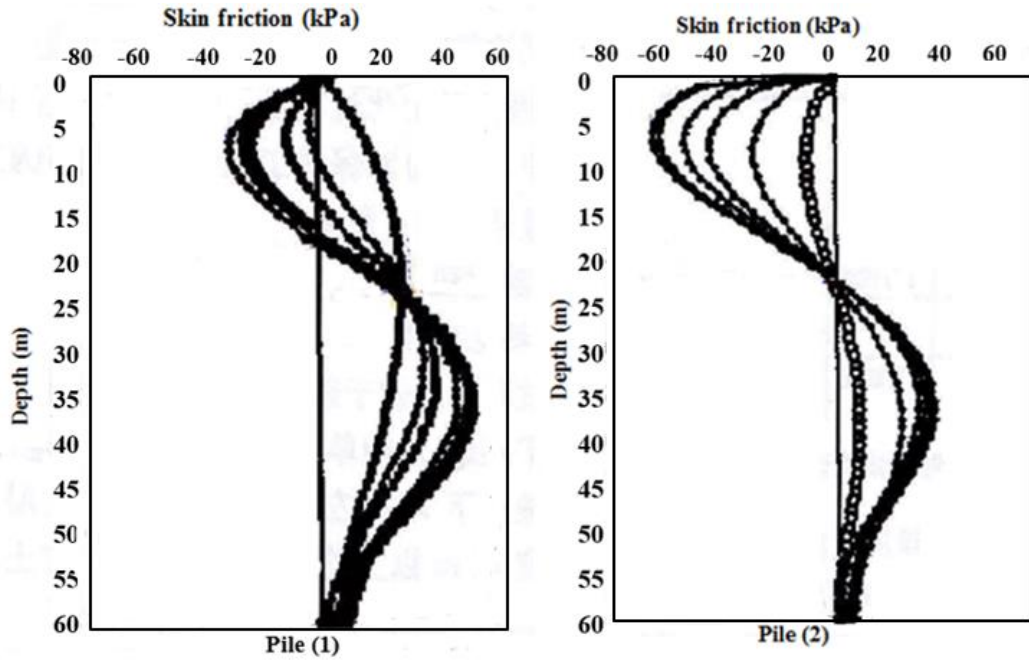
Figure 2.17 Friction stress development along pile depth during wetting (Ma et al. 2009)
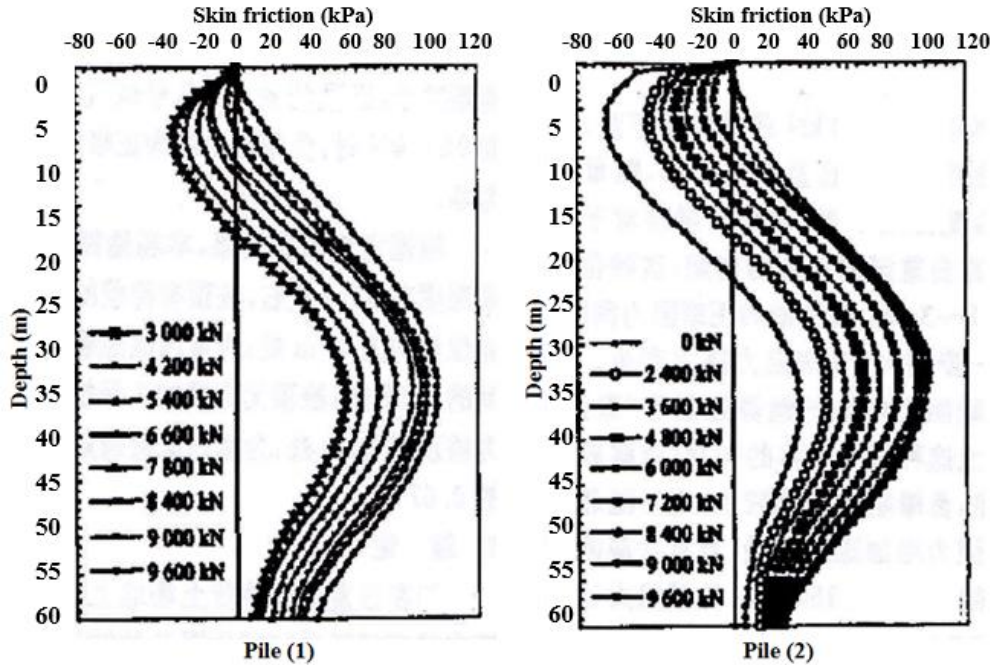
Figure 2.18 Friction distributions along pile depth after wetting (Ma et al. 2009)

Kakoli (2011) has introduced an axisymmetric finite-element model using software *PLAXIS 2D* software, for modelling piles in collapsible soil subject to inundation. Kakoli (2011) stated that the study was limited and many factors should be examined in further studies such as the consideration of different stages of partial inundation. Noor et al., (2013) extended the work introduced by Kakoli (2011) and introduced Equation [2.21] for predicting drag load on a single axially loaded vertical pile penetrating collapsible soil layer, taking into account the collapse potential.

$$Q_n = \pi \times H_{NA} \times C_p \, (m \times d_p + b) \dots \, [2.21]$$

where:

Q_n is the normalized drag load because of negative skin friction; m and b are two constants that can be estimated from Equations [2.22 and 2.23], knowing the depth of the collapsing soil (H_s).

$$m = 0.575 \, (Hs)^2 - 0.4575 \, H_s + 1.8525 \dots \, [2.22]$$

$$b = -0.0439 \, (Hs)^2 - 0.0489 \, H_s - 0.7914 \dots [2.23]$$

Figures 2.19 and 2.20 show shear stress distribution for inundation from bottom and top respectively after Kakoli (2011) and Noor et al., (2013).
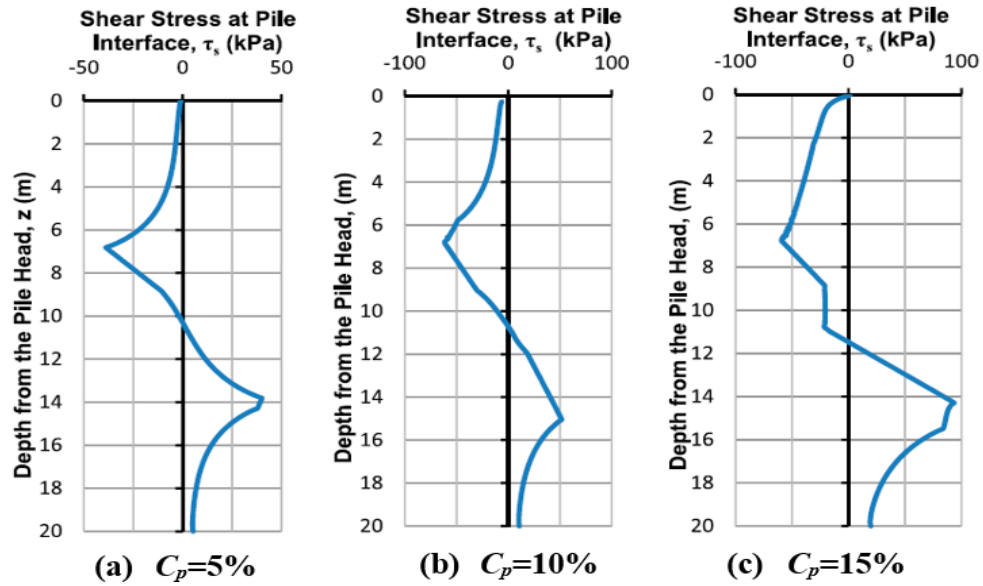
Figure 2.19 Shear stress distribution for inundation from bottom (for h=3m) after (Kakoli 2011) and (Noor et al., 2013)
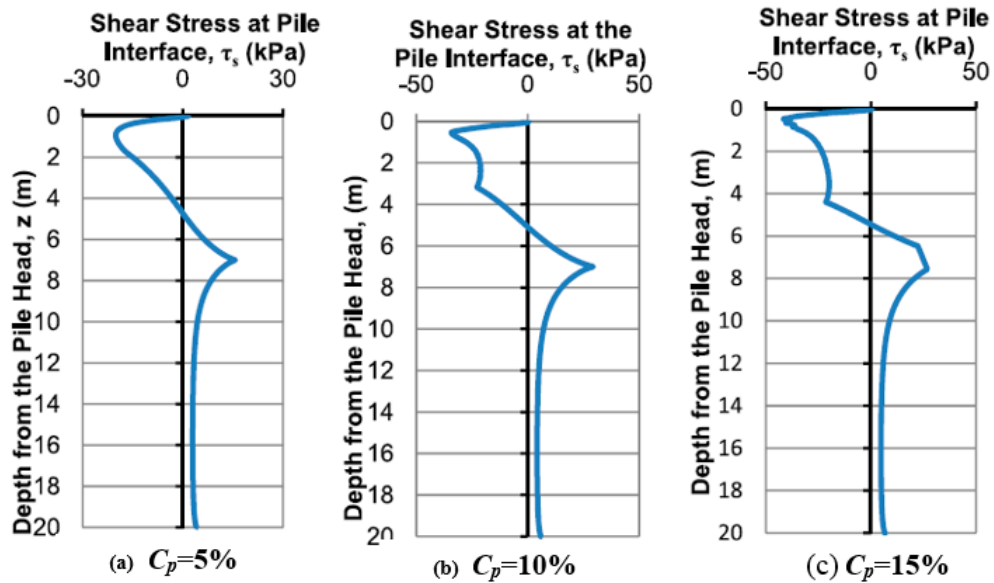
Figure 2.20 Shear stress distribution for inundation from top (for h=3m) after (Kakoli 2011) and (Noor et al. 2013)

Table 2.4 summarizes some of the experimental data reported in literature for studying the behaviour of piles in collapsible soils.

Table 2.4 Experimental data on piles in collapsible soils

Researcher	Foundation Type
Grigoryan and Grigoryan (1975)	Floating piles
Kalashnikova (1976)	Floating piles- soil stabilization
Grigoryan and Yushube (1986)	cast-in-place floating piles
Grigoryan and Chinenkov (1990)	Under-reamed floating piles
Li et al. (1994)	large diameter belled piles
Krutov (2003)	Floating piles
Gao et al. (2007)	Squeezed branch and plate pile
Chen et al. (2008)	Floating piles
Ma et al. (2009)	Floating piles
Mashhour (2009)	End-bearing pile - Prototype

Some measures have been suggested in literature to reduce or eliminate the effect of strength reduction and collapse settlement upon wetting of collapsible soils, including soil stabilization and coating with bitumen. Improving the performance of floating piles in collapsible soils by means of soil stabilization using sodium silicate grout through a leading hole has been studied by Kalashnikova (1976), where field tests have been carried out, to study the performance of piles in a stabilized collapsible soil using sodium silicate grout. These results have shown that soil stabilization, has increased the bearing capacity of the floating piles up to (50-65%) and the settlement has been reduced. The study has shown that the decrease in bearing capacity of collapsible soil upon wetting can be reduced or eliminated by soil stabilization.

2.4 Discussion

Numerous studies show that the design procedures developed for calculating negative skin friction for piles in clays undergoing consolidation settlement are not applicable for the case of collapsible soils. Furthermore, there is a lack of reliable methods for calculating negative skin friction on piles in collapsible soils. Several elastic solutions have been introduced in the literature to estimate NSF. However, these methods in general over predict the negative skin friction force acting on piles in clays (Lee et al., 2002). Pile failure and/or settlement occur as a result of a combination of forces acting on the pile from the super-structure and drag forces. Therefore, design procedures should take into consideration the development of NSF forces under different loading and soil-pile conditions with time. To date there is a lack in codes and standards for considering the effect of negative skin friction in pile design, as reported by Fellenius (2014).

Piles installed in collapsible soils are subjected to negative skin friction accompanied by a significant decrease in surrounding soil strength upon soil inundation. Different modes of failure resulting from NSF have been reported in the literature, including pile material failure, separation of the pile from the cap or building damage due to differential settlement. It can be noted also that the effect of NSF can be more critical for end-bearing piles, since the neutral plane and hence drag loads are relatively higher that these acting on floating piles. Such high values of NSF can exceed the structural capacity of the piles and result in pile failure (Fellenius1989).

Only a few full scale studies were carried out on piles in collapsible soils, as the testing procedure is highly expensive, time consuming and difficult to conduct (Grigoryan, 1997 and Chen et al., 2008). Although pile foundations were widely used in the 1960s in collapsible soils, and many studies were carried out in Russia to consider the effect of soil collapse upon wetting on pile

foundations, the design approach adopted by the Russian construction code of practice for pile foundations doesn't provide reliable results (Grigoryan 2005).

Since collapsible soils experience a sudden reduction in strength accompanied by a sudden volume change (settlement) upon wetting, the consideration of time factor is very important, in the analysis of NSF developed on piles in collapsible soils (Grigoryan, 2005). Therefore, in this study the effect of time factor and rate of inundation was considered. Since the effect of NSF is more critical for the end-bearing piles than the floating piles, and since the end-bearing piles are more commonly used in collapsible soils, it is necessary therefore to study the behaviour on end-bearing piles in this research.

It can be concluded from the literature review that the parameters that could impact the magnitude of negative skin friction in collapsible soils are but not limited to: collapse potential, inundation pressure, degree of wetting, rate of inundation, pile material and pile installation techniques. Different researchers have studied the effect of collapsible soil settlement due to wetting on negative skin friction, for specific site conditions, but less attention has been paid to the effect of collapse potential, inundation pressure and wetting schemes.

CHAPTER 3

EXPERIMENTAL INVESTIGATION

3.1 General

The main goal of this study is to provide a better understanding for the complex soil/pile interaction during collapsible soil inundation. An experimental prototype model was designed therefore, in order to simulate this complex interaction between collapsible soil and pile shaft over a wide range of parameters for different cases that can arise in the field.

3.2 Experimental Setup

The experimental setup simulates a single end-bearing pile embedded in collapsible soil subjected to inundation under a constant surcharge load. The prototype experimental setup consists of the following main components:

- Soil tank,
- Steel frame (reaction frame),
- Water supply system,
- Model pile (stainless steel rod),
- Loading system,
- Measurement devices: load cell, linear variable differential transducers (LVDTs) and data acquisition system.

These components are shown in Figure 3.1 and are explained in details in the following sections of this chapter.
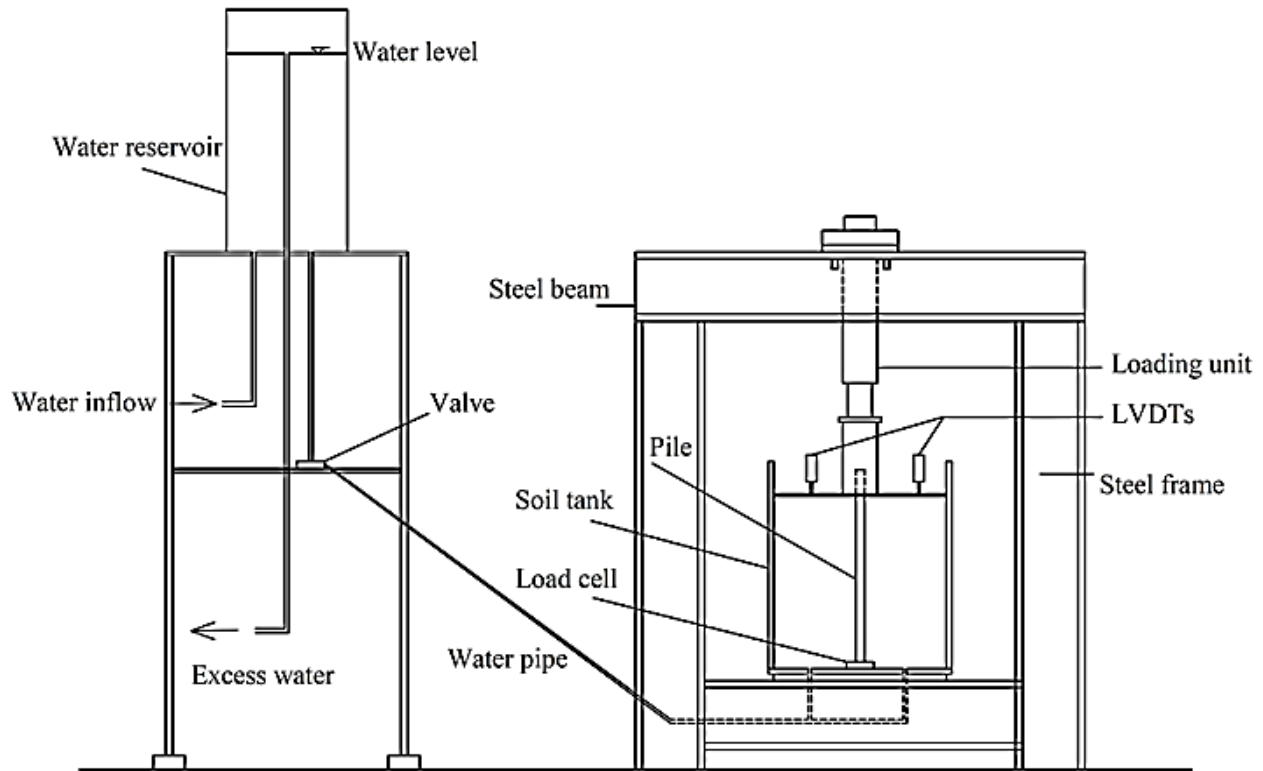
Figure 3.1 Experimental setup

3.2.1 Soil Tank and Water Supply System

The Plexiglas testing tank has a square cross section with dimensions of 50 cm length and 60 cm height. The tank is reinforced by steel angles and aluminum channels to provide rigidity as shown in figure 3.2. The bottom of the tank is made of a rigid steel plate. Eight pipes were connected to the bottom of the tank to introduce water inflow to the soil during the test, providing a uniform distribution of water.

Figure 3.2 Soil tank

The water supply system consists of a constant-head elevated tank made of Plexiglas to supply water to the soil tank during the test. The water tank is connected to an inflow pipe at the base of the tank to introduce water to the tank, and two outflow pipes. One of the outflow pipes is located at a constant height to maintain a constant water level in the tank by draining the excess water as shown in figure 3.3. The second outflow pipe is connected to a water distributer that provides water to the soil tank through eight water inlets at the base of the soil tank. A water valve was used to control the percentage of water flow to be allowed, which was used to control inundation rate.
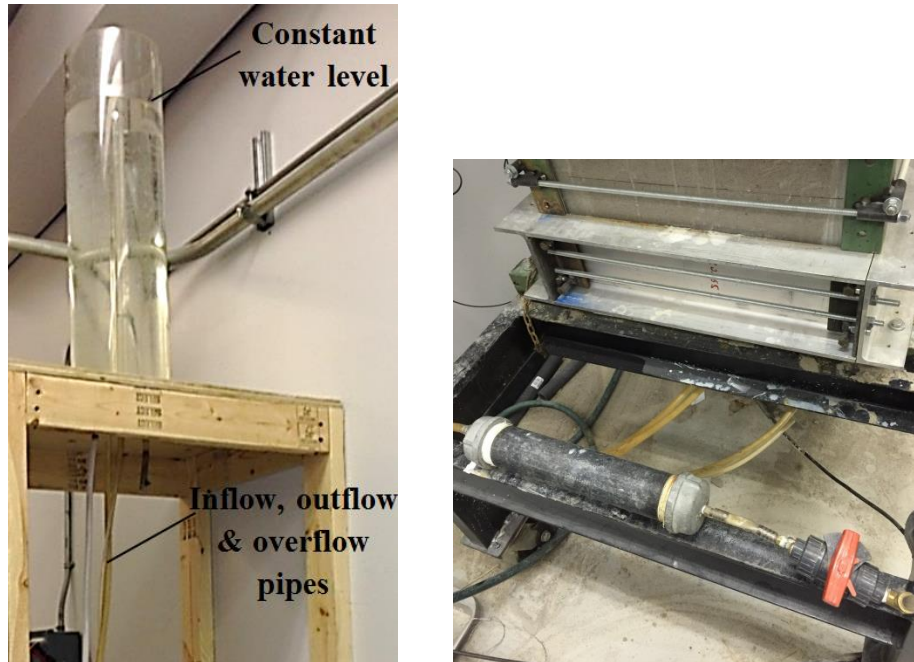
Figure 3.3 (a) Water tank (b) Water distributer and valve

3.2.2 Model Pile

The pile used in this study is made of a stainless steel rod that has a diameter of 2.5 cm and a length of 75 cm. The stainless steel rod surface was made rough by means of knurling, simulating the roughness of steel piles used in practice, as shown in figure 3.4.
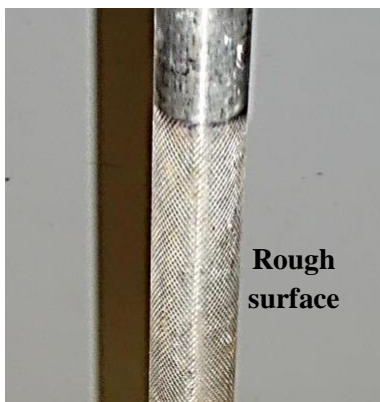
Figure 3.4 Model pile photograph

The roughness of the pile surface is very important as it affects the development of friction on pile-soil interface, upon relative movement between the soil and the pile. Roughness tests were carried out using a contact profilometer equipped with a diamond stylus, in order to plot the surface profile as shown in figure 3.5 and to measure roughness parameters of the pile.
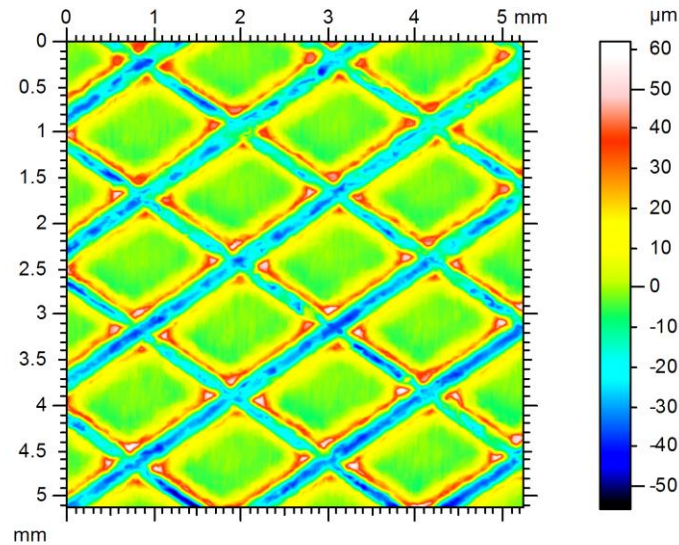
(a) 2D Profile
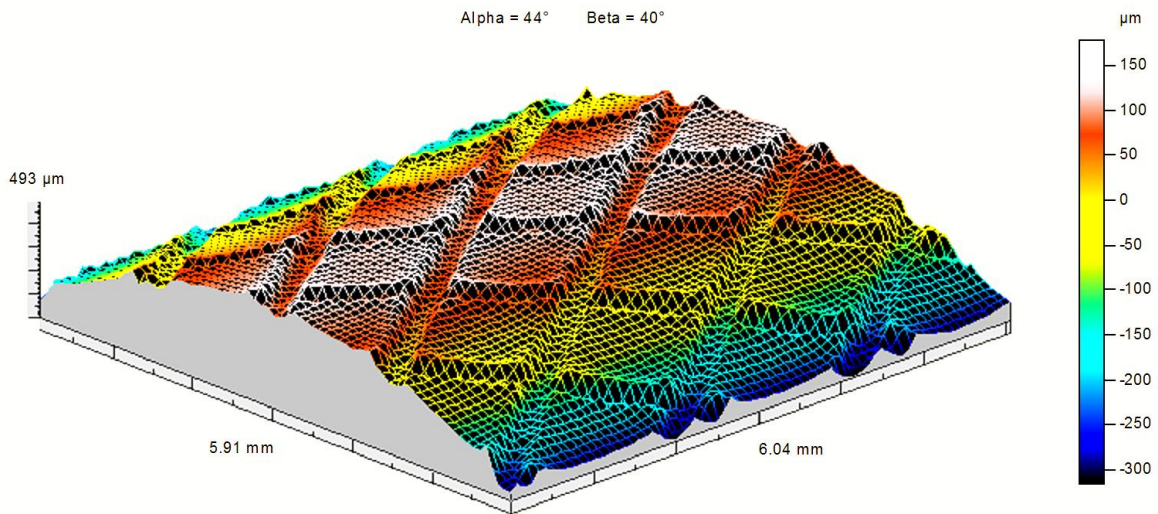
(b) 3D Profile

Figure 3.5 Pile-surface topography

Table 3.1 present roughness parameters calculated as average values of all sampling lengths, where micro-roughness filtering was used, with a ratio of 2.5 μm.

Table 3.1 Roughness parameters

R_a (μm): arithmetic average of absolute values	10.3
R_p (μm): maximum peak height	25.3
R_v (μm): maximum valley depth	20.6
R_t (μm): maximum height of the profile	59.8
R_q (μm): root mean squared	12.7

3.2.3 Loading System

A static loading system was used to apply stress on soil surface during the test that consists of a loading cylinder connected to a hydraulic pump through hoses as shown in figure 3.6. The stress applied on soil simulates the overburden pressure acting on collapsible soil layer in the field.
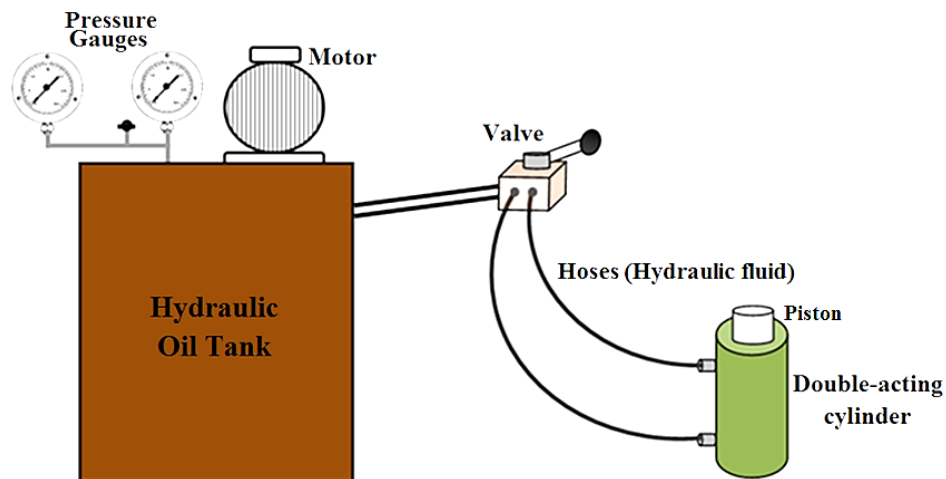
Figure 3.6 Hydraulic loading system

 The load is transferred to soil via a square steel plate placed on the soil surface, with lengths equal to 49.8 cm each, covering the entire surface area of the soil. The steel plate has a circular hole in the centre of diameter 2.56 cm to allow the pile to pass through. A steel post was used to transfer the load from the piston to the steel plate, allowing the pile to stand freely. The loading cylinder is

connected to the steel frame, as shown in figure 3.7 (a). Figure 3.7 (b) shows the main components of the loading system. Placing the steel post in order to transfer the load to the soil surface and the different load transfer elements used are shown in figures 3.8 and 3.9 respectively and a photograph of the main components of experimental setup is shown on Figure 3.10
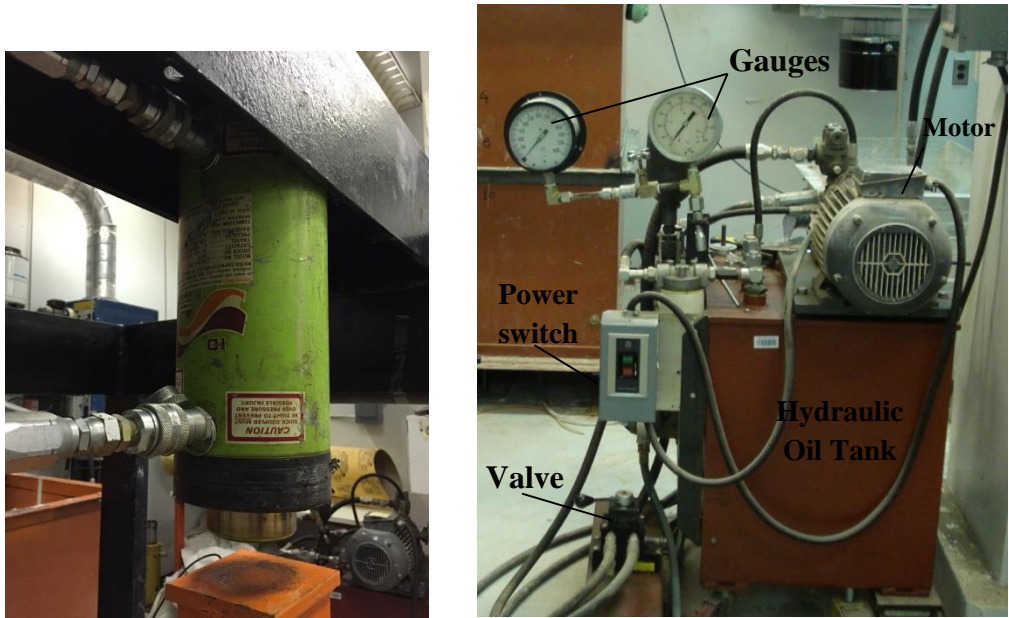
(a) Loading cylinder   (b) Loading system

Figure 3.7 Photo of Hydraulic loading system
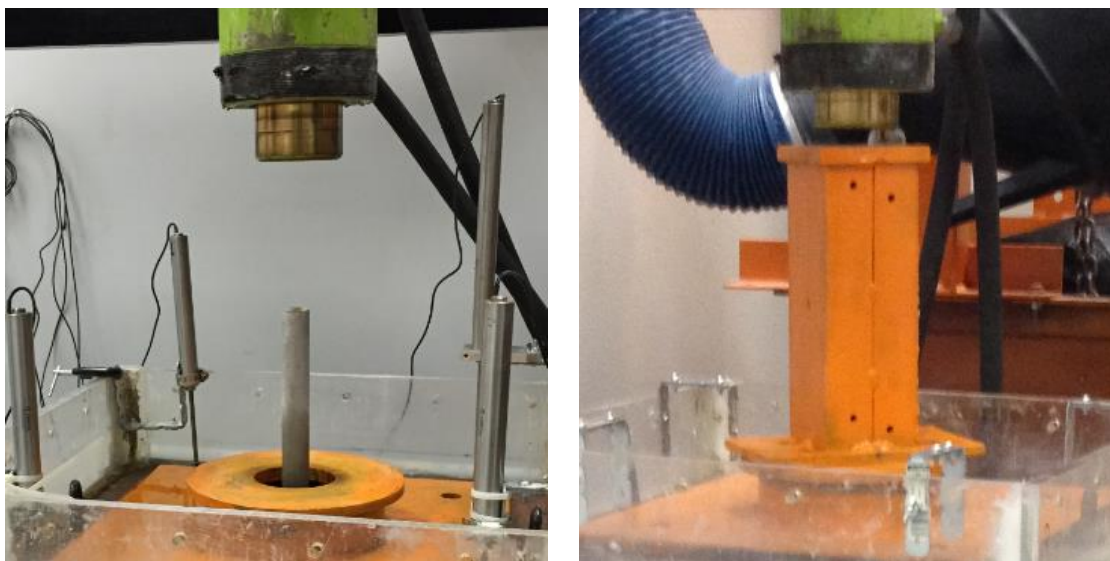
(a) Before placing post   (b) After placing post

Figure 3.8 Photo of Load transfer elements
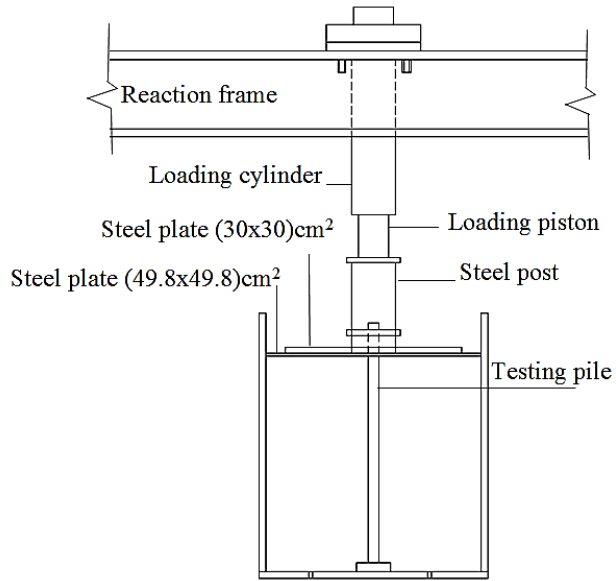
Figure 3.9 Load transfer schematic drawing

Figure 3.10 Experimental setup photograph

3.2.4 Measurement devices

The load cell used in this study has a capacity up to 1000 kg, and a rating of IP67 for dust and water immersion protection. In order to simulate end bearing piles, the load cell was attached to the tank bottom in order to measure the loads acting on the pile tip. The load cell dimensions and the pile-load cell connection are shown in Figure 3.11, while figure 3.12 is a photograph that shows the load cell fixed to the tank bottom.

(a) Cross-sectional view   (b) Plan view
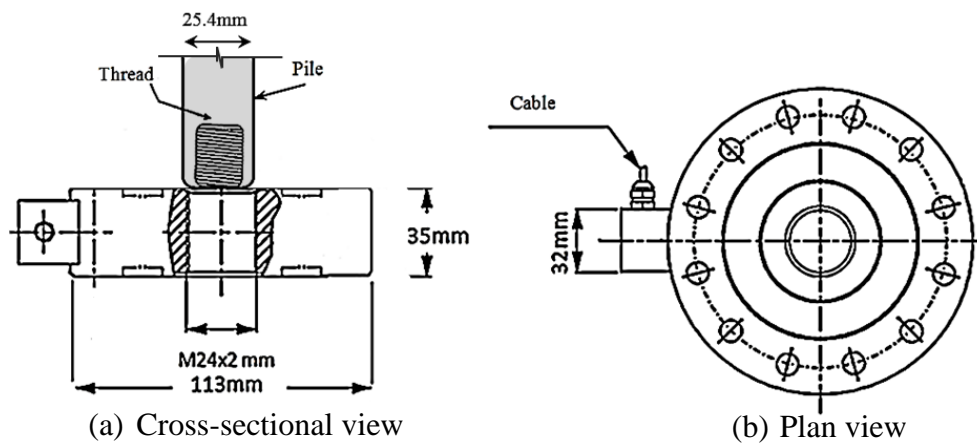
Figure 3.11 Load cell detailing

Figure 3.12 Photo of the Load cell

Four LVDTs were placed on top of the steel plate applying load on the soil surface, to measure the settlement of soil upon loading, and upon inundation with water. An electric current of a constant voltage was introduced during the tests, through a voltage unit, to the load cells and LVDTs as expressed in figure 3.13. A data acquisition system that is connected to the load cells and LVDTS,

displayed readings voltage on a computer, and converted into forces in grams and millimetres for both load cells and LVDTS respectively, using formulae developed from calibration of each instrument individually. A computer program (VEE pro 8.5) was used to control readings from the four LVDTs and the load cell in the desired time intervals. The program applies the formulae for each device to convert units from voltage to kilograms and millimetres for load cells and LVDTs respectively, and it imports readings in millimetres and kg versus time to an excel sheet throughout the test.
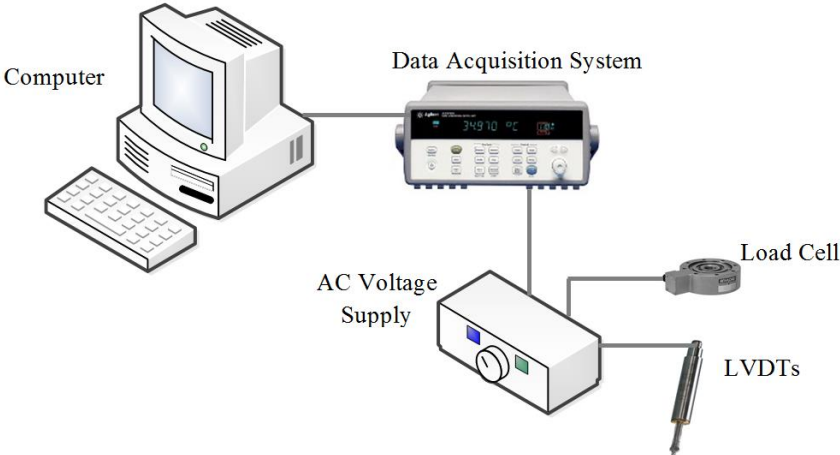
Figure 3.13 Data acquisition system and measuring equipment

3.2 Collapsible Soil Preparation

In this study, collapsible soil mixtures were prepared in the laboratory by mixing the sand and clay and water contents. The water content and clay percentage for each soil mixture were very carefully controlled using a highly accurate sensitive balance shown in figure 3.14 in order to obtain the desired soil properties for each collapsible soil mixture. The soil mixtures were uniformly mixed using a concrete mixer shown in figure 3.15, where the mixing procedure was carefully done over a sufficient period of time, to obtain uniform mixtures.

Figure 3.14 Sensitive balance

Figure 3.15 Concrete mixer

Collapse potential (C_p) is the key parameter used to define collapsible soils, and it depends mainly on initial water content, compaction effort and clay content. Therefore in order to determine the appropriate mixture properties for soils having collapse potential values between 4.2 and 12.5% a series of response-to-wetting single oedometer tests were carried out in Concordia University after (Mashhour 2009 and Soliman 2010) for sand-clay mixtures using kaolinite clay at different levels

of compaction, water and clay contents. An additional collapsible soil mixture that has a collapse potential of 18% was designed and introduced in this study based on different iterations, as shown in Table 3.2, where each oedometer test was repeated at least three times to ensure reliability. Figure 3.16 shows the compaction of soil sample in oedometer ring before carrying out oedometer test, while figure 3.17 shows the oedometer ring test, where soil was submerged at 200 kPa inundation stress.
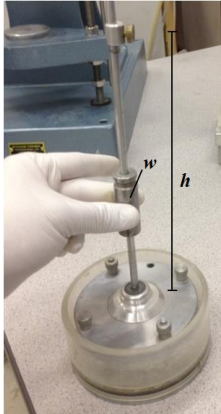
Figure 3.16 Soil compaction in oedometer ring

Figure 3.17 Oedometer test

Table 3.2 Response-to-wetting Oedometer tests on different sand-clay mixtures

| Researcher | Kaolin Clay Type | Clay Content (%) | Initial Water Content (%) | Compaction weight (100 gm) | | C_p (%) |
				# Drops	Height of drop (mm)	
Mashhour (2009) and Soliman (2010)	KT-Cast	5	5	10	200	1.5
	KT-Cast	10	5	10	200	3.2
	KT-Cast	15	5	10	200	7
	Sapphire	5	5	10	200	2
	Sapphire	10	5	10	200	6.2
	Sapphire	15	5	10	200	9.8
	Rogers	5	5	10	200	5
	Rogers	10	5	10	200	9
	Rogers	15	5	10	200	13
	Rogers	5	5	20	200	0.5
	Rogers	10	5	20	200	4
	Rogers	15	5	20	200	7.5
	Rogers	5	5	15	200	0.7
	Rogers	10	5	15	200	6.5
	Rogers	15	5	15	200	10.5
	Rogers	10	9	8	150	2
	Rogers	10	7	8	150	4
	Rogers	6	5	8	150	4.2
	Rogers	8	5	8	150	9
	Rogers	10	5	8	150	12.5
Present study	Rogers	14	5	8	150	16
	Rogers	14	5	6	150	18
	Rogers	14	4	8	150	15
	Rogers	14	4.5	8	150	17

In this investigation, the collapsible soil was prepared in the laboratory by mixing fine sand with Kaolin clay commercially known as "rogers clay", using a concrete mixer, then a compaction effort was applied on the soil mixture to reach the desired unit weight. The kaolin clay acts as the cementing material that bonds sand particles together at low water content (5%). The chemical analysis and physical properties of the clay is shown in Table 3.3 while the particle size distribution for clay and sand obtained from hydrometer test and sieve analysis are shown in figures 3.18 and 3.19 respectively.

Table 3.3 Chemical analysis and physical properties for clay

Silicon dioxide SiO_2 (%)	46.5
Aluminium oxide Al_2O_3 (%)	37.5
Ferric oxide Fe_2O_3 (%)	1
Titanium dioxide TiO_2 (%)	1.3
Calcium oxide (quicklime) CaO (%)	0.3
Magnesium oxide MgO (%)	0.3
Potassium oxide K_2O (%)	0.2
Sodium oxide Na_2O (%)	0.1
%Carbon	0.1
%Sulfur	0.13
Dry Modulus of Rupture (psi)	950
Surface Area, (m^2/g)	24
PH	4.5
G_s	2.6
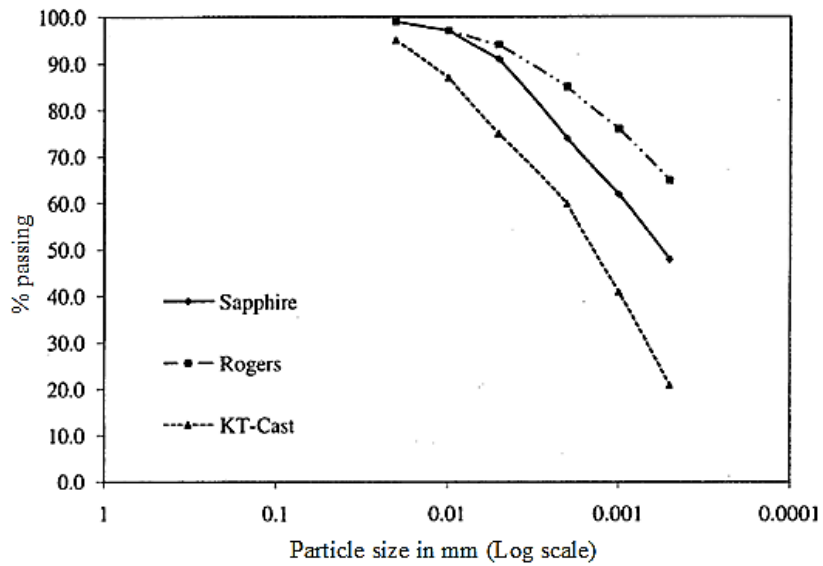
Figure 3.18 Particle size distribution for kaolin clay after Soliman (2010)

Four mixtures of collapsible soil CS-1, CS-2, CS-3 and CS-4 were used in this investigation having different clay contents and thus, different levels of collapse potential C_P. The collapse potential of these mixtures, were determined from the results of the Oedometer tests, following the procedure suggested by (Knight 1963). Table 3.4 presents a summary of properties of collapsible soil mixtures used in the current study obtained from soil tests, where shear strength parameters were obtained from direct shear tests. Sieve analysis for sand and collapsible soil mixtures used in this study is presented in figure 3.19.

Table 3.4 Collapsible soil properties

Soil Mix	Clay Content (%)	e	w (%)	S (%)	G_s	γ_d (kN/m³)	γ (kN/m³)	c (kPa)	φ (°)	C_P (%)	k_{sat} (cm/sec)
CS-1	14	0.80	5	16.75	2.68	14.6	15.3	18	31	18.0	$1.33*10^{-03}$
CS-2	10	0.70	5	19.05	2.67	15.4	16.2	15.5	35	12.5	$4.83*10^{-03}$
CS-3	8	0.69	5	19.35	2.67	15.5	16.25	12.5	38.5	9.0	$6.50*10^{-03}$
CS-4	6	0.67	5	19.77	2.66	15.6	16.28	9	40	4.2	$8.33*10^{-03}$

where:

e: void ratio G_s : specific gravity

w: water content C_p : collapse potential

S: degree of saturation φ': friction angle

c': cohesion γ_d: dry unit weight

k_{sat} : saturated permeability coeff. γ : moist water content
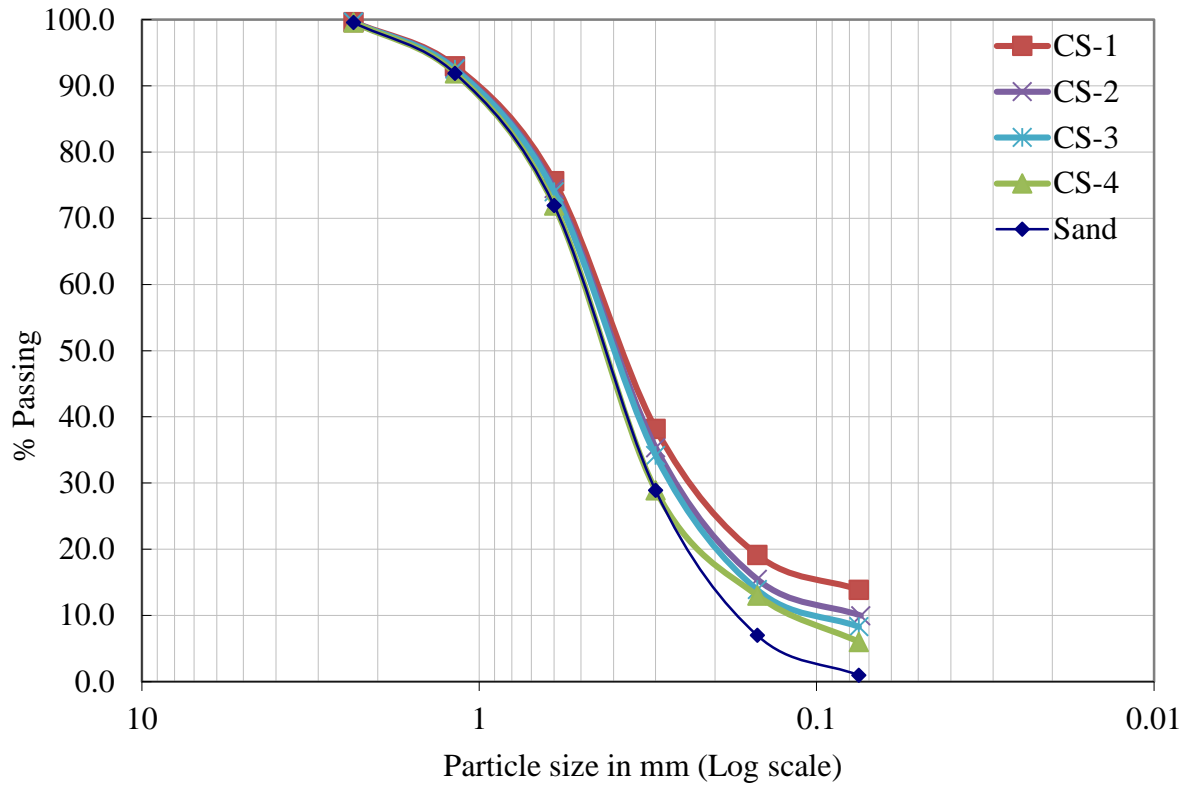
Figure 3.19 Particle size distribution for sand and collapsible soil mixtures

Soil properties obtained from grain size distribution and atterberg limits tests are summarized in Table 3.5. Where C_c is the coefficient of curvature, $C_c=D_{60}/D_{10}$. While C_u is the coefficient of uniformity $C_u= (D_{30})^2/D_{10} D_6$.

Table 3.5 Index properties for collapsible soil mixtures

Soil Mix	D60 (mm)	D30 (mm)	D10 (mm)	Cc	Cu	LL (%)	PL (%)	PI (%)
CS-1	0.45	0.24	0.015	8.53	30	24.70	17.3	7.40
CS-2	0.46	0.25	0.021	6.47	21.9	15.9	13.35	2.55
CS-3	0.47	0.26	0.086	1.65	5.4	---	---	---
CS-4	0.50	0.29	0.132	1.27	4.0	---	---	---

The compaction unit used in the experiments consists of a hammer weighing 12.5 kg, allowed to fall freely from a height of 20 cm to hit an aluminum plate placed on top of the soil. The aluminum plate placed on top of soil has a surface area of $30.5*50$ cm^2 and it contains a hole in the middle to allow the pile to pass through during the compaction as shown in figure 3.20.

(a)   (b)
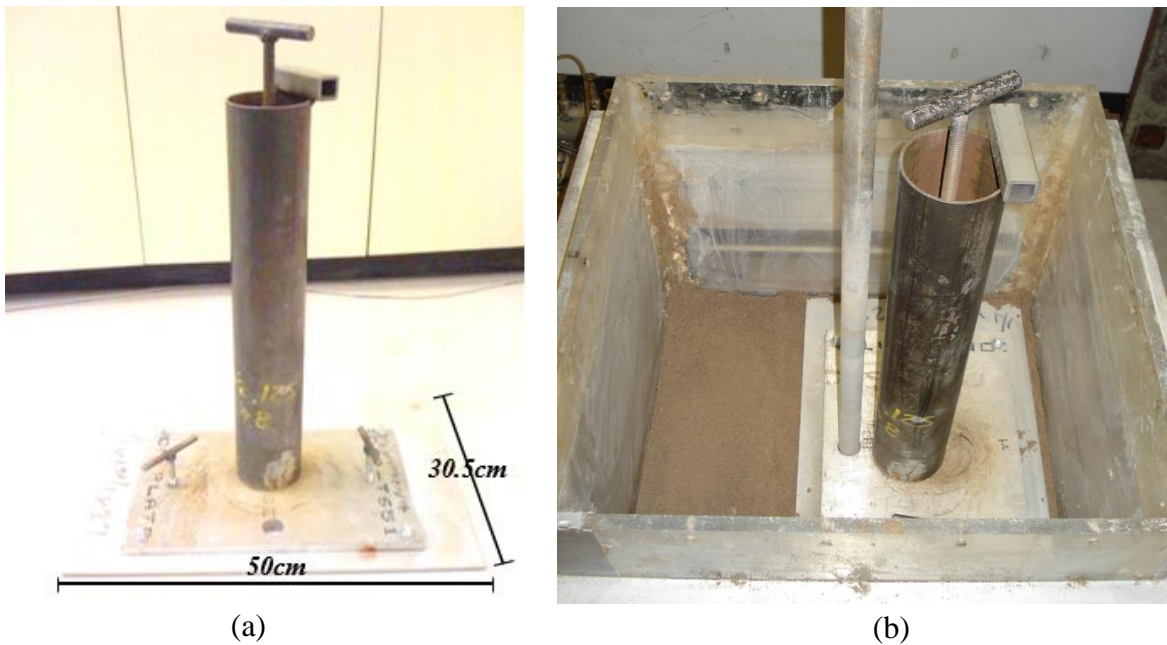
Figure 3.20 Compaction hammer and plate

The compaction energy per unit volume E can be calculated using Equation [3.1] used by (Proctor 1933), as following:

$$E = \frac{N * W * H * L}{V} \quad ... ... \quad [3.1]$$

Where the compaction energy per unit volume (E) values are summarized in Table 3.6, for number of blows $N = 30$ for collapsible soil mixture CS-1 and while for other mixtures $N = 36$ blows, weight of the hammer $W = 12500$ gm, height of drop $H = 20$ cm, number of layers $L = 5$, volume of soil being compacted $V = 50*50*30.5 = 76,250$ cm^3.

Table 3.6 Compaction energy

Soil mixture (%)	C_p (%)	Number of blows (N)	Compaction Energy (E) (gm.cm/cm^3)
CS-1	18	30	491.8
CS-2	12.5	36	590.16
CS-3	9	36	590.16
CS-4	4.2	36	590.16

3.3 Soil-Pile Friction

In order to determine friction angle between soil and steel pile surfaces used in the present study, five tests were carried out, where different sandpaper types were used having different grit numbers. In these experiments the sand papers were glued to the pile shaft, and resulting friction on the sandpaper was compared to that acting on the pile steel surface under similar conditions. In these tests the model pile was attached to a load cell fixed to the bottom of the tank, and soil was placed in sublayers each compacted with a fixed energy. Stress (σ) was applied on the soil surface on increments up to 80 kPa resulting in soil settlement. The relative movement between soil and pile resulted in drag load measured by the load cell at the pile tip. A summary of the parameters used is presented in Table 3.7.

Table 3.7 Summary of experiments for determining soil-pile friction

Test #	Series	Test Series	Pile surface	σ (kPa)
1		PR-GR100	Grit #100	80
2		PR-S	Steel	80
3	Pile Surface Roughness	PR-GR120	Grit #120	80
4		PR-GR140	Grit #140	80
5		PR-GR220	Grit #220	80

The results of these tests are summarized in figure 3.21, where the surcharge applied on soil is plotted versus the measured drag load acting on pile shaft as shown below.
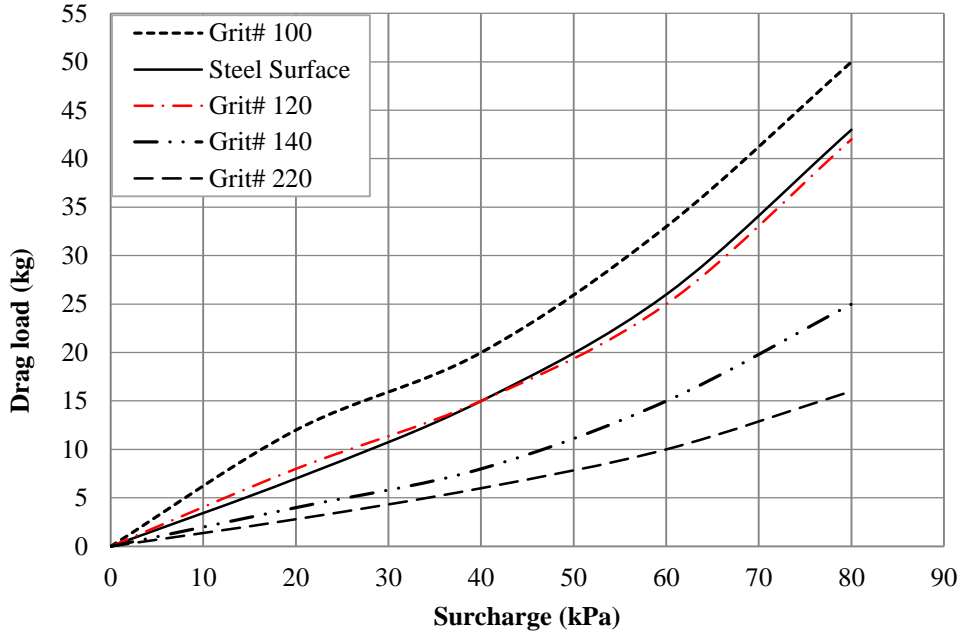
Figure 3.21 Drag load VS surcharge for different sandpaper grit numbers

These test results showed that sandpaper grit number 120 gave nearly the same friction as the pile steel surface, as shown in figure 3.21.

A series of direct shear tests were carried out to determine the friction angle between the sand and sandpaper grit # 120 to determine the angle of friction between soil particles and pile surface (δ) and thus we can determine the (δ/ϕ) ratio for different soil mixtures used in the experimental investigation. The angle of friction between soil particles and other materials (δ) could be determined from the direct shear test using the following equation:

$$\delta = \tan^{-1}\left(\frac{\tau}{\sigma'_v}\right)\dots\dots[3.2]$$

Where, σ'_v and τ are the effective vertical stress and shear stress, respectively.

From the direct shear tests the ratio between the angle of internal friction of soil and soil-pile friction (δ / ϕ) was found equal to 0.7.

3.4 Testing Procedure

The testing procedure is established in a unique and precise sequence in order to simulate a single end-bearing pile embedded in a collapsible soil layer subjected to over burden pressure, where at a certain pressure level (inundation pressure) inundation with water was introduced. The inundation of collapsible soil layer causes a substantial and a rapid settlement, and this settlement applies additional stresses on pile (NSF) that were measured for different cases. In order to simulate the situation described previously, the following testing procedure was established.

Before placing soil in the tank, pile is connected to the load cell attached to the bottom of the tank to simulate an end-bearing pile, as the tank has a rigid bottom to restrict pile movement. After soil mixture has been prepared, soil was spread uniformly in the tank on five overlying layers, where soil is being spread then compacted for each layer as described in the previous section. The compaction energy was maintained throughout the experiments to obtain the desired properties for collapsible soil mixtures. Figure 3.22 shows the compaction process performed in the soil tank on a sub-layer.

Figure 3.22 Compaction in soil tank

After soil has been placed and compacted in the testing tank, the loading plate was placed on the top of soil, allowing the pile to pass through the hole in the steel plate, so that the stress is only applied on the soil. Four LVDTs were be placed on the top of the loading plate to record the soil settlement throughout the test, preliminary tests show that the pile dead weight was enough to ensure full contact between the pile and the load cell during the test.

The loading plate placed on the top of the soil, and the loading system used to apply stress on the soil, has built-in stress gauges, to allow applying the desired stresses on increments, providing a stress-controlled loading scheme. The load was applied on the soil incrementally, until the desired inundation pressure was reached. Inundation pressure was kept constant, and water flow was introduced.

The surcharge acting on soil, soil settlement and the load at the bottom of the pile were monitored throughout the test, using the stress gauges, LVDTs and load cell respectively.

Two different procedures were used for inundation: inundation from bottom simulating full saturation due to rise of groundwater table, and inundation from top, simulating partial saturation (staged inundation) due to rainfall and surface leakage.

3.5.1 Inundation from Bottom

Inundation from bottom was carried out in order to take into consideration the effect of collapse potential, inundation pressure and rate of inundation on drag loads.

In these tests, a coarse, silica sand layer was placed at the bottom of the tank, forming a 2.5 cm thick filter layer that provided a uniform distribution of water to simulate inundation from bottom due to rise in groundwater level. Elevated water tank was used as explained in the previous sections, and water was introduced to the soil via eight openings in the tank bottom as shown in figure 3.23. During the tests, when the desired inundation pressure was reached. Inundation pressure was kept constant, and water flow was introduced from bottom upwards, until soil is being fully inundated with water. In these tests, three different inundation rates were applied such that inundation took place over 30, 60 and 90 minutes till full inundation was reached, where the inundation rate was controlled by adjusting the valve opening.

In preliminary tests, water pipes (piezometers) were connected to the tank to monitor the water level in the soil throughout inundation and the full saturation was confirmed by visual inspection and by obtaining the maximum soil settlement.
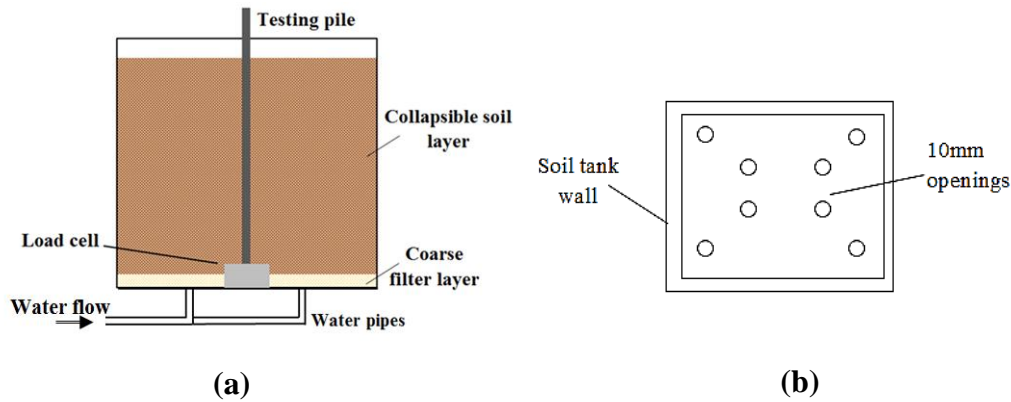
Figure 3.23 (a) Soil layers schematic view (b) Soil tank bottom schematic plan view

3.5.2 Inundation from Top

Tests simulating inundation with water from upwards due to rain and pipe leakage were carried out to take into consideration the effect of partial saturation. At the inundation pressure, water was purred from upwards on four equal increments (inundation stages). After soil was placed in a procedure similar to that described in the previous sections, silica sand layer was placed on top to ensure even water flow. Load was applied on increments till the inundation pressure was reached, at which water was introduced from top. Water penetrated the soil through gaps between the loading steel plate at the four sides of the tank (2 mm gaps) and also through four 10 mm holes in the steel plate placed on the top of the soil, as shown in figure 3.24. The inundation pressure was maintained for all inundation stages, such that for each stage enough time was allowed to reach the maximum settlement and drag load. Where the amount of water needed in each increment was calculated based on total soil volume and void ratio of soil, such that the average percentage of inundation (degree of wetting (D_W)) increases by 25% for each increment.

Each inundation stage represents a separate test, such that the average degree of wetting reaches: 25% for the first increment, 50%, for the second, 75% for the third and 100% (full saturation) for the fourth stage.
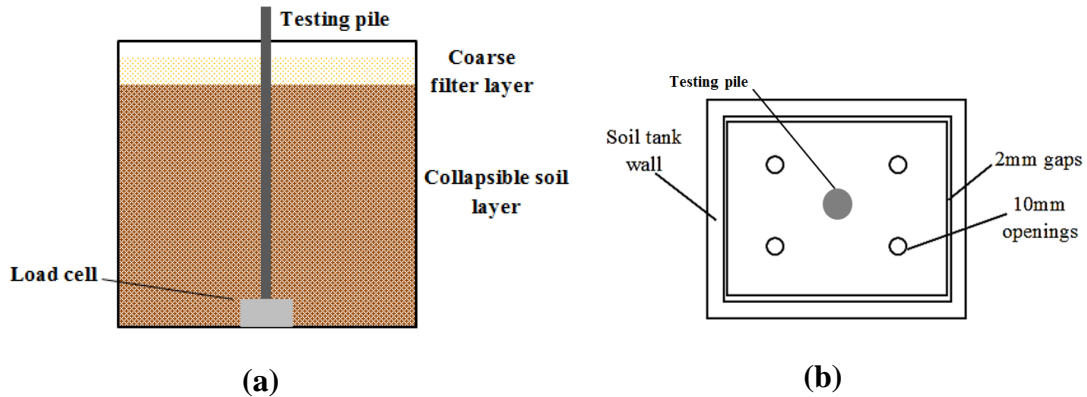
Figure 3.24 (a) Soil layers schematic view (b) Soil tank top, schematic plan view

3.5 Experimental Program

Series of tests were carried out, to study the effect of the governing parameters to include: rate of inundation, collapse potential of soil, wetting scheme and inundation pressure. A summary of experimental testing program is shown in Table 3.8, providing type of collapsible soil mixture, inundation pressure applied on soil and time needed for soil inundation with water. Where soil and pile properties are explained in details in section 3.2.3.

It is shown in Tables 3.8 and 3.9 that there are two main categories of tests, full inundation and partial inundation. For each test a legend has been given to define the soil, loading and inundation condition, such that for test 1 through test 45, the first letter indicates the direction of inundation, for inundation from bottom tests are given the letter B while for inundation from top tests are given the letter T.

The second part indicates the type of soil (CS1, CS2, CS3 and CS4), while for the third part indicates the surcharge stress applied on soil (S40, S80 or S120), and the fourth part indicates inundation time (T30, T60 and T90). For partial inundation tests where inundation took place from top, the last part indicates percentage of inundation achieved in the test (P25, P50, P75 and P100).

Table 3.8 Experimental program part A

Test #	Series	Test Series	C_p (%)	σ (kPa)	Inundation (%)	Inundation time (min)
1		B-CS1-S40-T30	18	40	100	30
2		B-CS1-S80-T30	18	80	100	30
3		B-CS1-S120-T30	18	120	100	30
4		B-CS2-S120-T30	12.5	120	100	30
5		B-CS3-S40-T30	9	40	100	30
6		B-CS3-S120-T30	9	120	100	30
7		B-CS4-S40-T30	4.2	40	100	30
8		B-CS4-S120-T30	4.2	120	100	30
9		B-CS1-S40-T60	18	40	100	60
10		B-CS1-S80-T60	18	80	100	60
11	**Full Inundation**	B-CS1-S120-T60	18	120	100	60
12		B-CS2-S40-T60	12.5	40	100	60
13		B-CS2-S80-T60	12.5	80	100	60
14		B-CS2-S120-T60	12.5	120	100	60
15		B-CS3-S40-T60	9	40	100	60
16		B-CS3-S80-T60	9	80	100	60
17		B-CS3-S120-T60	9	120	100	60
18		B-CS4-S40-T60	4.2	40	100	60
19		B-CS4-S80-T60	4.2	80	100	60
20		B-CS4-S120-T60	4.2	120	100	60
21		B-CS2-S80-T90	12.5	80	100	90

Table 3.9 Experimental program part B

Test #	Series	Test Series	C_p (%)	σ (kPa)	Inundation (%)	Inundation time (min)
22		T-CS1-S80-P25	18	80	25	20
23		T-CS1-S80-P50	18	80	50	20
24		T-CS1-S80-P75	18	80	75	20
25		T-CS1-S80-P100	18	80	100	20
26		T-CS2-S40-P25	12.5	40	25	20
27		T-CS2-S40-P50	12.5	40	50	20
28		T-CS2-S40-P75	12.5	40	75	20
29		T-CS2-S40-P100	12.5	40	100	20
30		T-CS2-S80-P25	12.5	80	25	20
31		T-CS2-S80-P50	12.5	80	50	20
32		T-CS2-S80-P75	12.5	80	75	20
33	**Partial Inundation**	T-CS2-S80-P100	12.5	80	100	20
34		T-CS2-S120-P25	12.5	120	25	20
35		T-CS2-S120-P50	12.5	120	50	20
36		T-CS2-S120-P75	12.5	120	75	20
37		T-CS2-S120-P100	12.5	120	100	20
38		T-CS3-S80-P25	9	80	25	20
39		T-CS3-S80-P50	9	80	50	20
40		T-CS3-S80-P75	9	80	75	20
41		T-CS3-S80-P100	9	80	100	20
42		T-CS4-S80-P25	4.2	80	25	20
43		T-CS4-S80-P50	4.2	80	50	20
44		T-CS4-S80-P75	4.2	80	75	20
45		T-CS4-S80-P100	4.2	80	100	20

CHAPTER 4

EXPERIMENTAL RESULTS

4.1General

In this chapter, results obtained from the present experimental investigation are presented in figures, followed by analysis and discussion of these results. For each test, the pressure acting on the soil surface, soil settlement and load acting on the tip of the pile were measured throughout. Each test is being presented by a single figure. For tests 1 through 45, the figures demonstrate the change in surcharge applied on soil, soil settlement and negative skin friction measured at the tip of the pile. For tests 46 through 50, the results are presented in a single figure demonstrating the change in the measured negative drag load with respect to the surcharge load applied on soil for different pile surfaces.

4.2 Full Inundation Tests Results

In order to study the development of drag forces due to the rise of the groundwater table, tests 1 through 21 were carried out, where water was introduced to the testing tank from bottom upwards. In order to examine the effect of collapse potential, tests were carried out on four collapsible soil mixtures, having collapse potential values 4.2, 9, 12.5 and 18%. While in order to examine the effect of inundation surcharge, tests were carried out at inundation pressures of 40, 80 and 120kPa. The inundation process took place in about 30 minutes for eight tests, 60 minutes for twelve tests and 90 minutes for one test.

Figures 4.1 to 4.21 present test results in the form of time versus: surcharge pressure applied on soil surface (kPa), measured soil settlement (mm) and measured drag load acting on pile (kg).
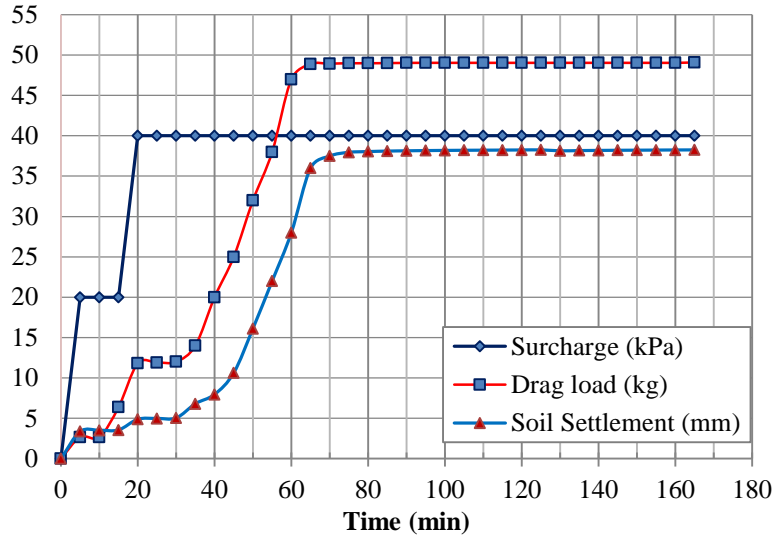
Figure 4.1 Test 1 (B-CS1-S40-T30) Surcharge, settlement and drag load VS time for C_p=18%, inundation time (30 min)
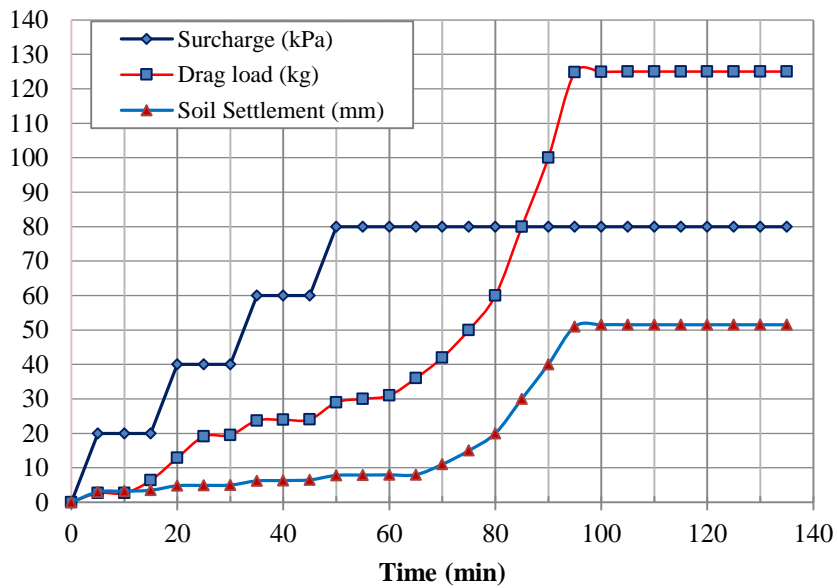
Figure 4.2 Test 2 (B-CS1-S80-T30) Surcharge, settlement and drag load VS time for C_p = 18%, inundation time (30 min)
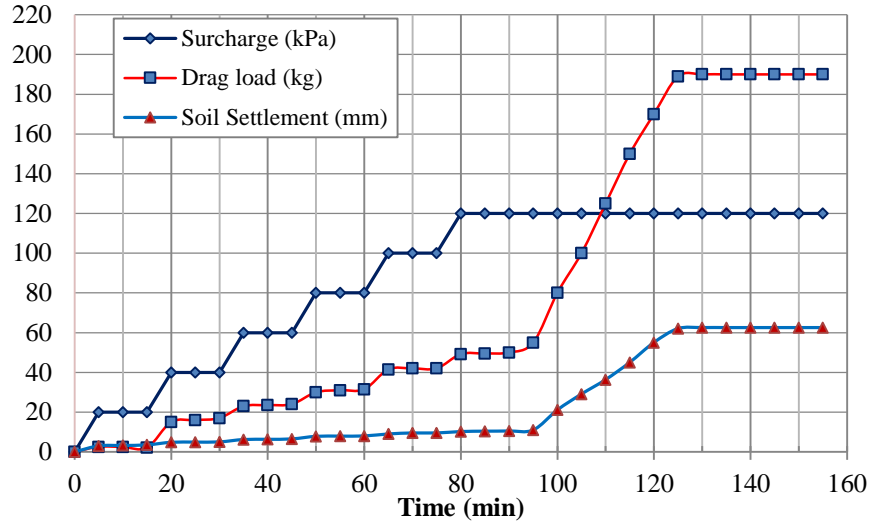
Figure 4.3 Test 3 (B-CS1-S120-T30) Surcharge, settlement and **drag load** VS time for C_p

=18%, inundation time (30 min)
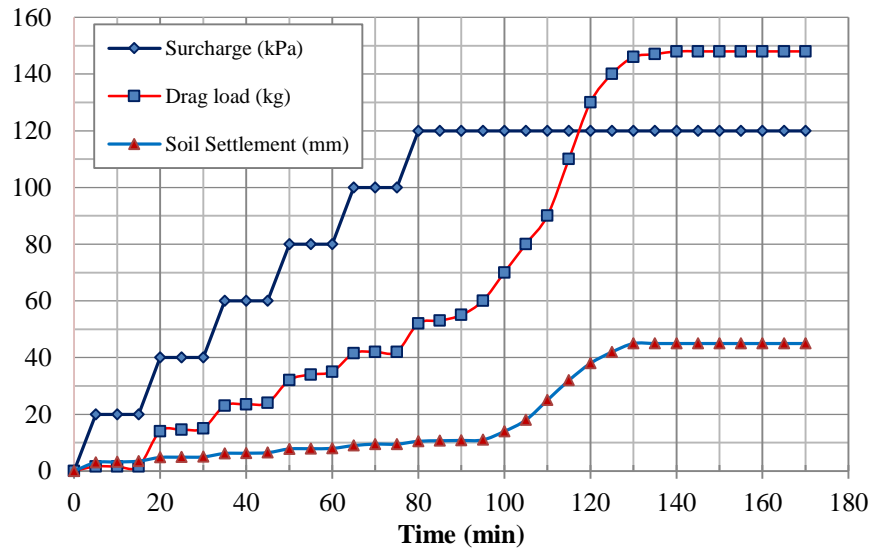
Figure 4.4 Test 4 (B-CS2-S120-T30) Surcharge, settlement and drag load **VS** time for $C_p =$ 12.5%, inundation time (30 min)
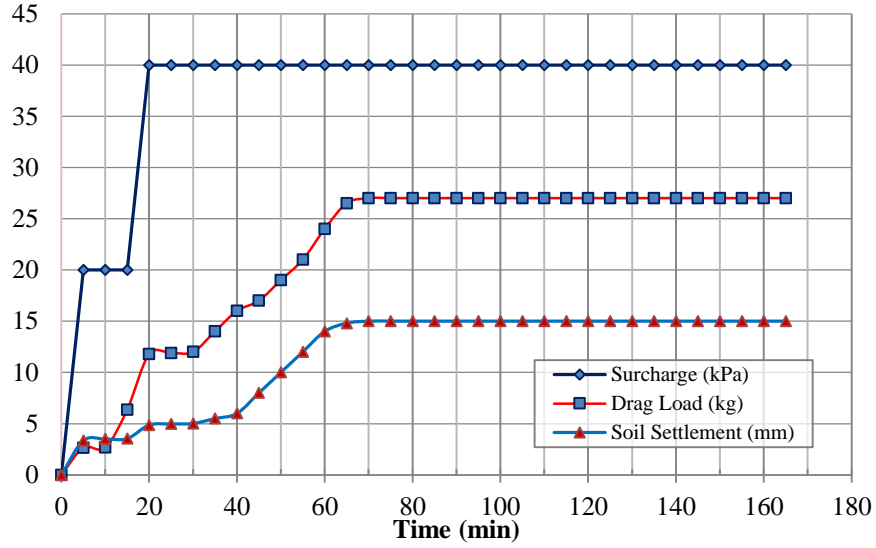
Figure 4.5 Test 5 (B-CS3-S40-T30) Surcharge, settlement and drag load **VS** time for $C_p = 9\%$, inundation time (30 min)
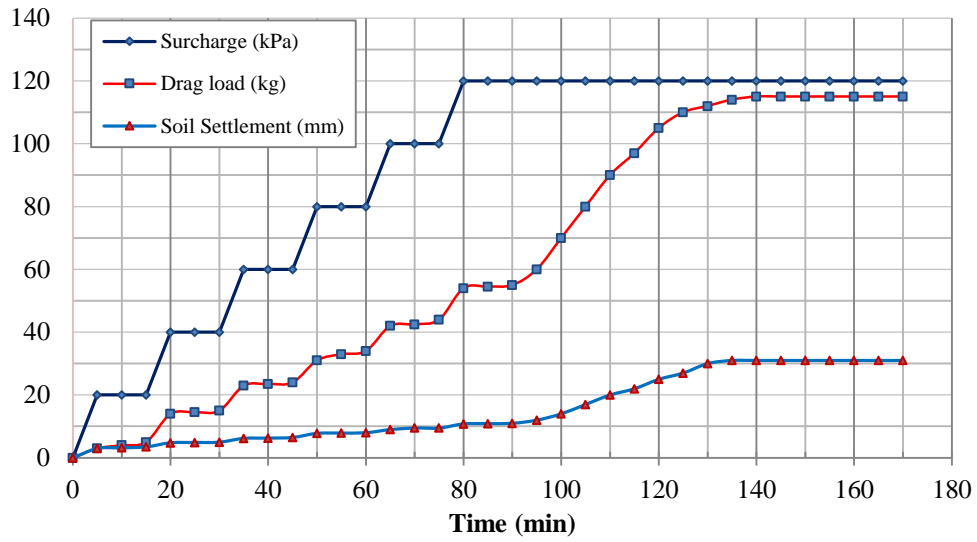
Figure 4.6 Test 6 (B-CS3-S120-T30) Surcharge, settlement and drag load **VS** time for $C_p = 9\%$, inundation time (30 min)
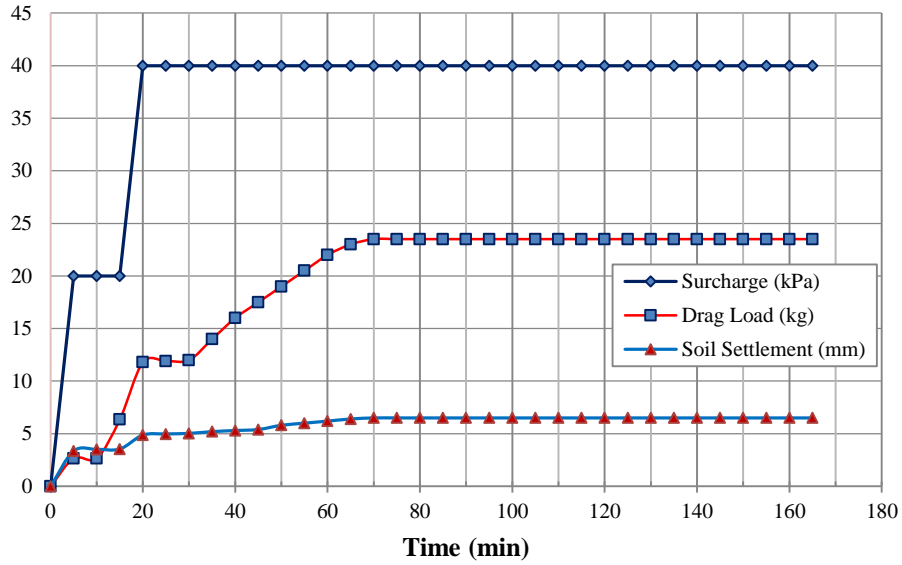
Figure 4.7 Test 7 (B-CS4-S40-T30) Surcharge, settlement and drag load **VS** time for $C_p =$ 4.2%, inundation time (30 min)
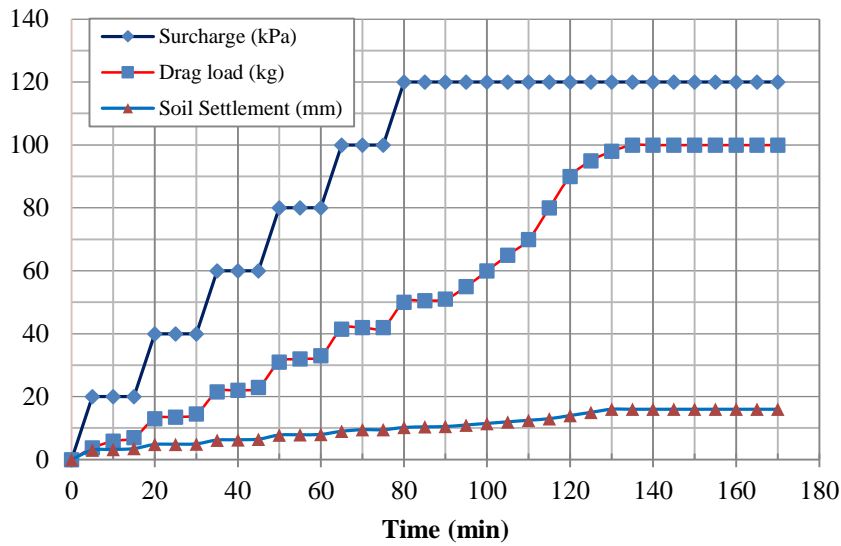
Figure 4.8 Test 8 (B-CS4-S120-T30) Surcharge, settlement and drag load **VS** time for C_p =4.2%, inundation time (30 min)
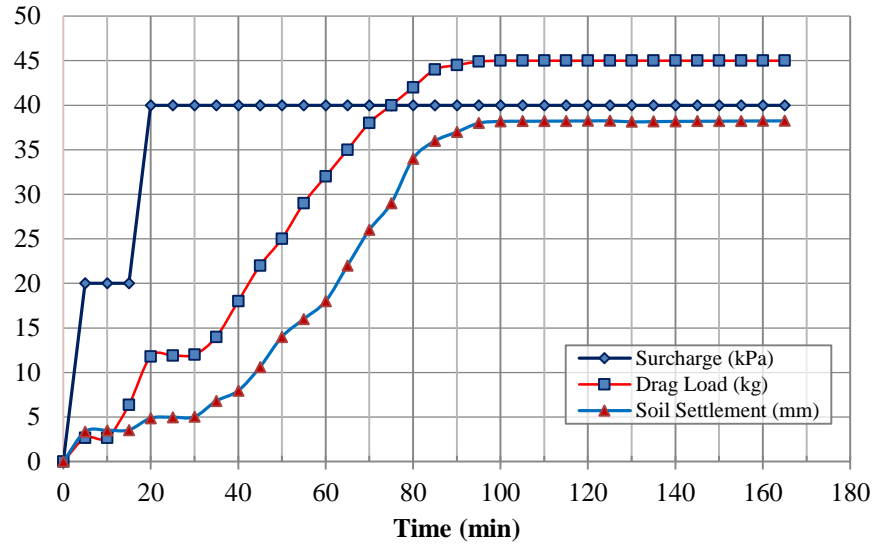
Figure 4.9 Test 9 (B-CS1-S40-T60) Surcharge, settlement and drag load **VS** time for C_p = 18%, inundation time (60 min)
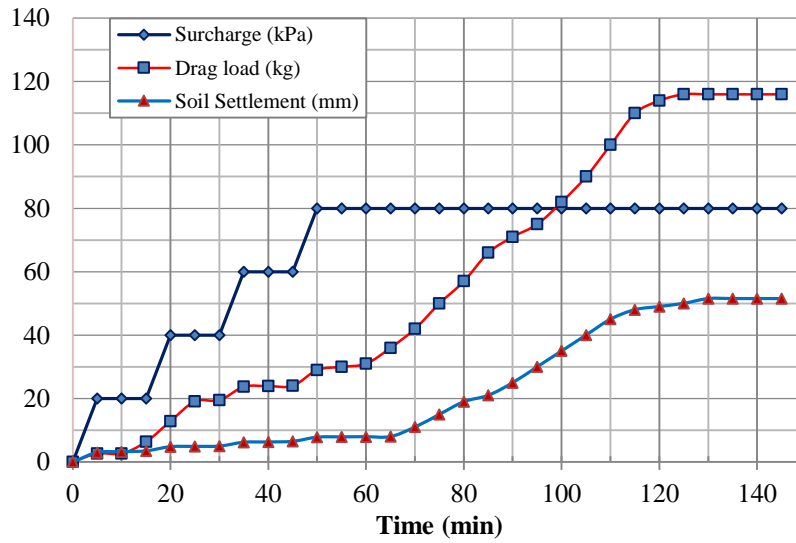
Figure 4.10 Test 10 (B-CS1-S80-T60) Surcharge, settlement and drag load **VS** time for C_p =18%, inundation time (60 min)
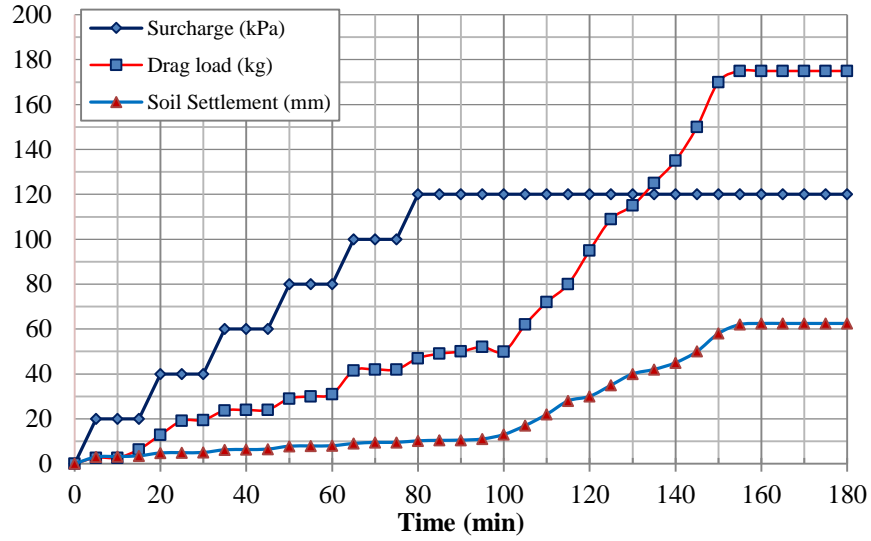
Figure 4.11 Test 11 (B-CS1-S120-T60) Surcharge, settlement and drag load **VS** time for C_p =18%, inundation time (60 min)
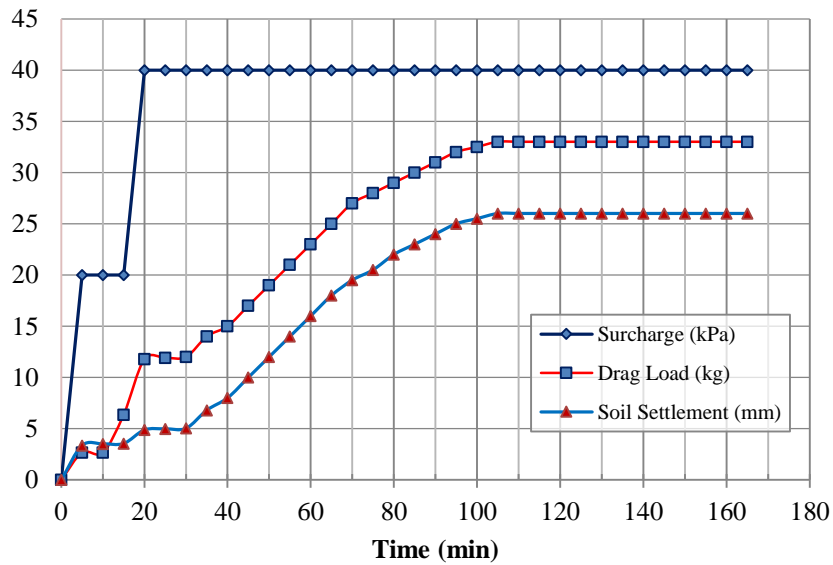
Figure 4.12 Test 12 (B-CS2-S40-T60) Surcharge, settlement and drag load **VS** time for C_p =12.5%, inundation time (60 min)
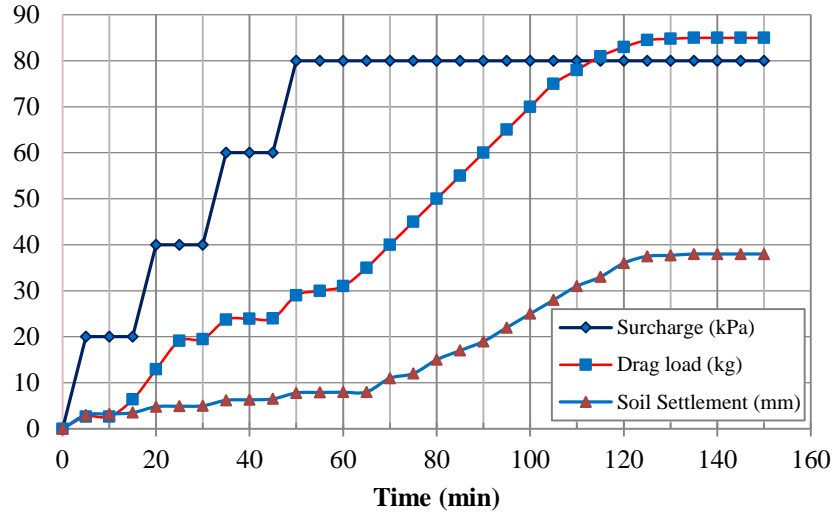
Figure 4.13 Test 13 (B-CS2-S80-T60) Surcharge, settlement and drag load VS time for C_p =12%, inundation time (60 min)
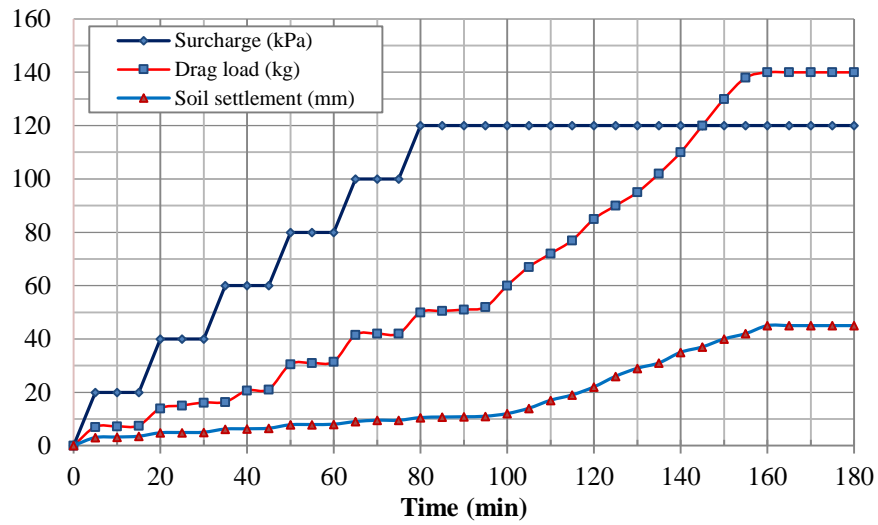
Figure 4.14 Test 14 (B-CS2-S80-T60) Surcharge, settlement and drag load VS time for C_p = 12%, inundation time (60 min)
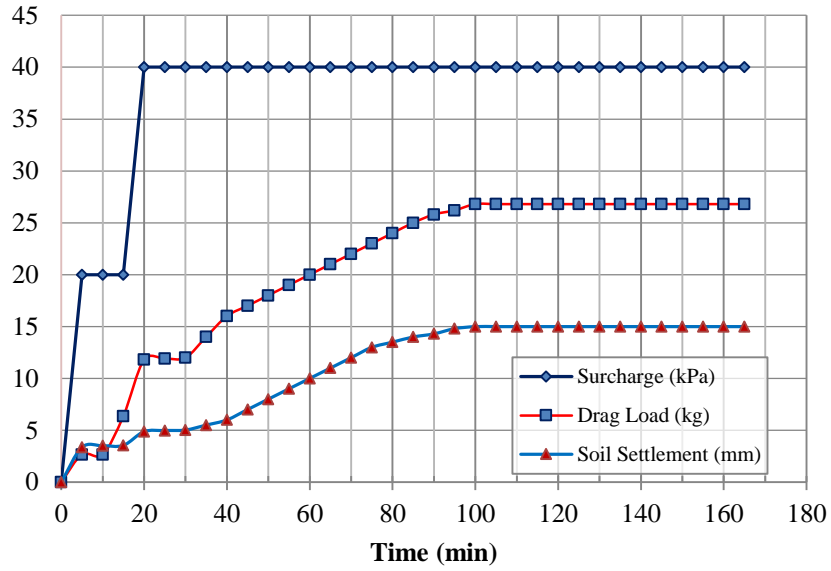
Figure 4.15 Test 15 (B-CS3-S40-T60) Surcharge, settlement and drag load **VS** time for $C_p =$ 9%, inundation time (60 min)
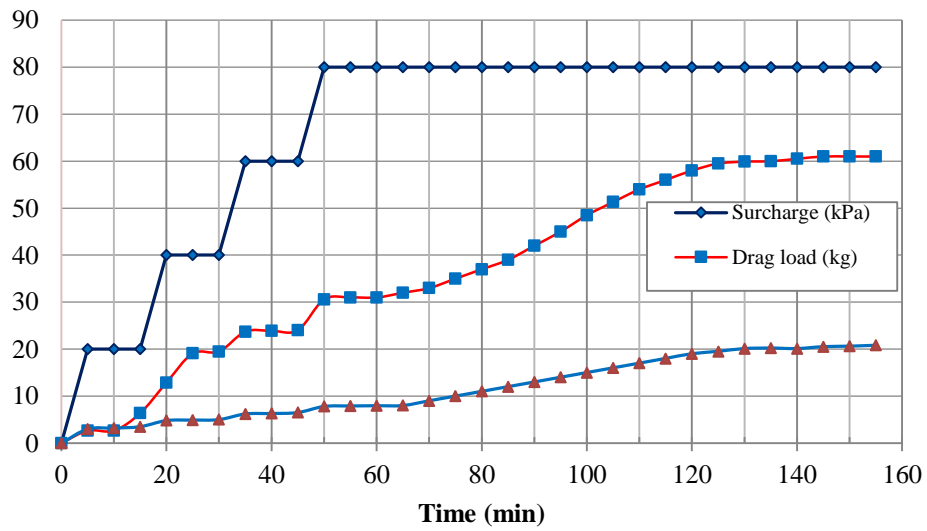
Figure 4.16 Test 16 (B-CS3-S80-T60) Surcharge, settlement and drag load **VS** time for $C_p =$ 9%, inundation time (60 min)
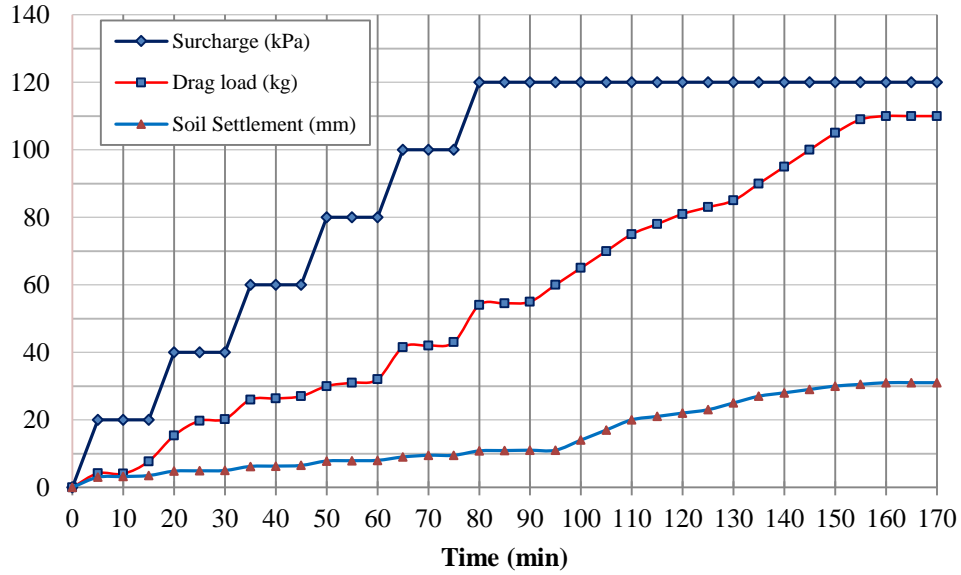
Figure 4.17 Test 17 (B-CS3-S120-T60) Surcharge, settlement and drag load **VS** time for $C_p =$ 9%, inundation time (60 min)
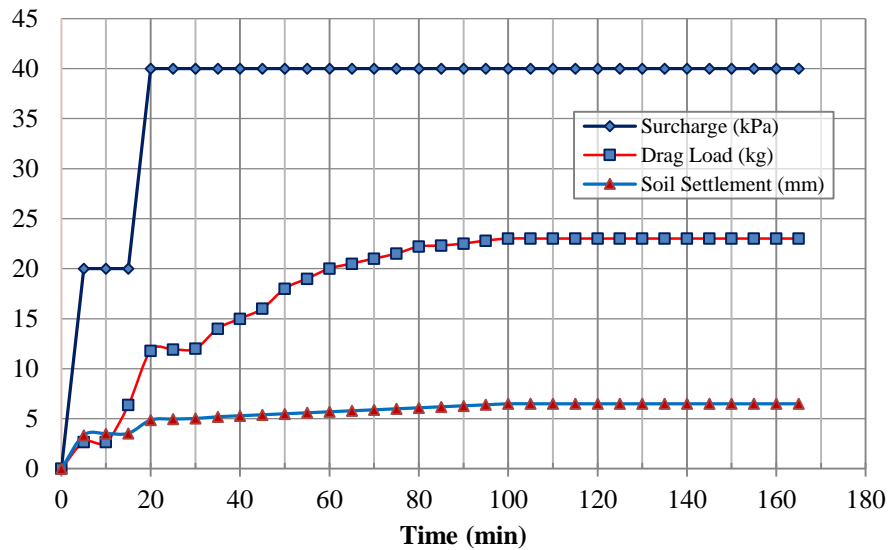
Figure 4.18 Test 18 (B-CS4-S40-T60) Surcharge, settlement and drag load **VS** time for C_p =4.2%, inundation time (60 min)
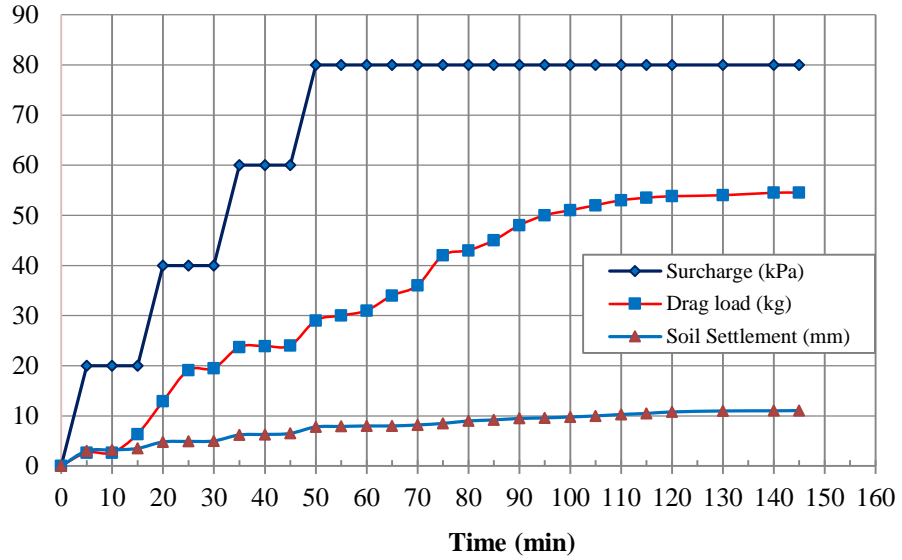
Figure 4.19 Test 19 (B-CS4-S80-T60) Surcharge, settlement and drag load **VS** time for C_p =4.2%, inundation time (60 min)
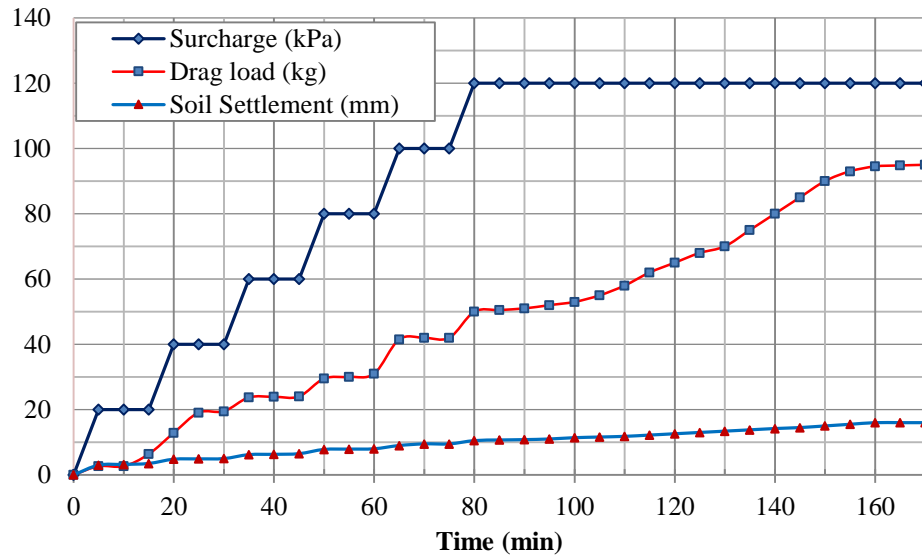
Figure 4.20 Test 20 (B-CS4-S120-T60) Surcharge, settlement and drag load VS time for C_p = 4.2%, inundation time (60 min)
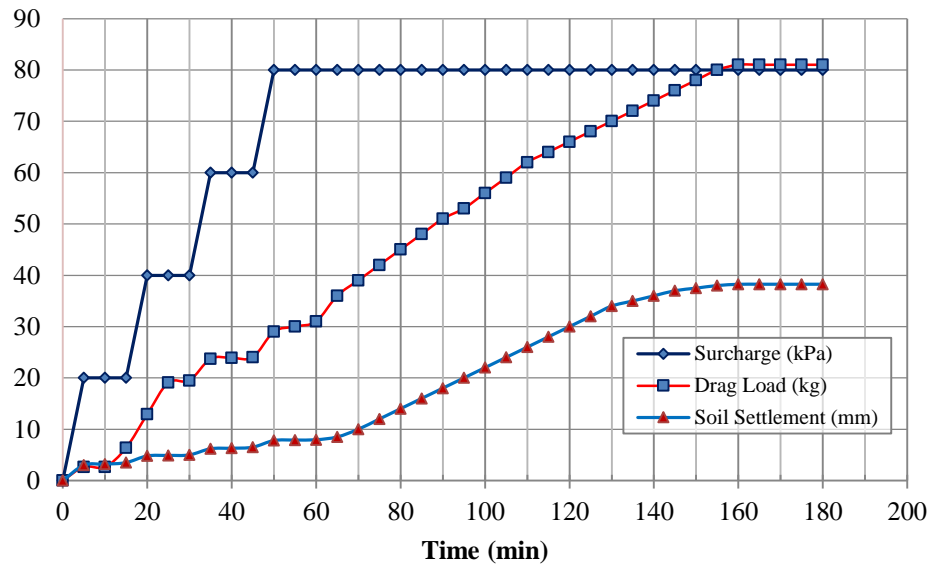
Figure 4.21 Test 21 (B-CS2-S80-T90) Surcharge, settlement and drag load **VS** time for $C_p = 12.5\%$, inundation time (90 min)

The variation of drag load with respect to inundation pressure and soil settlement for different collapsible soil mixtures (CS1, CS2, CS3 and CS4) subjected to inundation from bottom were presented in Figures 4.1 through 4.21. It can be noticed from these figures that the measured soil settlement and associated drag forces increased significantly upon inundation with water, where inundation took place over different inundation rates. These test results have shown that the drag load is directly proportional to collapse potential, inundation pressure and rate of inundation. The effect of collapse potential on NSF was more significant for highly collapsible soil mixtures CS1 and CS2. The increase in drag force with respect to inundation pressure was significant only up to 80 kPa, where at 120 kPa it becomes less significant, for different soil mixtures. The effect of inundation rate was pronounced only for higher rate approaching critical flow conditions, where this effect was almost negligible for lower inundation rates.

4.3 Partial Inundation Test Results

In order to examine the development of skin friction at different stages of inundation, tests 22 through 25 were carried out, where soil was inundated from top at different degrees of inundation (25, 50, 75, and 100 %). Test results are presented in the form of time versus measured drag load (kg) and soil settlement (mm) on the vertical axis. Time plotted on the horizontal axis is the time needed for adding water to reach the desired degree of saturation for each test, (i.e from 25 to 50%, from 50 to 75% and from 75 to 100%)
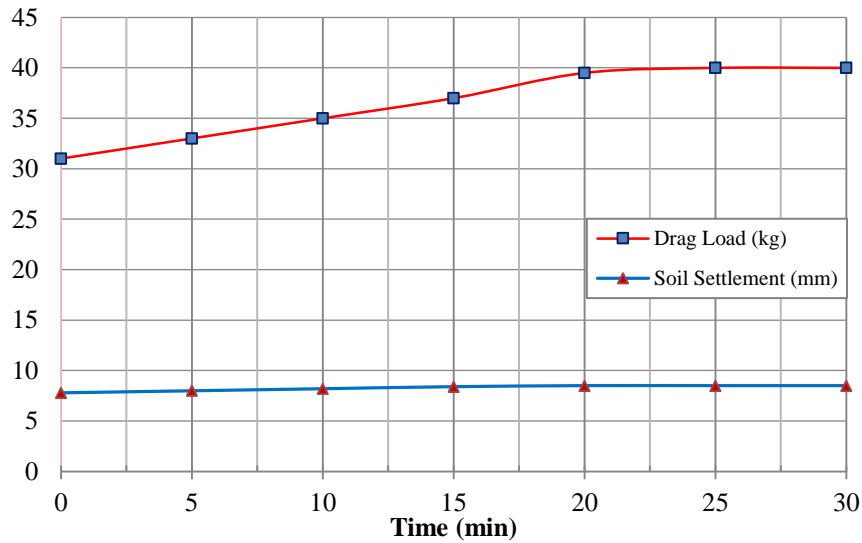
Figure 4.22 Test 15. Soil settlement and drag load **VS** time for C_p = 4.2%, σ = 80kPa, for partial inundation (0-25) %

Figure 4.23 Test 16 Soil settlement and drag load **VS** time for C_p = 4.2%, σ =80kPa, for partial inundation (25-50) %

Figure 4.24 Test 17 Soil settlement and drag load **VS** time for C_p = 4.2%, σ = 80kPa, for partial inundation (50-75) %

Figure 4.25 Test 18 Soil settlement and drag load **VS** time for $C_p = 4.2\%$, $\sigma = 80$kPa, for partial inundation (75-100) %
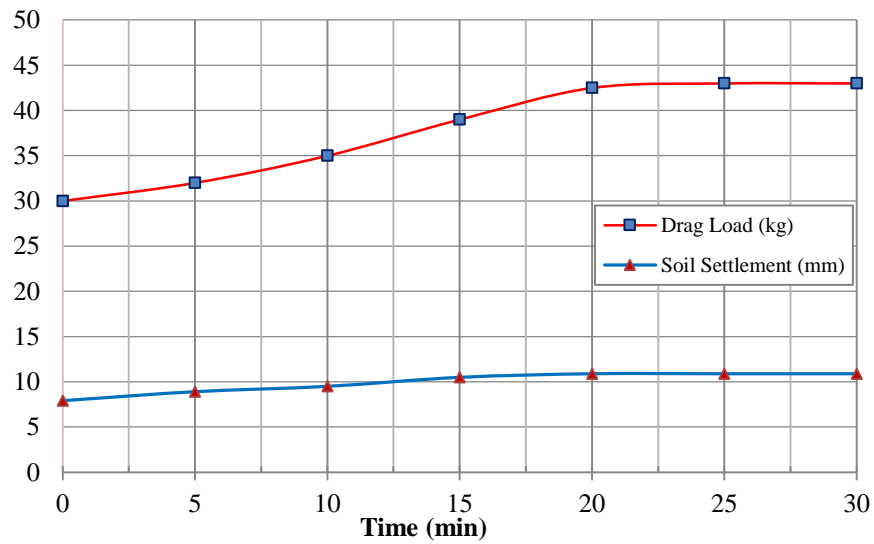
Figure 4.26 Test 19 Soil settlement and drag load **VS** time for $C_p = 9\%$, $\sigma = 80$kPa, for partial inundation (0-25) %
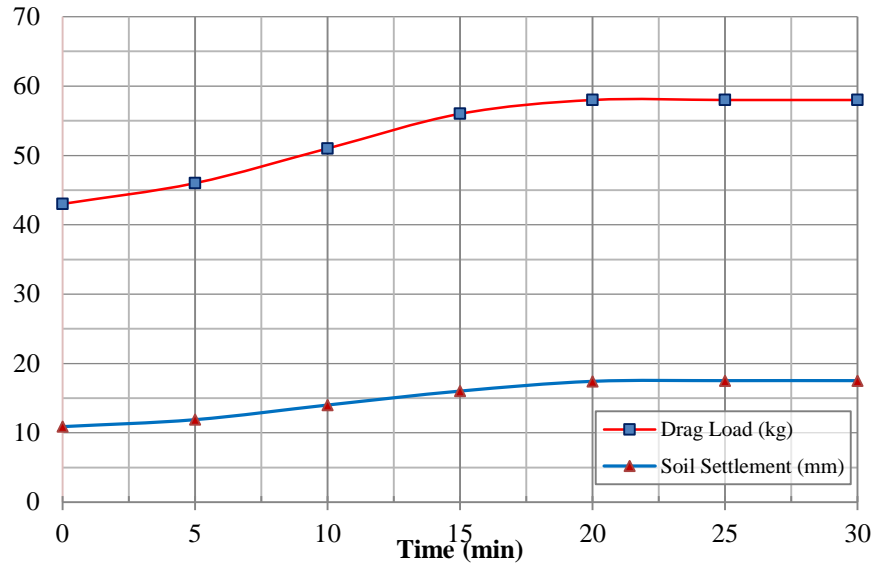
Figure 4.27 Test 20 Soil settlement and drag load **VS** time for $C_p = 9\%$, $\sigma = 80$kPa, for partial inundation (25-50) %
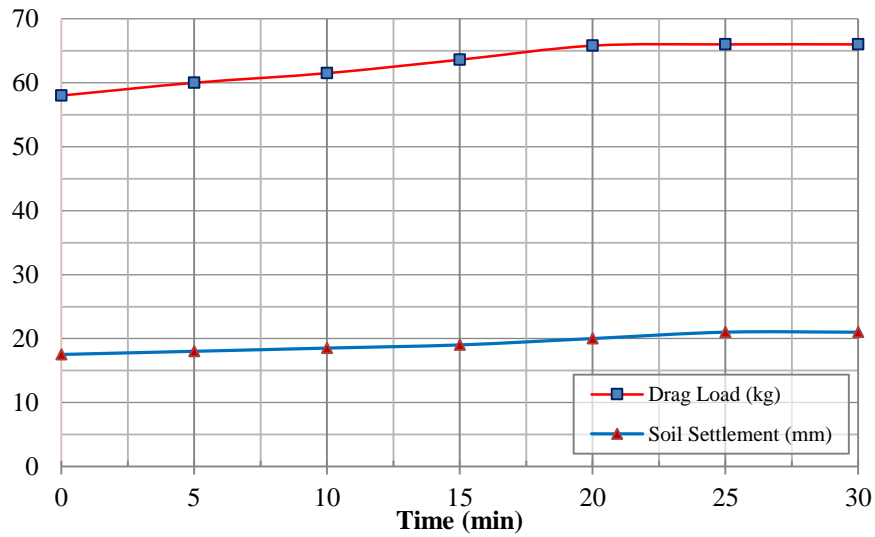
Figure 4.28 Test 21 Soil settlement and drag load **VS** time for $C_p = 9\%$, $\sigma = 80$kPa, for partial inundation (50-75) %
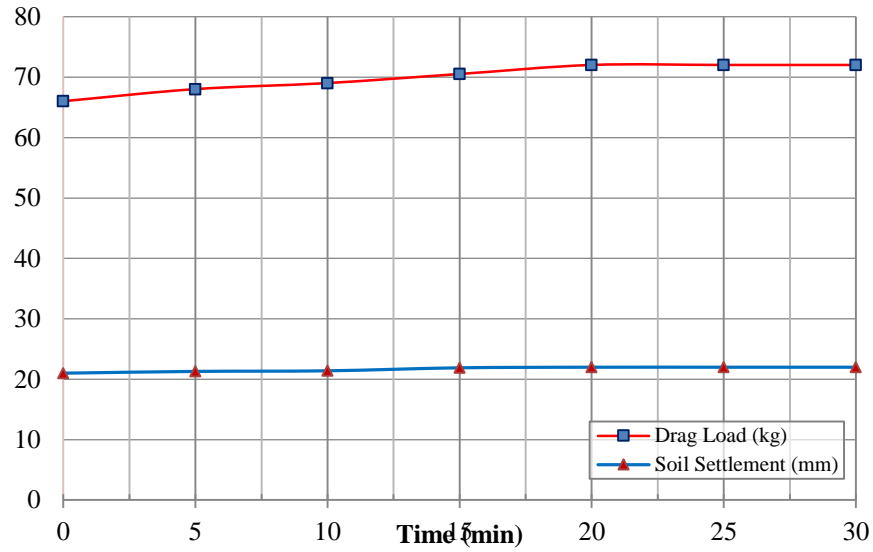
Figure 4.29 Test 22 Soil settlement and drag load **VS** time for $C_p = 9\%$, $\sigma = 80\text{kPa}$, for partial inundation (75-100) %
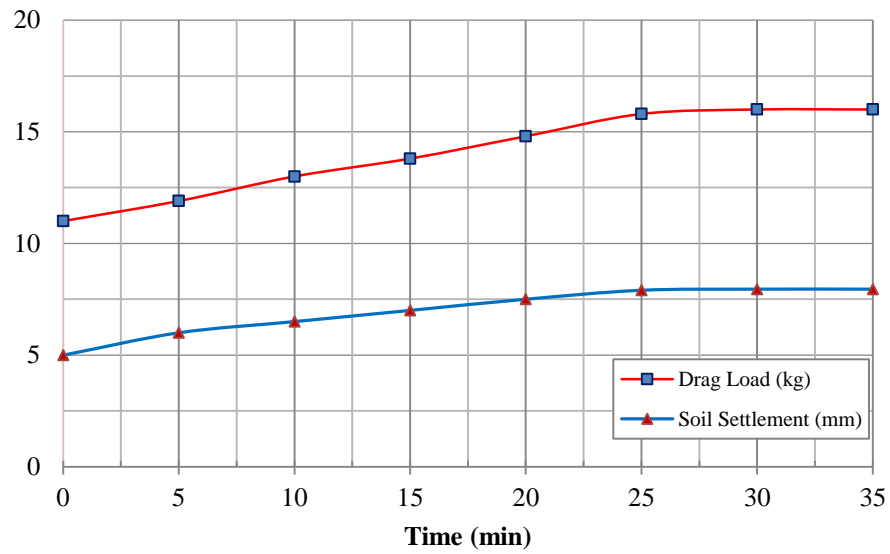
Figure 4.30 Test 23 Soil settlement and drag load **VS** time for $C_p = 12.5\%$, $\sigma = 40\text{kPa}$, for partial inundation (0-25) %
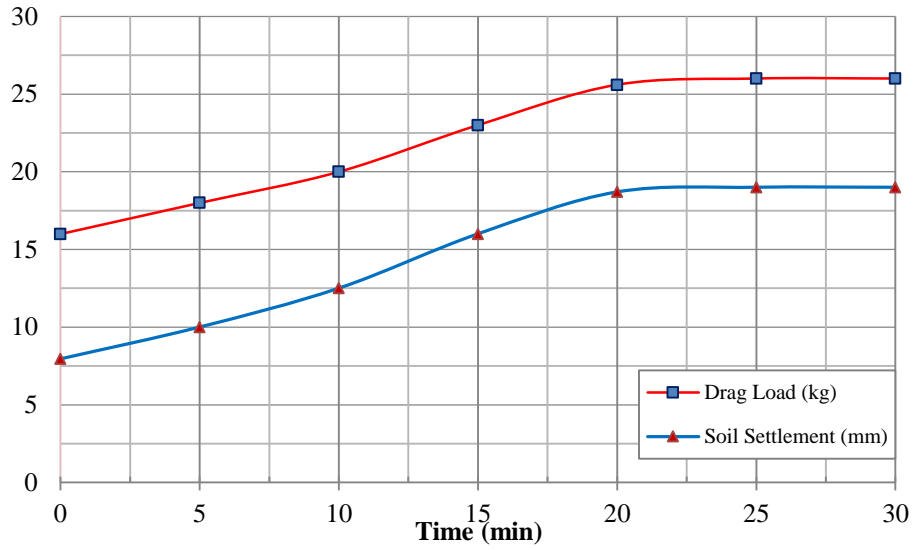
Figure 4.31 Test 24 Soil settlement and drag load **VS** time for $C_p = 12.5\%$, $\sigma = 40\text{kPa}$, for partial inundation (25-50) %
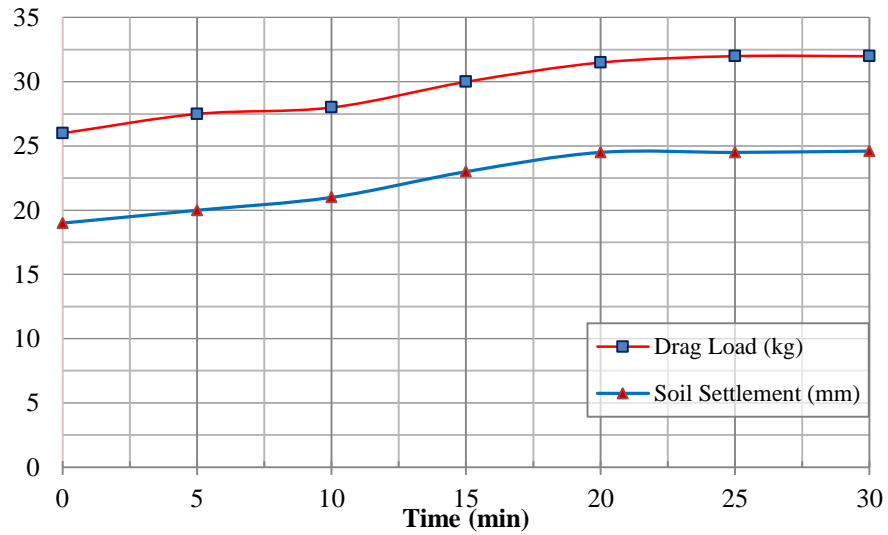
Figure 4.32 Test 25 Soil settlement and drag load **VS** time for $C_p = 12.5\%$, $\sigma = 40\text{kPa}$, for partial inundation (50-75) %
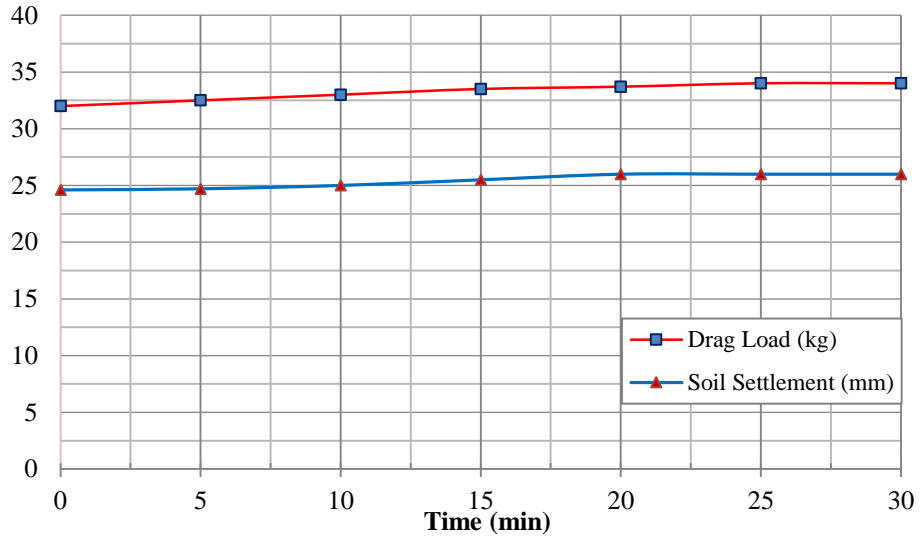
Figure 4.33 Test 26 Soil settlement and drag load **VS** time for $C_p = 12.5\%$, $\sigma = 40$kPa, for partial inundation (75-100) %
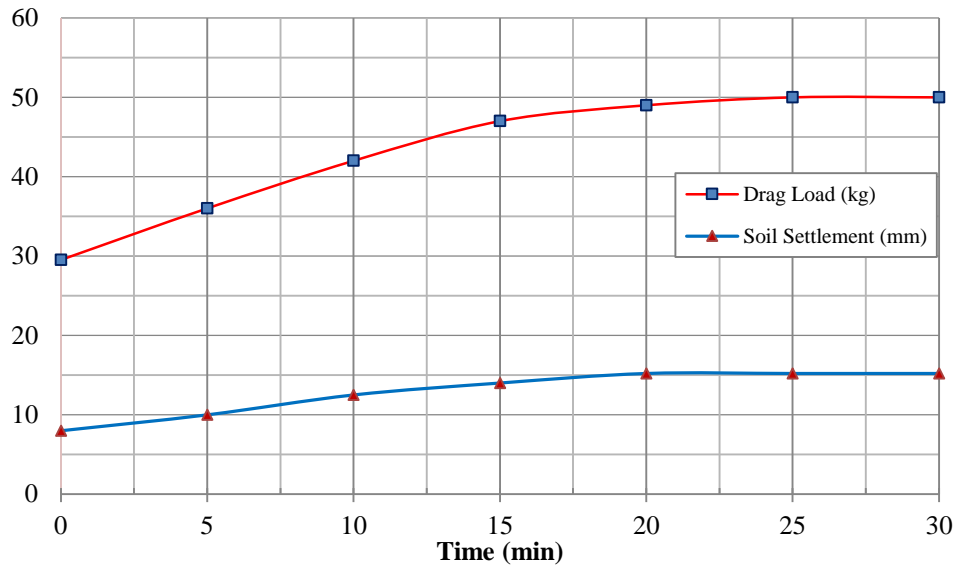
Figure 4.34 Test 27 Soil settlement and drag load **VS** time for $C_p = 12.5\%$, $\sigma = 80$kPa, for partial inundation (0-25) %
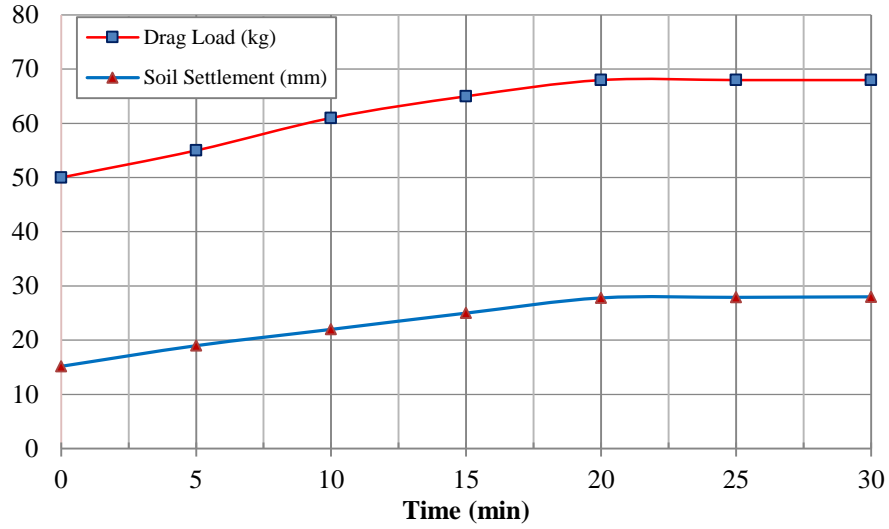
Figure 4.35 Test 28 Soil settlement and drag load **VS** time for $C_p = 12.5\%$, $\sigma = 80$kPa, for partial inundation (25-50) %
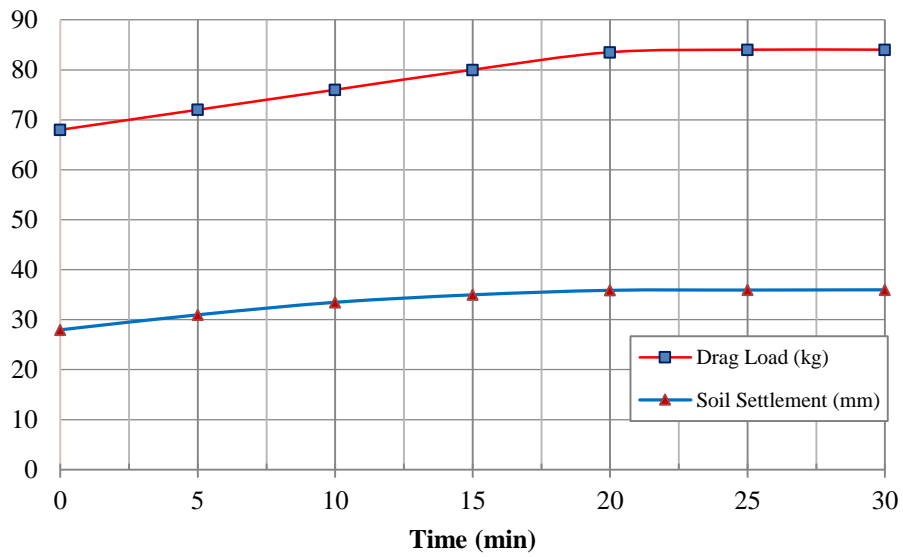
Figure 4.36 Test 29 Soil settlement and drag load **VS** time for $C_p = 12.5\%$, $\sigma = 80$kPa, for partial inundation (50-75) %
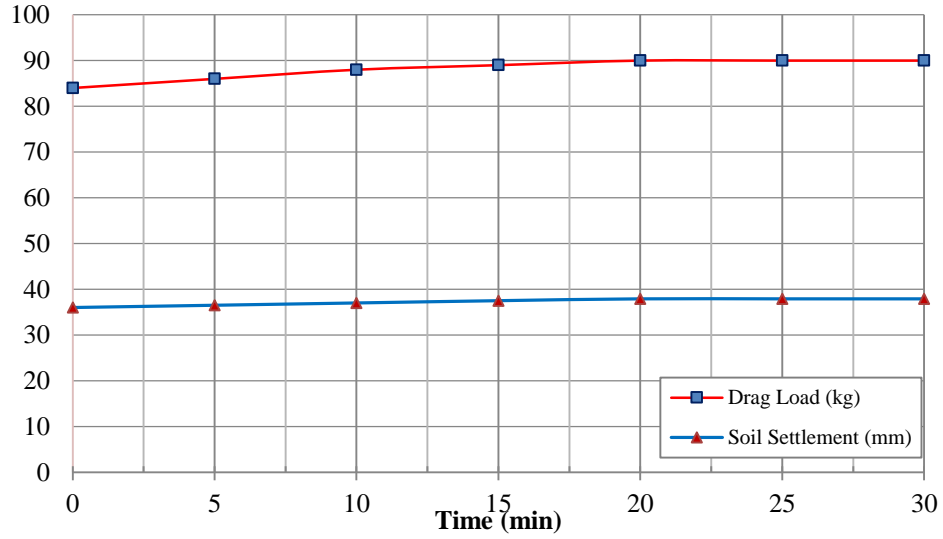
Figure 4.37 Test 30 Soil settlement and drag load **VS** time for $C_p = 12.5\%$, $\sigma = 80\text{kPa}$, for partial inundation (75-100)%
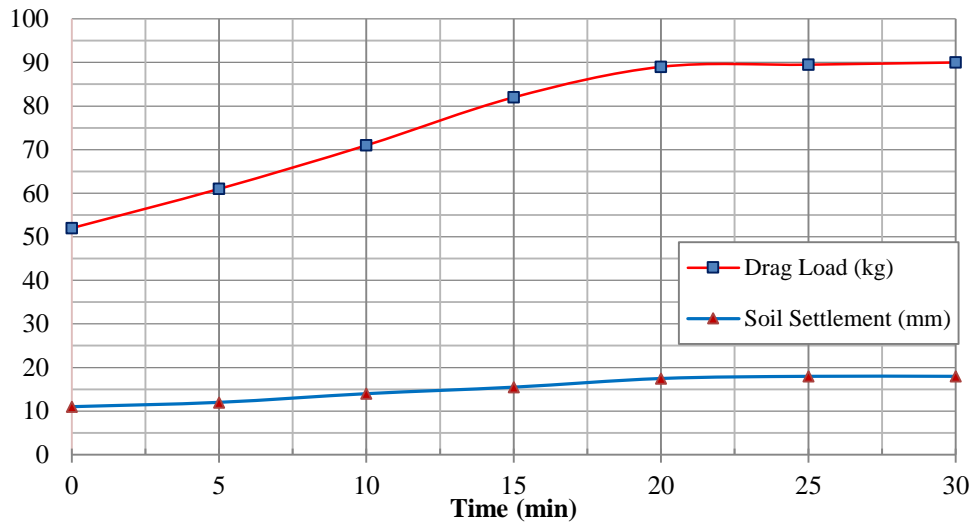
Figure 4.38 Test 31 Soil settlement and drag load **VS** time for $C_p = 12.5\%$, $\sigma = 120\text{kPa}$, for partial inundation (0-25) %
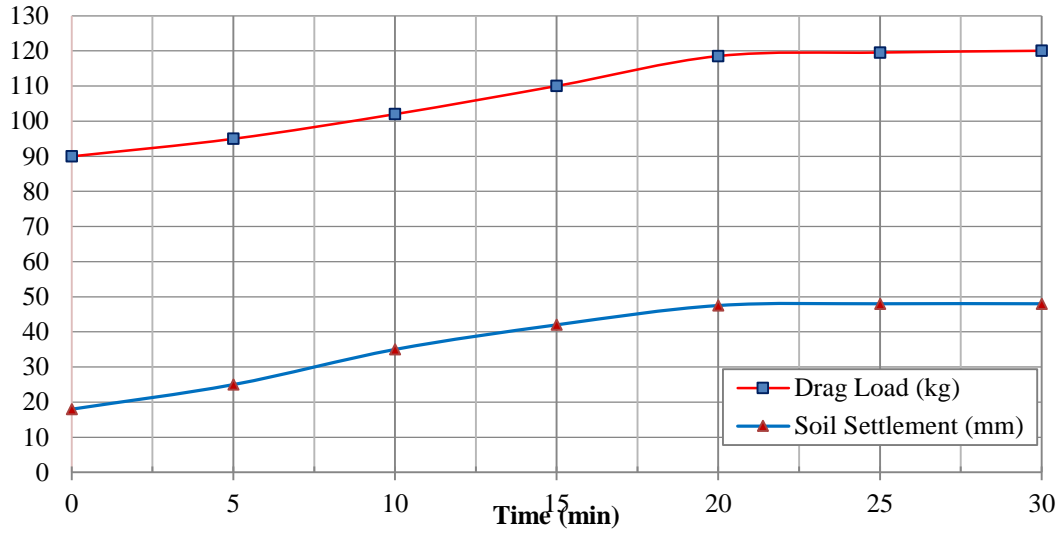
Figure 4.39 Test 32 Soil settlement and drag load **VS** time for $C_p = 12.5\%$, $\sigma = 120$kPa, for partial inundation (25-50) %
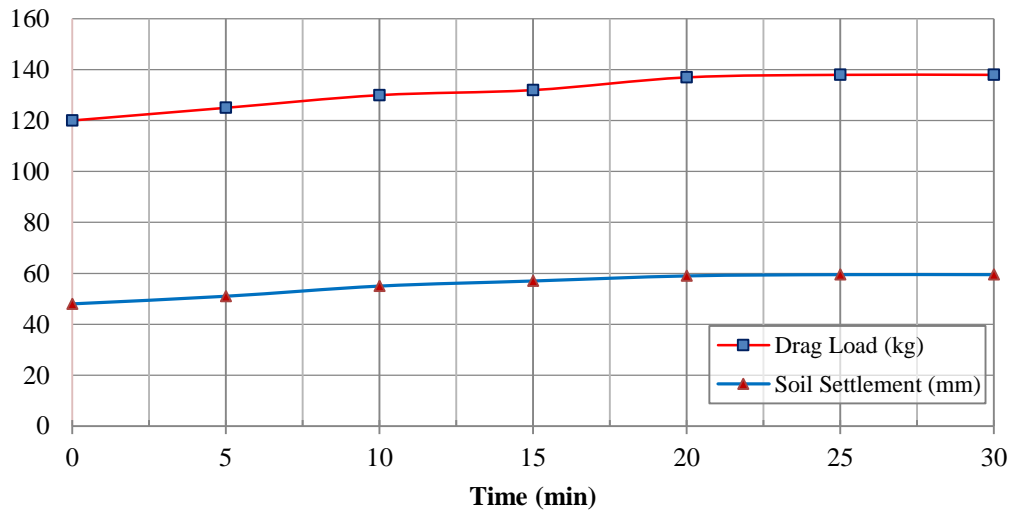
Figure 4.40 Test 33 Soil settlement and drag load **VS** time for $C_p = 12.5\%$, $\sigma = 120$kPa, for partial inundation (50-75) %
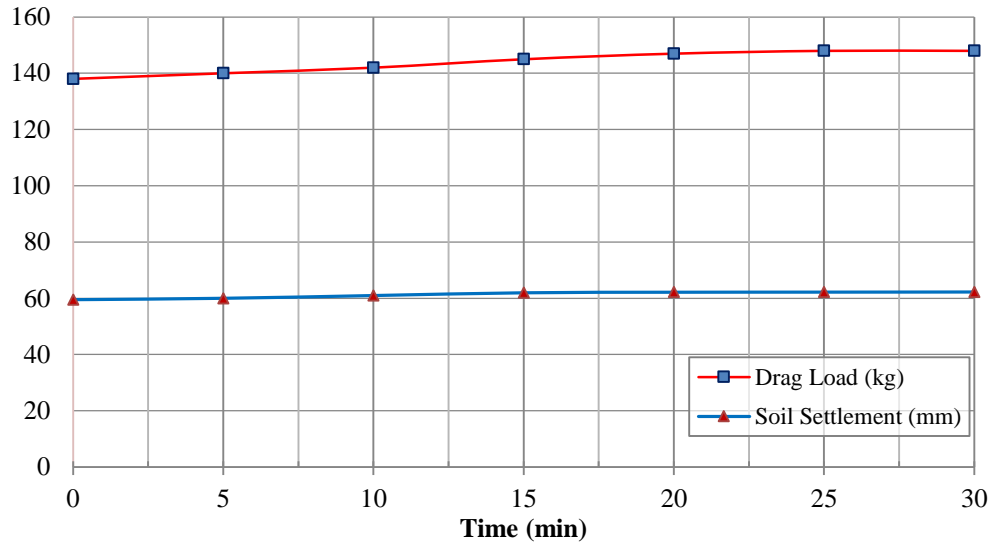
Figure 4.41 Test 34 Soil settlement and drag load **VS** time for $C_p = 12.5\%$, $\sigma = 120\text{kPa}$, for partial inundation (75-100) %
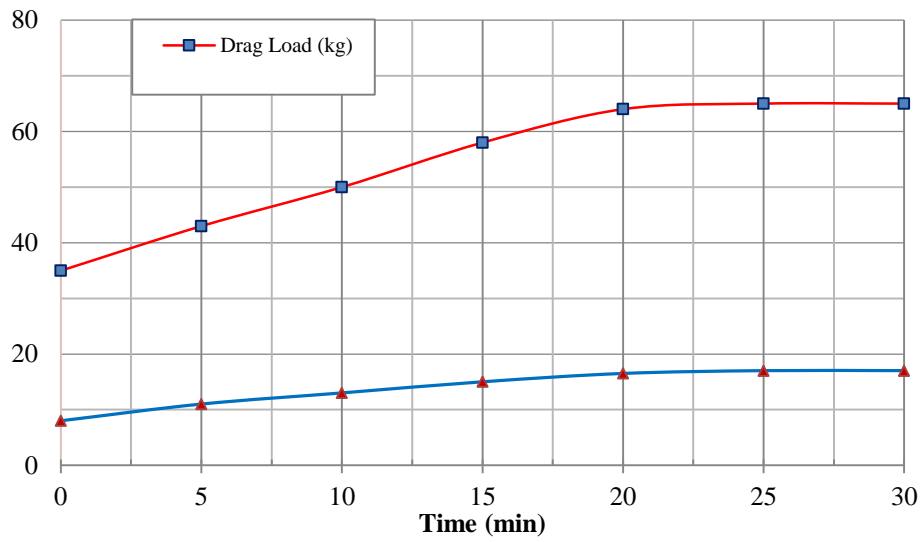
Figure 4.42 Test 35 Soil settlement and drag load **VS** time for $C_p = 18\%$, $\sigma = 80\text{kPa}$, for partial inundation (0-25) %
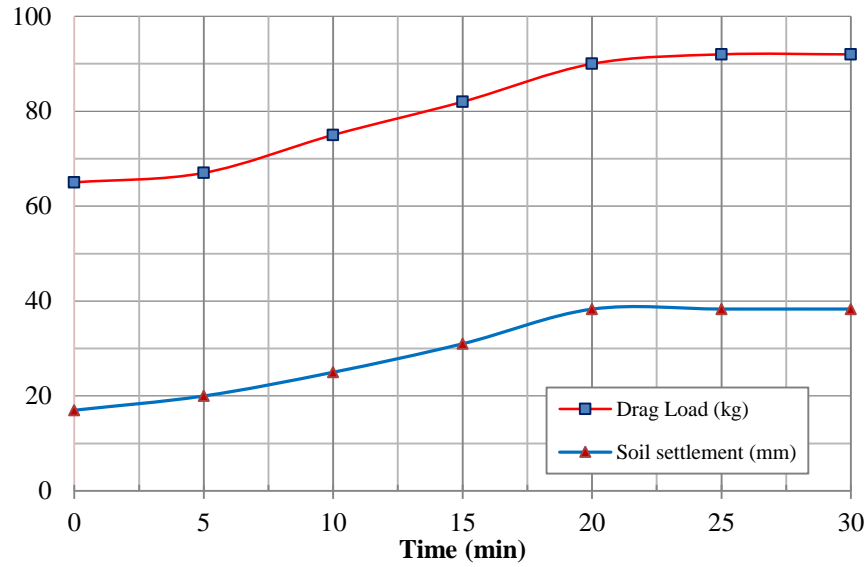
Figure 4.43 Test 36 Soil settlement and drag load **VS** time for $C_p = 18\%$, $\sigma = 80\text{kPa}$, for partial inundation (25-50) %
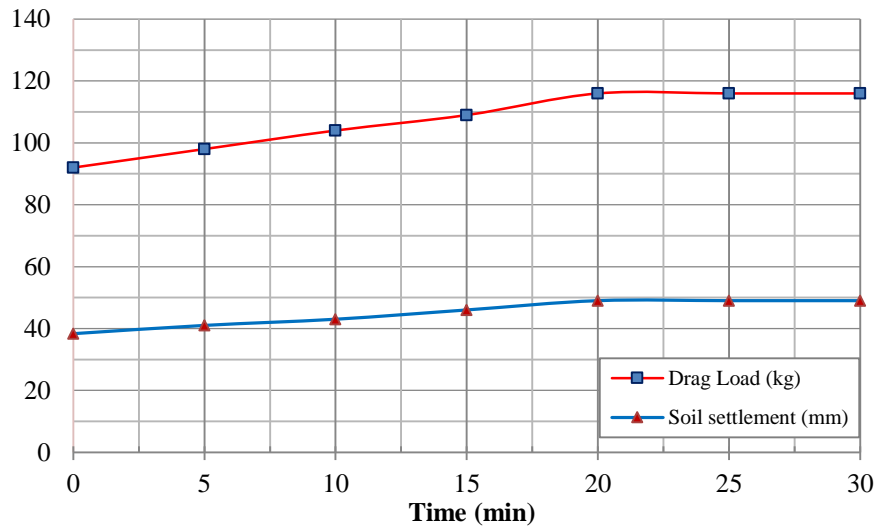
Figure 4.44 Test 37 Soil settlement and drag load **VS** time for $C_p = 18\%$, $\sigma = 80\text{kPa}$, for partial inundation (50-75) %
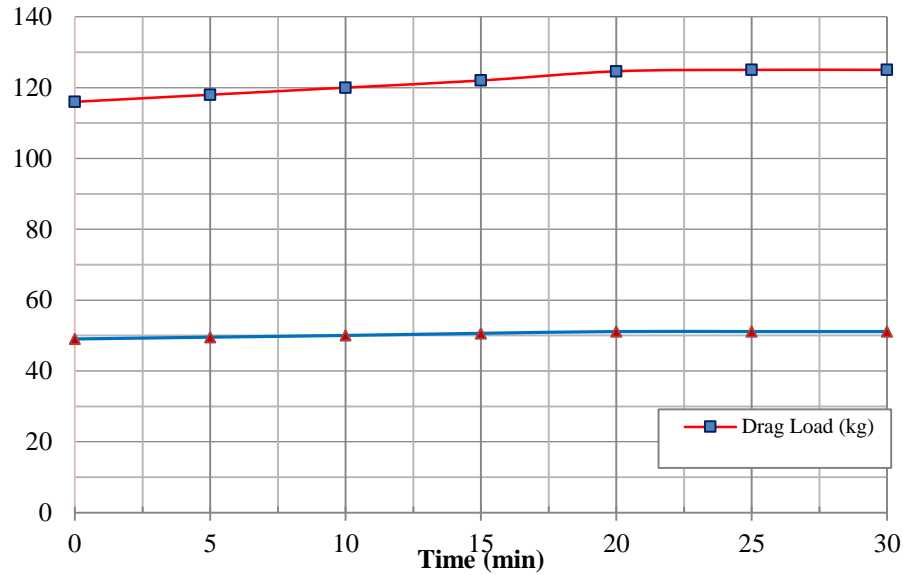
Figure 4.45 Test 38 Soil settlement and drag load **VS** time for $C_p = 18\%$, $\sigma = 80$kPa, for partial inundation (75-100) %

The effect of partial inundation on collapse settlement and drag load was noticed from tests 22 through 45, where both settlement and drag force increased significantly upon increasing the degree of wetting up to a certain value about 75% after which this increase becomes less significant. These test results have shown that the drag load is directly proportional to collapse potential, inundation pressure and degree of wetting. The effect of degree of wetting on NSF was more significant for highly collapsible soil mixtures CS1 and CS2.

4.4 Analysis of Results

Results obtained from experimental work are presented in this section in tables and figures, comparing different tests results, rather than expressing individual test results as in the previous sections. The analysis of experimental results in this section aims at showing the effect of different parameters on soil settlement due to inundation and the resulting drag load acting on the pile, where the results of five tests obtained by Mashhour (2009) were also used along with the results obtained in the current research. Maximum values measured of soil strain due to inundation as well as drag

load are summarized in Table 4.1. It can be noticed that for inundation from bottom, the rate of inundation has an effect on the magnitude of drag load, where the drag load increases with the increase in inundation rate. While the magnitude of soil strain upon inundation stays nearly constant for different inundation rates.

Table 4.1 Increase in NSF due to inundation from experimental results

C_p (%)	σ (kPa)	Inundation direction	Inundation time (min)	Soil Strain due to inundation (%)	Max. drag load before inundation (kg)	Max. drag load after 100% inundation (kg)
4.2	40			0.43	12	23.5
9	40			2.00	12	27
12.5	40			4.20	14	33
18	40			6.64	12	48
4.2	80			0.80	31	56
9	80		30	2.40	31	62
12.5	80			6.00	31	89
18	80			8.62	30	125
4.2	120			1.60	55	100
9	120			3.90	55	115
12.5	120			7.00	52	148
18	120	From Bottom		10.70	50	190
4.2	40			0.43	12	22.5
9	40			2.13	11.7	26
12.5	40			4.10	12	34
18	40			6.60	12	48
4.2	80			0.74	31	56
9	80		60	2.50	30.5	62
12.5	80			6.34	30	89
18	80			9.15	30	125
4.2	120			1.60	50	95
9	120			4.02	55	110
12.5	120			7.00	50	140
18	120			10.20	49	175
12.5	80		90	6.06	30	80.5
4.2	80			0.82	31	60
9	80			2.82	30	72
12.5	80	From Top	20	5.98	29.5	90
18	80			8.62	35	125
12.5	40			4.20	11	34
12.5	120			10.26	52	148

4.4.1 Collapse Strain due to Full Inundation

In this study four different collapsible soils mixtures were used, where each mixture was designed having a specific collapse potential ranging between 4.2 to 18%. Single oedometer tests were performed to obtain the collapse potential values, where inundation pressure in these oedometer tests of 200 kPa was applied, following the procedure of Knight (1963). Throughout the experiments performed in the testing set up for the soil-pile system, different inundation pressures were applied ranging from 40 to 120 kPa. The relationship between collapse strain caused by inundation and inundation pressure for different soil mixtures is illustrated in Figures 4.46 and 4.47, showing the effect of surcharge and collapse potential on collapse strain as obtained from the current experimental study. The collapse strain was calculated using Equation [4.1], where at inundation pressure 200 kPa, the collapse strain is equal to the collapse potential value of the soil mixture.

$$\%\text{Collapse Strain} = \frac{\Delta e}{1 + e_0} \times 100 = \frac{H_0 - H_f}{H_0} \times 100 \dots\dots [4.1]$$

H_0: Height of soil before inundation (cm)

H_f: Height of soil after inundation (cm)
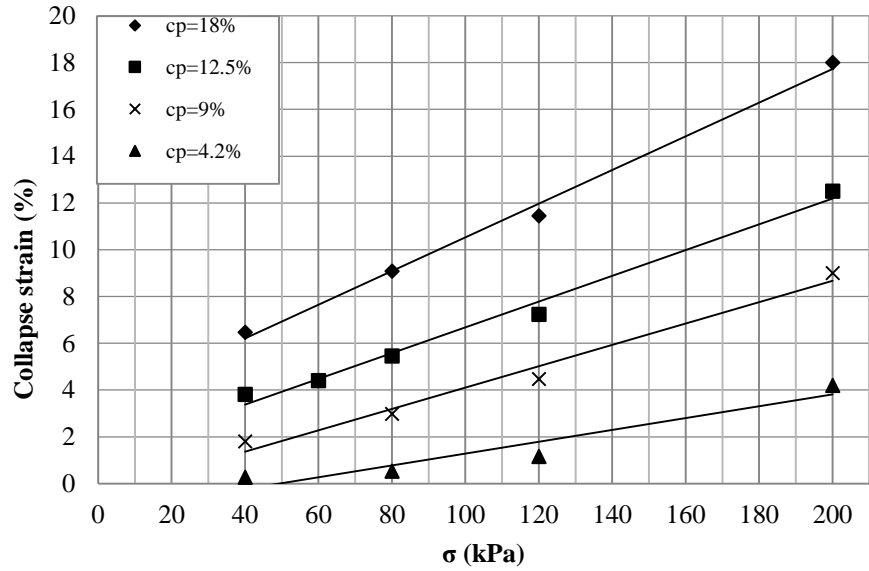
Figure 4.46 Inundation pressure (kPa) VS collapse strain (%)
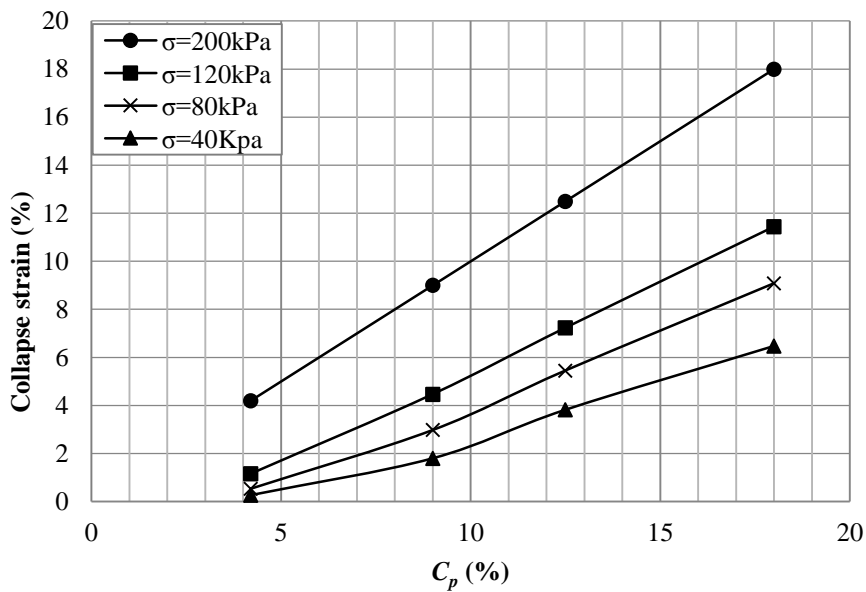
Figure 4.47 Collapse potential (%) VS collapse strain (%)

The relationships in Figures 4.46 and 4.47 show a good agreement with data reported in literature, where the collapse strain is directly proportional to the surcharge load and collapse potential of the soil mixtures. It can be noticed from Figures 4.46 and 4.47, that soil mixtures having collapse potential of 12.5% and above, can collapse upon inundation without additional surcharge.

4.4.2 Drag Load due to Full Inundation

In the following section, the results of tests are compared to each other, in order to show the effect of rate of inundation, collapse potential and inundation pressure on drag load developing on pile shaft upon inundation of collapsible soil subjected to surcharge load. In order to establish these relationships, three sets of tests were done where water inundation (100% saturation from bottom) took place over 30, 60 and 90 minutes.

Figures 4.48 and 4.49 present the relationship between inundation pressure and maximum measured drag load, for different inundation rates and different soil mixtures. While Figures 4.50 and 4.51 present the relationship between the maximum measured drag load and the period needed for 100% inundation for each test, for different soil mixtures at different inundation pressures.
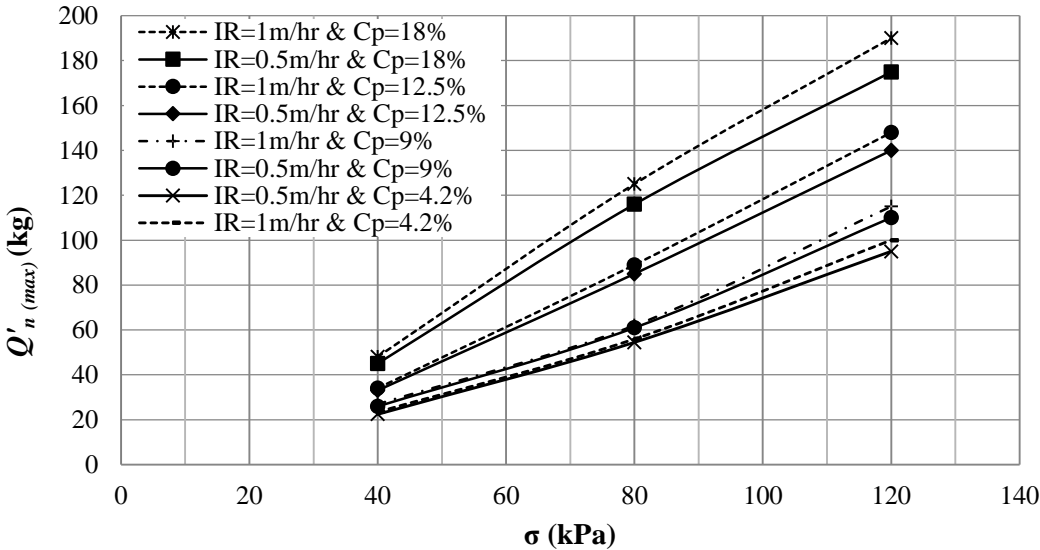
Figure 4.48 Inundation pressure (σ) VS the maximum drag load after inundation
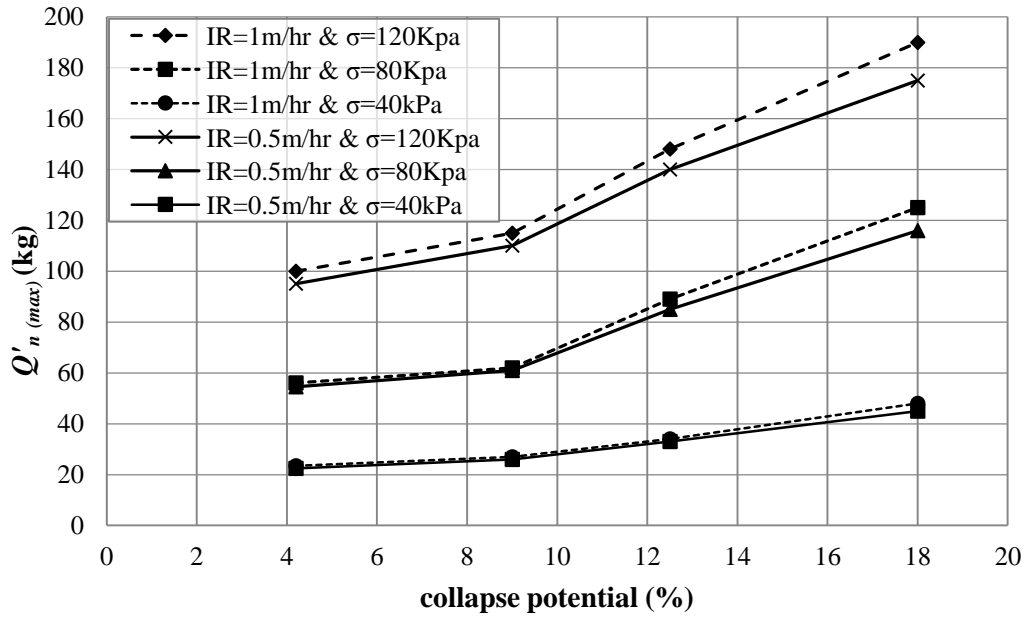
Figure 4.49 Maximum drag load measured after inundation VS collapse potential (C_p)
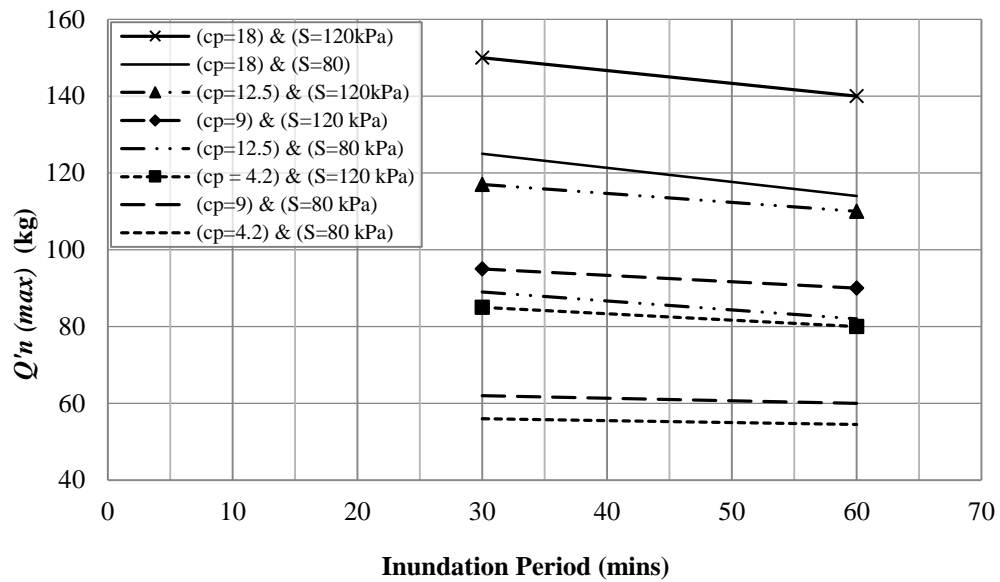
Figure 4.50 Maximum drag load (kg) VS inundation period (min)
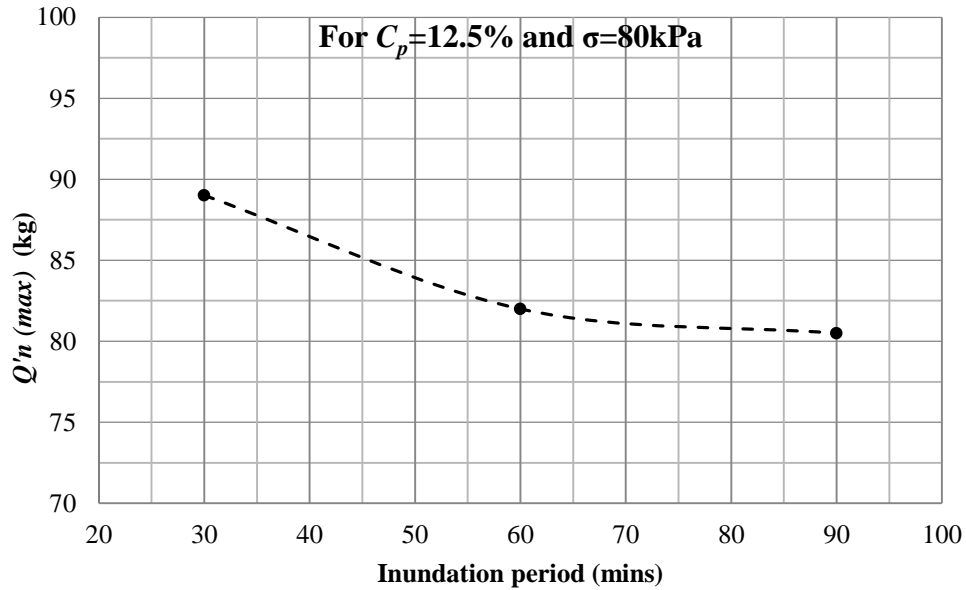
Figure 4.51 Maximum drag load (kg) VS inundation time (min)

It can be noticed in Figures 4.48, 4.49 and 4.50 that the maximum measured drag load, is directly proportional to inundation rate for different soil mixtures. The effect of inundation rate was significant only for highly collapsible soils (C_p=12.5 and 18%), and for higher surcharge values (σ = 80 and 120 kPa). On the other hand it can be noticed from Figure 4.51 that the effect of inundation rate becomes significant for higher inundation rates where the hydraulic gradient approaches the critical value at IR=1 m/hr, and this effect becomes minimal to negligible for inundation rate below 0.5 m/hr.

4.4.3 Collapse Strain due to Partial Inundation

In the following section, the results of tests are demonstrated to show the effect of different parameters on drag load developing on pile shaft upon partial wetting of collapsible soil subjected to surcharge load, and on soil settlement. In order to establish these relationships, tests were done where water was added to soil from top, over four equal increments, so that after each inundation stage degree of wetting of soil increased by 25%.

A typical relationship between the percentage of collapse due to wetting is plotted versus the degree of wetting in Figure 4.52. Where the percent of collapse due to wetting is the ratio between the collapse settlements due to increase of degree of saturation at a point, divided by the full collapse due to full inundation.
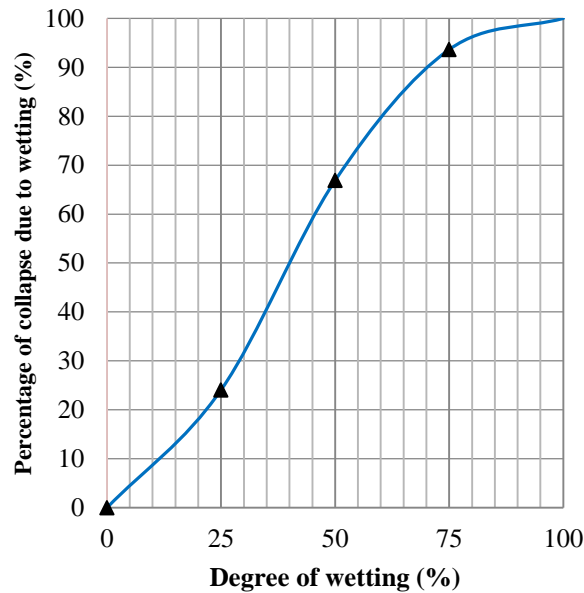
Figure 4.52 Percentage of collapse VS degree of wetting for $\sigma = 80kPa$

Figure 4.53 presents the relationship between collapse potential of the soil on the horizontal axis, and the collapse strain due to wetting on the vertical axis for different degrees of inundation. While Figures 4.54 and 4.55 present the relationship between the percentages of inundation the soil on the horizontal axis versus the collapse strain and soil settlement due to wetting respectively on the vertical axis, for different soil mixtures.
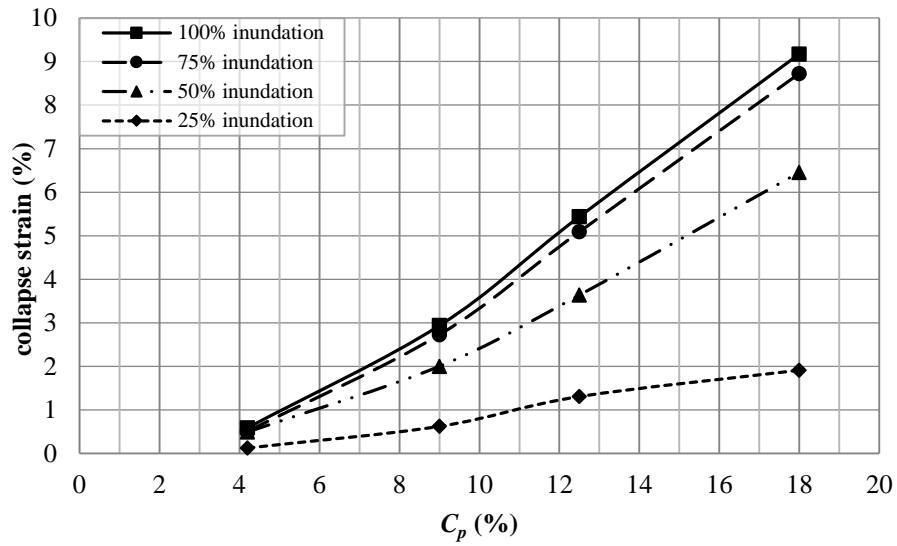
Figure 4.53 Collapse strain (%) VS C_p (%) for inundation pressure σ = 80kPa
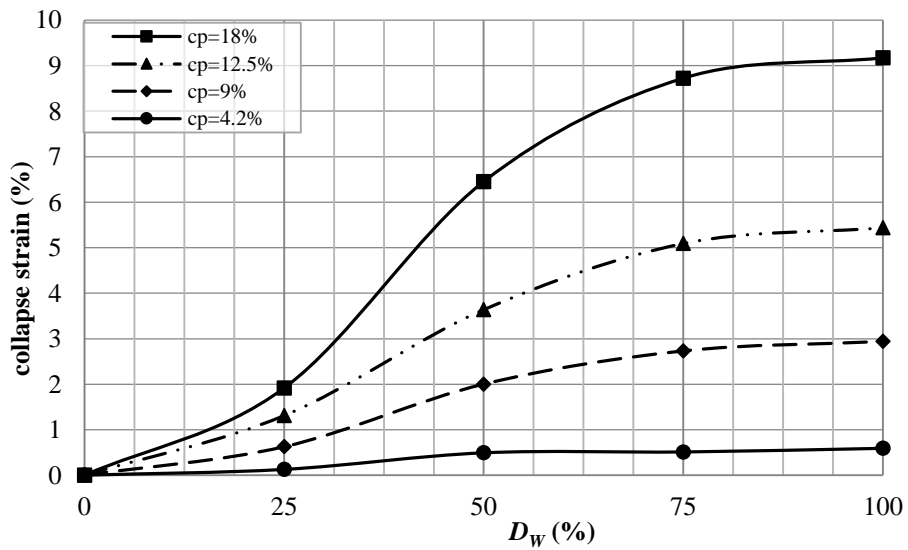
Figure 4.54 Collapse strain (%) VS degree of wetting for σ = 80kPa
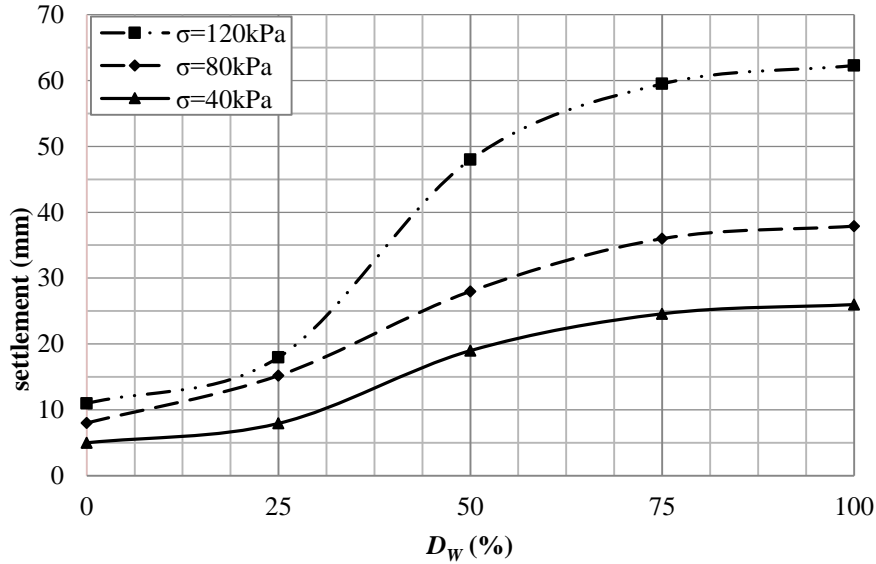
Figure 4.55 Soil Settlement VS degree of wetting for $C_p=12.5\%$

The tests showed that the collapse strain caused by wetting, increases significantly upon an increase in degree of wetting up to 75% as shown in figure 4.52. These relationship trends presented in figure 4.52 are in a good agreement with the findings reported by El-Ehwany and Houston (1990), Houston et al., (1993), Houston et al., (2001) and Elkady (2002).

4.4.4 Drag Load due to Partial Inundation

In order to consider the effect of partial wetting of collapsible soil subjected to inundation pressure, on the drag load, the results of tests carried out in this research were partial inundation took place, are being compared in this section. Where figures 4.56 and 4.57 demonstrate the relationship between collapse potential and drag load for different degrees of wetting for inundation pressure equal to 80 kPa. While figures 4.58 and 4.59 present relationships between inundation pressure and drag load for different degrees of wetting.
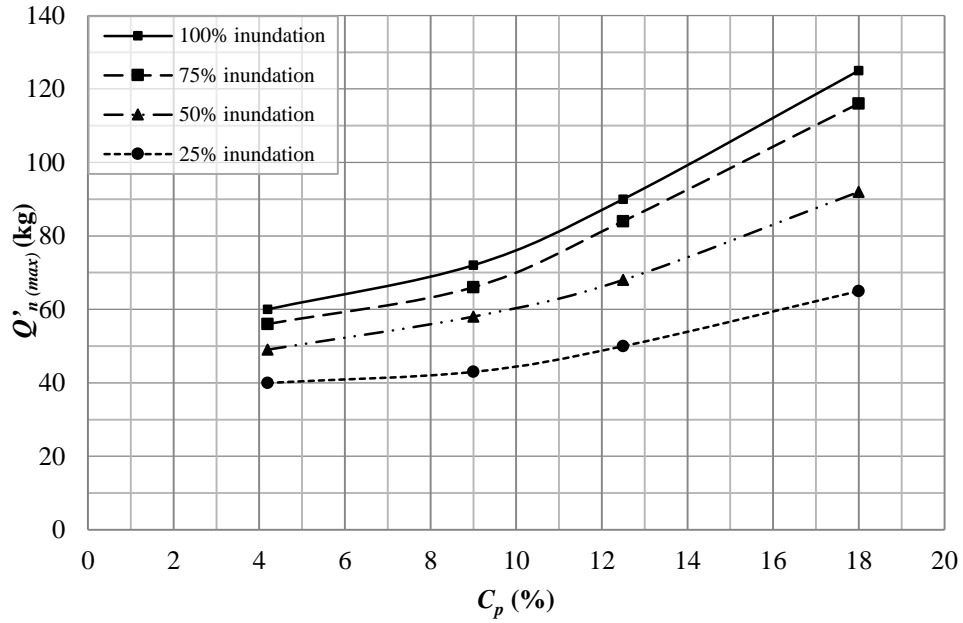
Figure 4.56 Maximum drag load VS collapse potential (C_p), for $\sigma = 80$kPa
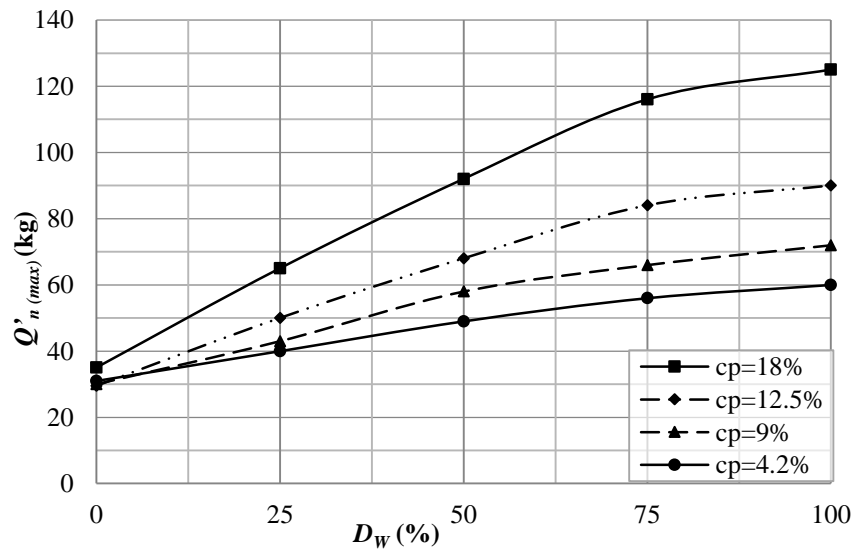
Figure 4.57 Maximum drag load VS degree of wetting for $\sigma = 80$kPa
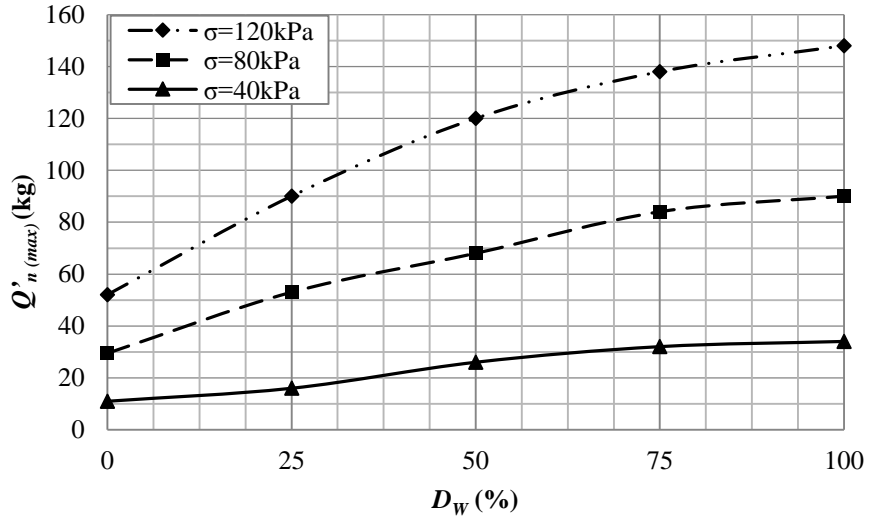
Figure 4.58 Maximum drag load VS degree of wetting for C_p=12.5%
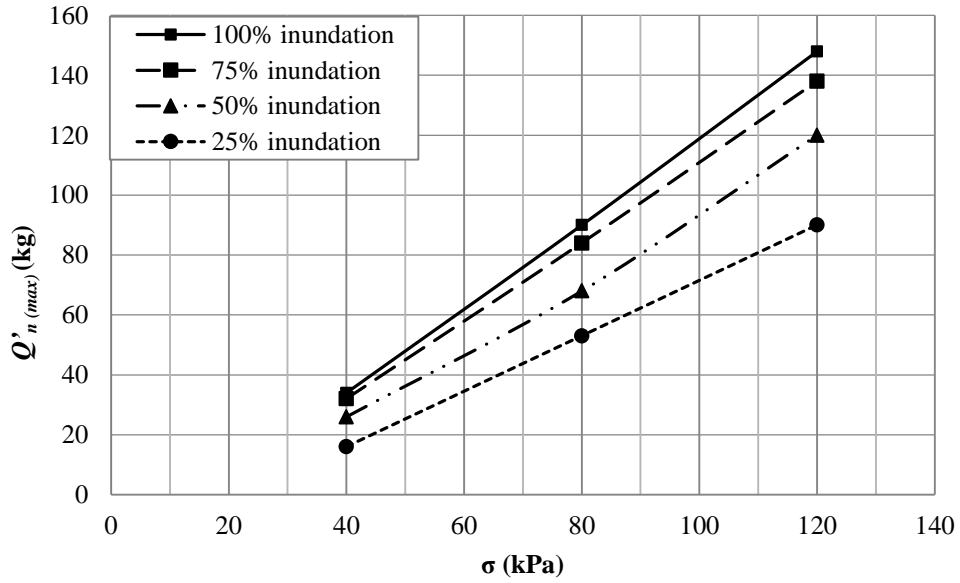
Figure 4.59 Maximum drag load (kg) VS inundation pressure (kPa), for C_p=12.5%

4.5 Discussion

Based on the experimental results obtained in the present investigation, it can be noted that collapse potential, inundation pressure, inundation rate, inundation direction and degree of inundation have substantial influence on the drag loads developing on the pile's shaft due to the soil collapse during inundation.

The effect of inundation rate on drag load was most significant for higher collapse potential mixtures, where the increase in drag load between inundation rates 0.5 and 1 m/hrs, reached up to 9.65% for soil mixture CS-1 at inundation pressure 80kPa. While the effect of inundation rate, was found to be less significant for the lower inundation rate of 0.33m/hr.

It can be noted as well that the percentage of increase in drag load due to inundation is directly proportional to the increase in inundation pressure in the range of 40 to 80 kPa, whereas this increase in drag load due to inundation is inversely proportional for the range of 80 to 120 kPa.

For partial inundation the development of settlement and drag load is increasing in a very high rate between 25 and 75% inundation, whereas at 75% saturation the drag load reaches almost 92% of the maximum drag load $Q'_{n(max)}$.

CHAPTER 5

NUMERICAL MODELLING

5.1 General

The main goal of this chapter is to perform a parametric study by investigating the effects of the critical parameters on NSF in collapsible soil, extending the range of parameters used in the experimental results. A series of two-dimensional numerical analyses were performed using PLAXIS 2D 8.6 finite element software. The axis-symmetric numerical model was calibrated and validated with data obtained from the experimental tests conducted in the present study.

5.2 Finite Element Model

In order to develop reliable solutions using numerical techniques, it is necessary to develop a conceptual model that resembles the physical system. In this study the physical system was explained in detail in Chapter 3. Based on the conceptual model, the following main steps were implemented in the process of defining the numerical model; identifying: the domain geometry, boundary conditions, element types, mesh, analysis types, material properties and constitutive models. The finite element model components and the numerical model methodology adopted in this study are described in details in this section.

5.2.1 Geometry and Boundary Conditions

The first step of the modeling process, is to define the geometry of the domain consisting of the soil and the pile clusters. A single axially-loaded pile penetrating collapsible soil was simulated in the

axisymmetric finite element model. The axis of the pile is located at the centerline of the mesh. To limit the movement at the soil boundaries (the nodes at the boundaries of the domain) and to improve the computational complexity, boundary conditions were generated using standard fixities in PLAXIS software by defining prescribed displacement equal to zero at the geometry lines, thereby restricting transitional movements of the nodes at the domain bottom in both vertical and horizontal directions. For the nodes at the sides of the domain, only the lateral movement was restricted.

The outer vertical boundary of the mesh was placed at 50 times the pile diameter from the pile axis as suggested by several researchers including (Hanna and Sharif, 2006).

The axisymmetric model boundary conditions layout used for modeling the single end-bearing pile in collapsible soil resting on dense sand is presented in Figure 5.1.
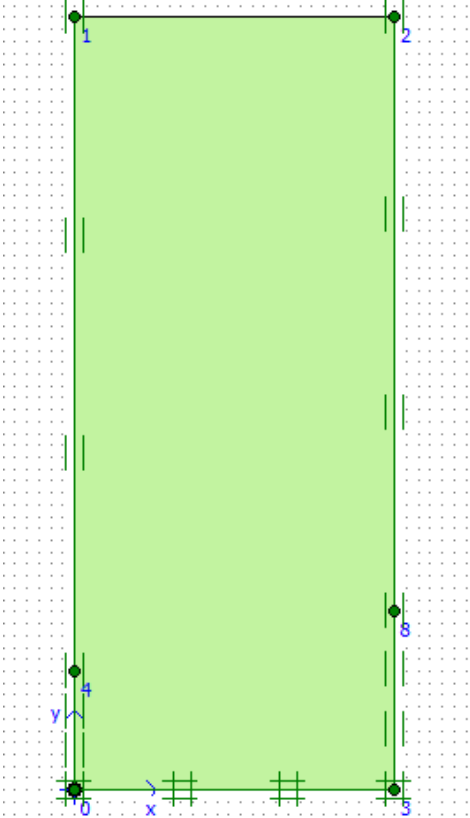
Figure 5.1 Model boundary conditions

5.2.2 Element Type

Higher order triangular elements were used for soil and pile clusters. These 15-node higher-order triangular elements often provide better accuracy than lower-order triangular elements with 6 or 9 nodes, since each of these higher order elements have more nodes providing a fourth order displacement interpolation. Triangular elements involve fewer nodes and accordingly less degrees of freedom than quadrilateral elements. Therefore, the time needed for finite element analysis using triangular elements is often less than that needed for quadrilateral elements for the same number of elements and order of interpolation. Figure 5.2 summarizes different types of nodes and stress points in triangular elements used in PLAXIS software.
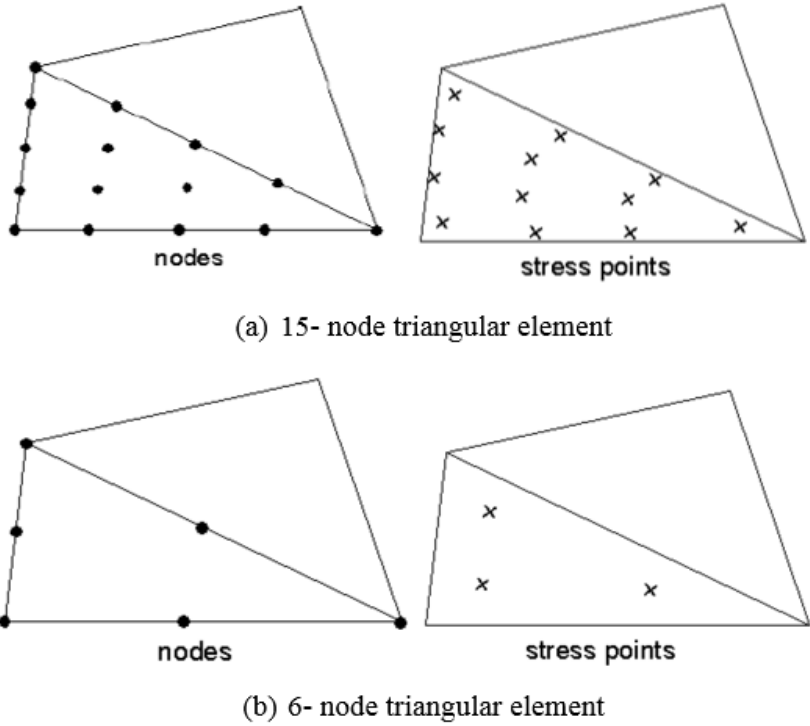
Figure 5.2 Nodes and stress points in triangular elements (PLAXIS 2D User's Manual, 2010)

5.2.3 Mesh Generation

Both soil and pile clusters were modeled using 15-node triangular elements providing a fourth-order interpolation for displacements. The numerical integration process involved twelve stress points for each element as shown in Figure 5.2 (a). At the interface between the soil and the pile, five-node line elements were used in order to take into consideration the soil-pile interaction that generates skin friction due to the relative movement. The connection between a 15 node triangular element and an interface element is shown in Figure 5.3.
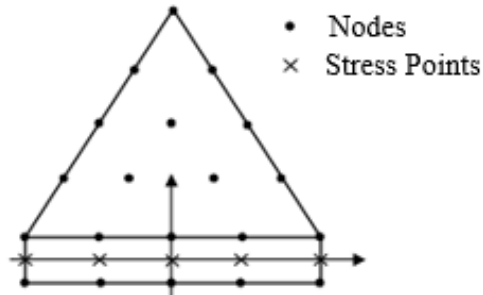
Figure 5.3 Nodes and stress points in an interface element connected to triangular element

(PLAXIS 2D User's Manual, 2010)

An automatic mesh generation option in the PLAXIS 2D finite element program was utilized, in which the mesh was automatically generated based on the boundary conditions, the model geometry and the soil and material properties. The generated mesh has a medium global coarseness as shown in Figure 5.4.
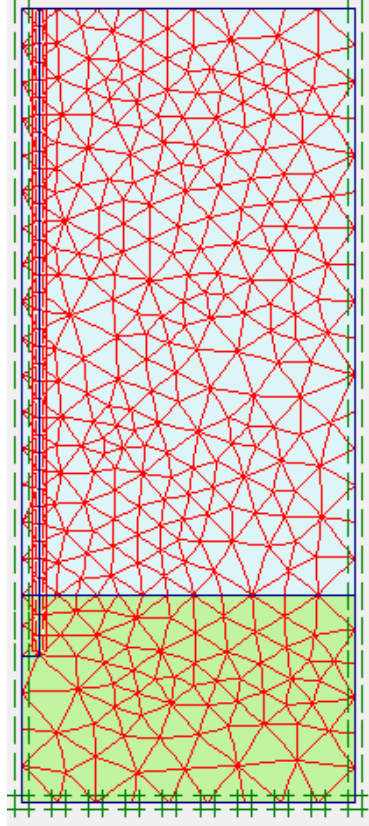
Figure 5.4 Finite element mesh

5.2.4 Material Properties

In this study, the pile material was defined as an isotropic linear elastic material where the constitutive relationship in this case can be defined by two input parameters Young's modulus (E_p) and Poisson's ratio (v_p). The isotropic linear elastic materials are governed by Hooke's law as expressed in the following set of equations.

$$\begin{bmatrix} \dot{\sigma}'_{xx} \\ \dot{\sigma}'_{yy} \\ \dot{\sigma}'_{zz} \\ \dot{\sigma}'_{xy} \\ \dot{\sigma}'_{zy} \\ \dot{\sigma}'_{zx} \end{bmatrix} = \frac{E'}{(1+v')(1-2v')} \begin{bmatrix} 1-v' & v' & v' & 0 & 0 & 0 \\ v & 1-v' & v' & 0 & 0 & 0 \\ v & v & 1-v' & 0 & 0 & 0 \\ 0 & 0 & 0 & 0.5-v' & 0 & 0 \\ 0 & 0 & 0 & 0 & 0.5-v' & 0 \\ 0 & 0 & 0 & 0 & 0 & 0.5-v' \end{bmatrix} \begin{bmatrix} \varepsilon_{xx} \\ \varepsilon_{yy} \\ \varepsilon_{zz} \\ \varepsilon_{xy} \\ \varepsilon_{zy} \\ \varepsilon_{zx} \end{bmatrix} \dots [5.1]$$

A linearly elastic perfectly plastic model was used to model collapsible soil behaviour upon inundation similar to that obtained from the laboratory investigation in this study. The typical stress-strain relationship in the elastic perfectly plastic model is demonstrated in Figure 5.5.
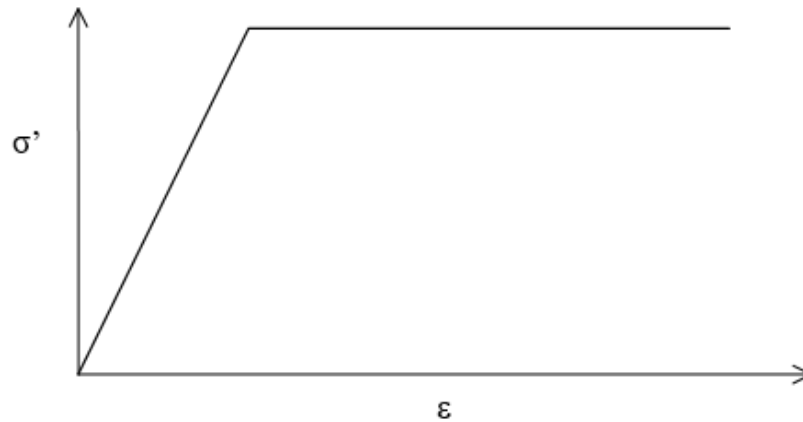
Figure 5.5 Stress strain relationship for an elastic perfectly plastic soil model

The stress-strain relationship for the linear elastic phase shown in Figure 5.5 is governed by Hooke's law, and can be expressed by the relationships in equation [5.2], so that the stress rates and elastic strain rate can be linked together by the subsequent equations.

$$\sigma = E.\varepsilon\ldots\ldots[5.2]$$

$$\dot{\sigma} = D^e \dot{\varepsilon}^e \ldots\ldots[5.3]$$

$$\varepsilon = \varepsilon^e + \varepsilon^p \ldots.[5.4]$$

$$\dot{\varepsilon} = \dot{\varepsilon}^e + \dot{\varepsilon}^p \ldots[5.5]$$

$$D^e = \frac{E'}{(1+v')(1-2v')} \begin{bmatrix} 1-v' & v' & v' & 0 & 0 & 0 \\ v & 1-v' & v' & 0 & 0 & 0 \\ v & v & 1-v' & 0 & 0 & 0 \\ 0 & 0 & 0 & 0.5-v' & 0 & 0 \\ 0 & 0 & 0 & 0 & 0.5-v' & 0 \\ 0 & 0 & 0 & 0 & 0 & 0.5-v' \end{bmatrix} \quad \dots [5.6]$$

The plastic behaviour in the elastic perfectly plastic model is governed by the theory of plasticity

equations, such that the rate of plastic strain is proportional to the derivative of the yield function

with respect to the stress. In order to avoid over prediction of dilatancy, plastic potential function

(g) was introduced in PLAXIS in addition to the yield function. The elastic perfectly plastic model

is governed by various equations including equations [5.7] and [5.8]:

$$\dot{\sigma} = (D^e - \frac{\alpha}{d} D^e \frac{\partial g}{\partial \sigma'} \frac{\partial f^T}{\partial \sigma'} D^e) \dot{\varepsilon} \dots [5.7]$$

$$d = (\frac{\partial f^T}{\partial \sigma'} D^e \frac{\partial g}{\partial \sigma'}) \; \dots\dots\dots\dots [5.8]$$

where:

σ : effective stress rate v' : effective Poisson's ratio

$\dot{\varepsilon}$: strain rate E' : effective Young's modulus

D^e: elastic material stiffness matrix φ : friction angle

c' : cohesion ψ: dilatancy angle

g: plastic potential function f : yield function

α: switch parameter

The soil material governed by Mohr-Coulomb failure criterion can therefore be defined with the

following material parameters: modulus of elasticity (E), Poisson's ratio (v), angle of internal

friction (φ), cohesion (c) and angle of dilatancy (ψ). The Mohr–Coulomb yield surface in principal stress space is shown in Figure 5.6.
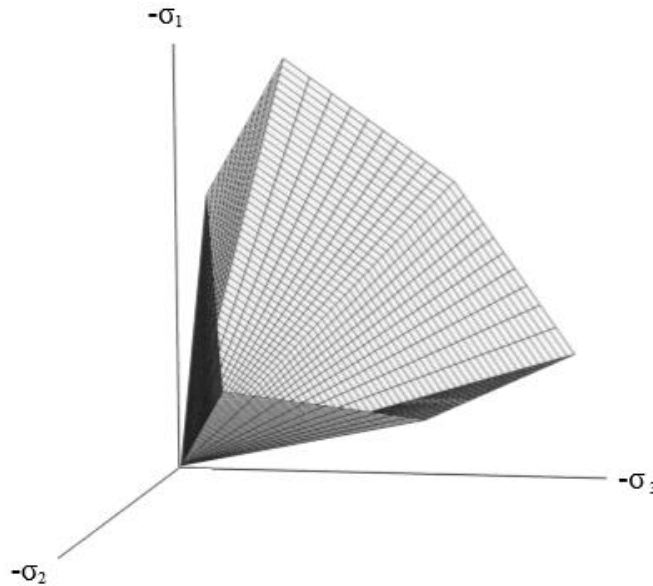
Figure 5.6 Mohr-Coulomb yield surface for $c = 0$ (PLAXIS 2D User's Manual, 2010)

The theory of scale model similitude defines the relationship between the prototype behaviour and the model in order to obtain similarity. Since the numerical model and the prototype setup were subject to identical density and stress conditions, material properties can be used without further scaling in order to obtain constitutive similarity as reported by Sedran et al., (2001). Therefore, the material properties were not scaled and a scaling factor of 1.0 was used for: the density (λ_ρ) and the stress (λ_σ) or strain (λ_ε). A scaling factor of 20 was used for the pile and soil dimensions ($\lambda_L = L_m/L_p$). The ratio between the pile diameter and soil grain diameter in the prototype tests is greater than 30 and so the effect of grain size in the prototype was neglected, as suggested by researchers including Sedran et al., (2001). The material properties of the soil layers used in the numerical analysis are

summarized in Table 5.1, while the pile material properties and dimensions are summarized in Table 5.2.

Table 5.1 Soil properties

Soil layer	G_s	Dry unit weight γ_d (kN/m³)	Moist unit weight γ (kN/m³)	Cohesion c (kPa)	Angle of internal friction φ (°)	Collapse Potential C_p (%)	Modulus of elasticity E (kPa)	Dialatancy ψ (°)
CS-0	2.69	14.0	14.50	25.0	25.0	30	30,000	2.0
CS-1	2.68	14.6	15.30	18.0	31.0	18	30,000	3.0
CS-2	2.67	15.4	16.20	15.5	35.0	12.5	30,000	5.0
CS-3	2.67	15.5	16.25	12.5	38.5	9	30,000	8.5
CS-4	2.66	15.6	16.28	9.0	40.0	4.2	30,000	10.0
End-bearing sand	2.65	18.2	21.0	1.0	42.0	-	45,000	12.0

Table 5.2 Parameter of pile model

Parameter	Symbol	Value	Unit
Diameter	D	0.50	(m)
Length	L	11.00	(m)
Unit weight	γ	24.50	(kN/m³)
Modulus of elasticity	E	30,000,000	(kPa)
Effective Poisson's ratio	v'	0.33	--

5.2.5 Numerical Model Methodology

The numerical model used in this study was developed following the methodology suggested by Noor et al., (2013) in order to take into account the effect of volume reduction on the soil-pile interaction during inundation of collapsible soil. Figure 5.7 presents the key steps adopted in the numerical model.
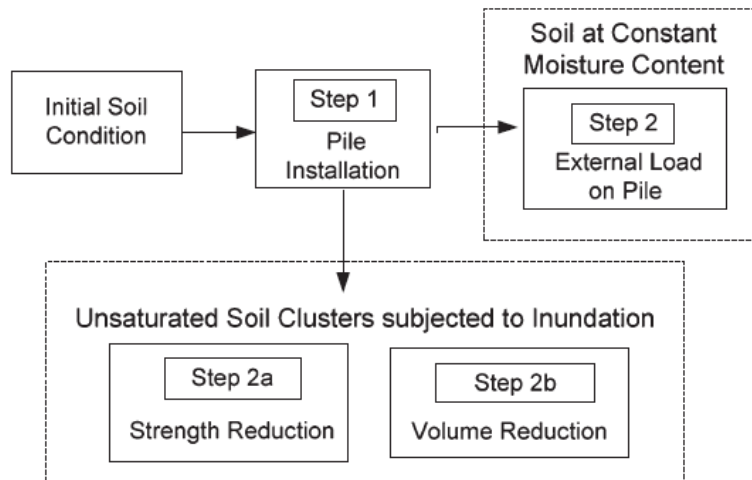
Figure 5.7 Critical sequence of inundation (Noor et al., 2013)

From Figure 5.7 it can be noted that steps 1 and 2 present the initial moisture conditions of the soil in the unsaturated phase (before inundation). In this initial phase, the Mohr-Coulomb failure criteria were assigned to the collapsible soil layer, which was defined as an elastic-plastic material with the material properties summarized in Table 5.1. The in-situ effective stresses were generated based on an earth pressure coefficient at rest and the static groundwater level. Pile installation was introduced, where pile properties were assigned to the predefined pile cluster.

Steps 2a and 2b were applied to simulate the effect of inundation on collapsible soil. Step 2a takes into account the soil inundation and the changing soil parameters from the unsaturated to the

saturated phase, while step 2b accounts for the collapse settlement that takes place due to the inundation of collapsible soil. In order to model the effect of collapse strain upon inundation, surcharge pressures (with values ranging from 20 to 200 kPa) and the associated prescribed displacements were applied on the soil surface.

The values of the prescribed displacements applied on top of the soil to take into account the collapse settlement upon inundation, were determined based on the experimental data, to which a calibration factor was applied. The values of the prescribed displacements were obtained by multiplying the calibration factor by the collapse settlement estimated from the graph shown in Figure 5.10.

Figure 5.8 shows a snapshot taken from the PLAXIS program for a typical prescribed displacement and surcharge applied on top of the soil in the finite element analysis.
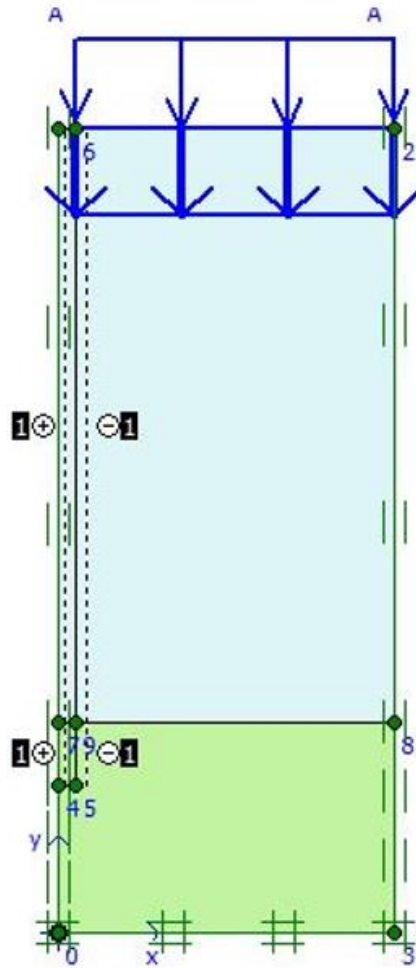
Figure 5.8 Prescribed displacement and surcharge applied on soil surface

5.3 Numerical Model Validation

Experimental data from the study presented here were used to validate the numerical model. The prototype tests were simulated in the numerical analysis taking into consideration the effect of collapsible soil inundation. The maximum drag load data obtained from the experimental investigation $Q_{n(max)}$ were compared to values obtained from the numerical model.

Table 5.3 and Figure 5.9 summarize selected results obtained from the numerical model compared to experimental results.

Table 5.3 Finite element analysis compared to experimental results

Soil Mix	C_p (%)	σ (kPa)	Collapse Stain (%)	$Q_{n(max)}$ Experimental	$Q_{n(max)}$ FEA
CS-1	18.0	80	9.08	125.21	127.93
CS-2	12.5	80	5.45	89.13	86.57
CS-3	9.0	80	2.98	61.98	60.35
CS-4	4.2	80	0.54	56.05	53.16
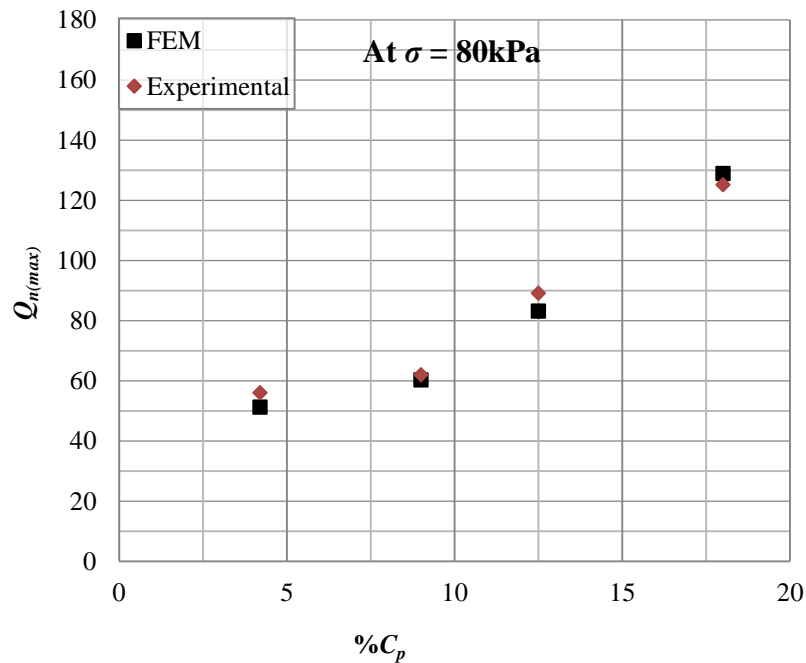
Figure 5.9 Finite element analysis data compared to experimental results

From Figure 5.9 it is clear that the numerical results are in good agreement with the values measured in the experimental investigation for the maximum drag load $Q_{n(max)}$ which takes place due to negative skin friction upon the inundation of collapsible soil.

5.4 Numerical Results Summary

A series of runs were performed using PLAXIS software in order to perform a parametric study, demonstrating the effect of key parameters on negative skin friction in collapsible soil due to inundation. The soil parameter values used in these runs for collapse potential ranged from $C_p = 4$ to 30%; and the range of values for the inundation pressure was from $\sigma = 20$ to 200 kPa.

The prescribed displacement values applied in these runs were assumed based on the collapsible soil stress strain relationships obtained from the response-to-wetting experimental data, in which the collapse strain is directly proportional to the inundation pressure and is equal to the value of collapse potential only at 200 kPa. The collapse strain under different inundation pressures was obtained from the response to wetting tests, as given in equation [5.9].

$$\%\text{Collapse Strain} = \frac{H_0 - H_f}{H_0} \times 100 \dots [5.9]$$

where:

H_0: Height of soil before inundation (cm)

H_f: Height of soil after inundation (cm)

Figure 5.10 shows the relationship between collapse strain and inundation pressure. This relationship was used as a guideline for the values entered as a prescribed deformation in the numerical analysis. This relationship was obtained based on response-to-wetting tests from experimental evaluations of collapsible soil mixtures CS-1 through CS-4, while for CS-5 these values were estimated based on data from the literature.
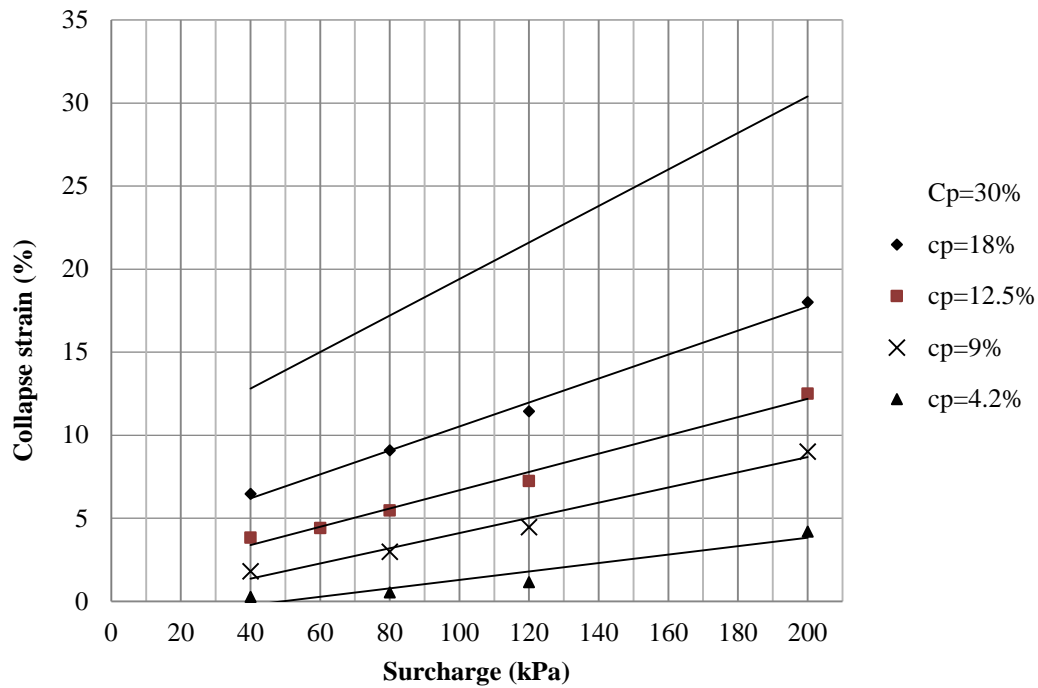
Figure 5.10 Collapse strain versus inundation pressure

After performing the numerical calculations for all phases in the finite element program, the calculated output can be viewed in various forms including deformed mesh, total displacement distribution, total strains, incremental displacements, internal forces acting on the structural elements, effective stresses, excess pore pressures, total stresses and plastic points. Most of these outputs can be viewed for a select phase as incremental values, or as envelope values from the beginning of the analysis up to the selected phase.

Figure 5.11 shows a typical deformed mesh obtained from the numerical model.
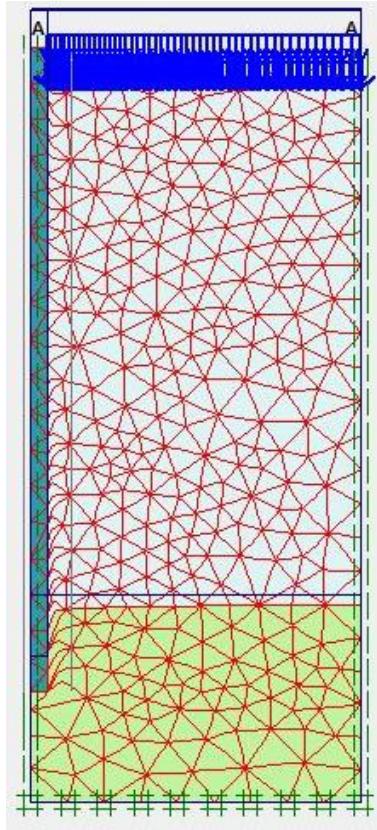
Figure 5.11 Deformed mesh

A typical total displacement distribution after all phases obtained from the numerical model representing collapse settlement upon inundation is shown in Figure 5.12. The total displacements of all nodes are presented in the figure as arrows indicating the relative magnitude of the resulting displacements along the collapsible soil profile. It should be noted that these total displacements can also be viewed in the program as contour lines.
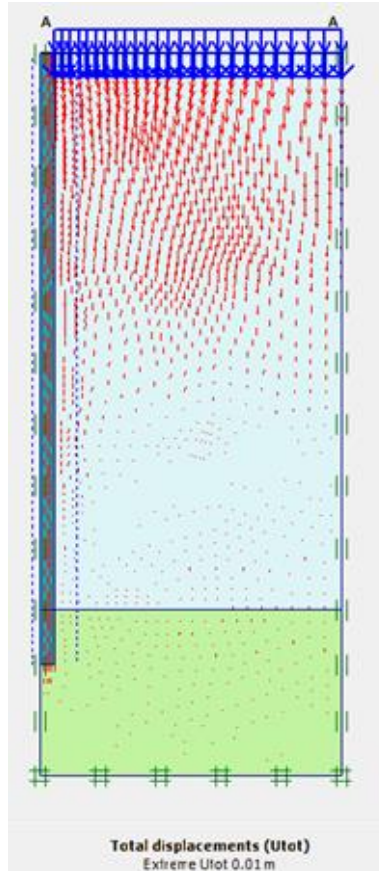
Figure 5.12 Typical total displacement distribution

The shear stresses present after all the analysis phases, representing shear stresses after inundation, were obtained from the finite element analysis for each element along the pile shaft. The drag load values were obtained from the numerical model by integrating the negative skin friction stresses along the pile shaft as shown in Equation [5.10].

$$Q'_{n(max)} = \int_0^L f_n(\pi D) \, dz \, ... [5.10]$$

A summary of the numerical analysis results is presented in Table 5.4 and represented graphically in Figure 5.13.

Table 5.4 Summary of the numerical analysis results

Soil Mix	C_p (%)	σ (kPa)	Collapse Strain (%)	$Q_{n(max)}$ from FEA
CS-0	30.0	20	11.1	23.1
		40	13.2	66.2
		60	15.0	112.3
		80	17.9	160.1
		120	21.2	240.1
		160	26.3	310.4
		200	30.0	380.3
CS-1	18.0	20	5.2	20.2
		80	9.1	127.93
		160	14.8	309.6
		200	18.0	320.4
CS-2	12.5	20	2.6	16.3
		80	5.5	86.6
		160	8.2	202.2
		200	12.5	260.1
CS-3	9.0	20	1.2	11.2
		80	2.9	60.4
		160	6.8	173.4
		200	9.0	219.8
CS-4	4.2	20	0.1	10.9
		80	0.6	53.2
		160	3.5	96.3
		200	4.2	180.1
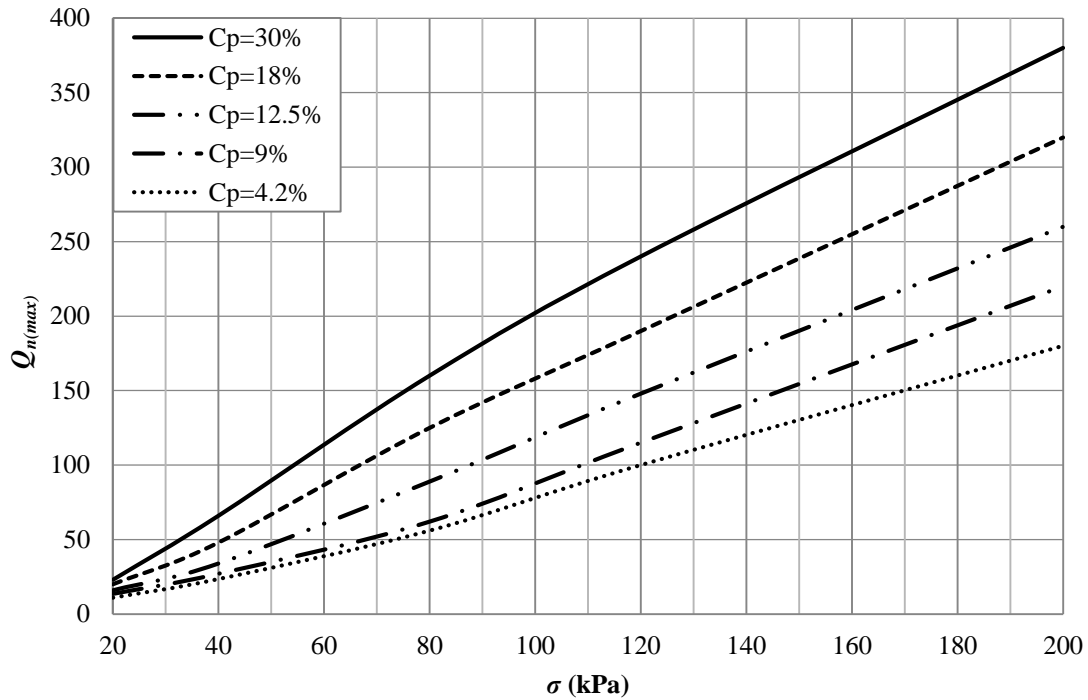
Figure 5.13 Maximum drag load VS σ

From the figures it can be observed that the numerical results were in good agreement with the experimental results, such that the rate of increase in the drag load with respect to inundation pressure for different types of soil did not change significantly.

The range of parameters applied in the numerical model was assumed based on field data reported in the literature for collapse potential and inundation pressure values. The collapse potential values applied in the numerical model reached up to 30% in order to cover the highly collapsible soils expected to result in severe foundation trouble.

CHAPTER 6

ANALYTICAL MODELS

6.1 General

A comparative study was performed to examine the effect of different parameters on the negative skin friction (NSF) developed along a pile shaft as a result of soil collapse settlement upon inundation. To date, there is no analytical model available in the literature that predicts the negative skin friction developed on piles upon soil collapse settlement caused by wetting based on experimental results, taking into account the effect of rate of inundation and the combined effect of different wetting schemes, soil properties, and loading conditions.

The analytical models suggested in this study can be divided into three main parts:

- Models for estimating the rate of increase in NSF upon inundation from the bottom;

- Models for estimating the maximum drag loads due to full inundation from the bottom; and

- Models for estimating drag loads at different degrees of saturation due to partial wetting from the top.

6.2 Analytical Models for Inundation from the Bottom

This section introduces analytical models for estimating the increase in drag load due to inundation from the bottom due to a rise in the groundwater table. The parameters that affect the maximum drag load acting on a pile embedded in collapsible soil due to soil inundation from the bottom upwards that were considered in analysis in this section can be divided into three main categories:

1. Inundation conditions:

   - Inundation pressure acting on the soil (σ)

   - Inundation rate (*IR*)

2. Soil conditions:

   - Collapse potential (*Cp*)

   - Angle of internal friction of the soil ϕ'

3. Soil-pile interface condition:

   - Friction angle at the soil-pile interface δ'.

6.2.1 Rate of Increase in Drag Load during Inundation

Three different inundation rates were studied in this research, 0.34, 0.5 and 1.0 m/hr, where soil inundation from the bottom took place over 90, 60 and 30 minutes respectively. Equations for predicting the rate of increase in drag loads due to inundation, including different cases where collapsible soil mixtures are subjected to different inundation rates and inundation pressures are developed and presented here. Drag Load $\underline{Q_n}$ is the product of negative skin friction f_n multiplied by the circumference area of the pile shaft, as demonstrated in Equation [6.1].

$$Q_n = f_n * \pi \, D \, l \; \ldots\ldots \; [6.1]$$

$f_n = f\,(C_p,\ \sigma,\ \delta',\ \phi',\ IR)$

$\delta' = k_{i.f} * \phi'$

where:

C_p: Collapse potential (%);

σ: inundation pressure: pressure applied at the middle depth of the soil during inundation (kPa);

ϕ': angle of internal friction of soil;

IR: inundation rate, where IR is equal to vertical distance water travels during inundation per time;

δ': friction angle between pile surface and soil; and

$k_{i,f}$: interface constant, that depends on pile material and installation method of the pile.

The effect of Cp, σ, and IR on the rate of increase in drag load due to inundation is expressed in Figures 6.1 through 6.5, where drag load in kg is plotted against inundation time in minutes. In these figures, each straight line is a line that connects the maximum drag load on the pile before inundation $Q_{n(max)}$ and the maximum drag load acting on the pile after inundation from the bottom $Q'_{n(max)}$.
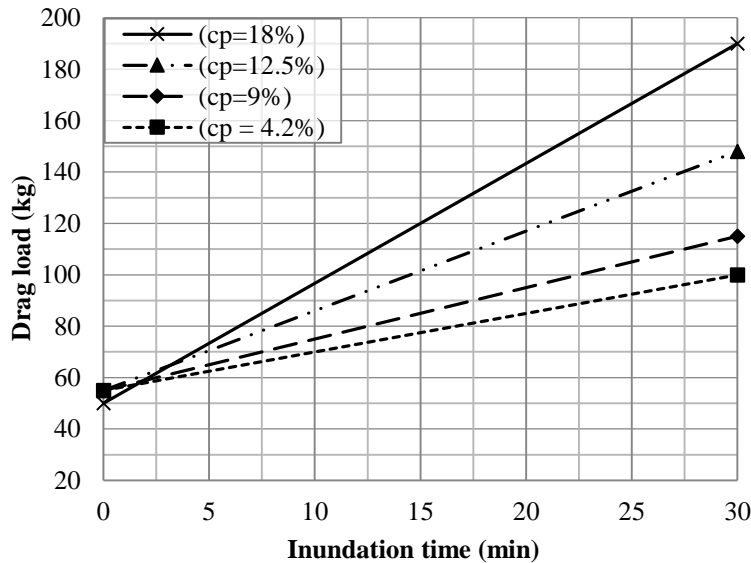
Figure 6.1 Drag load VS time of inundation, for IR=1m/hr & σ =120kPa
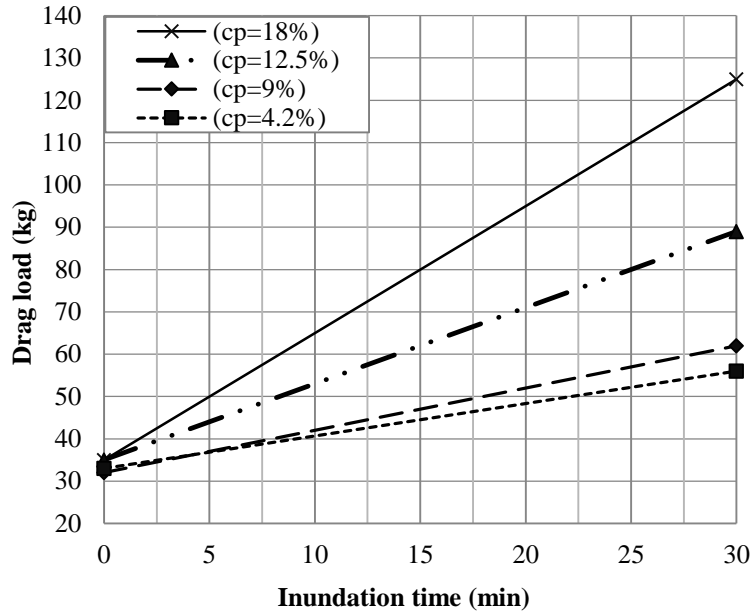
Figure 6.2 Drag load VS time of inundation (min) for IR=1m/hr & σ =80kPa
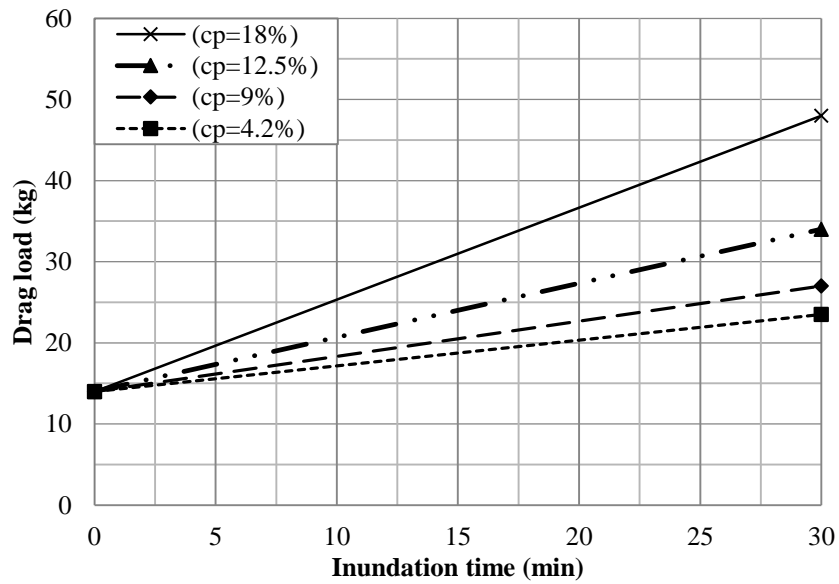
Figure 6.3 Drag load VS time of inundation, for IR=1m/hr & σ =40kPa
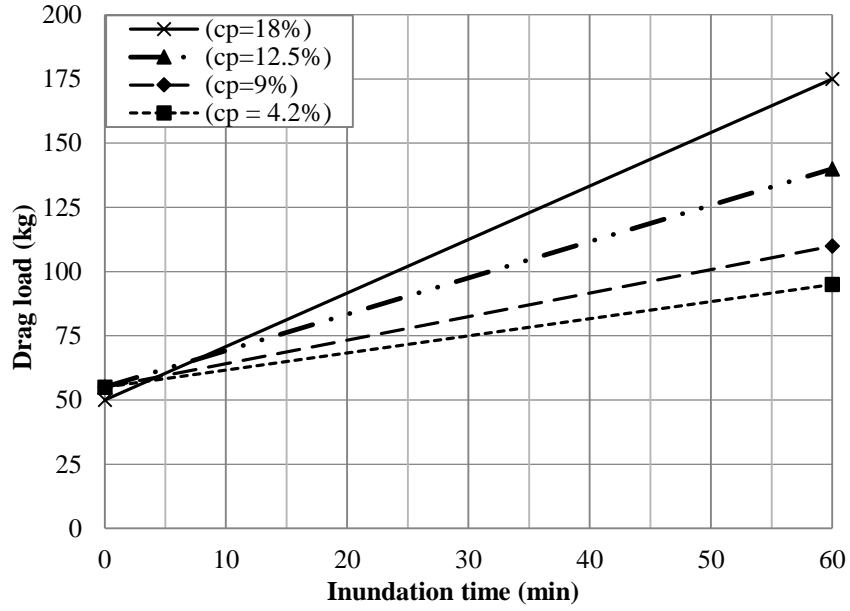
Figure 6.4 Drag load VS time of inundation, for IR=0.5m/hr & σ =120kPa
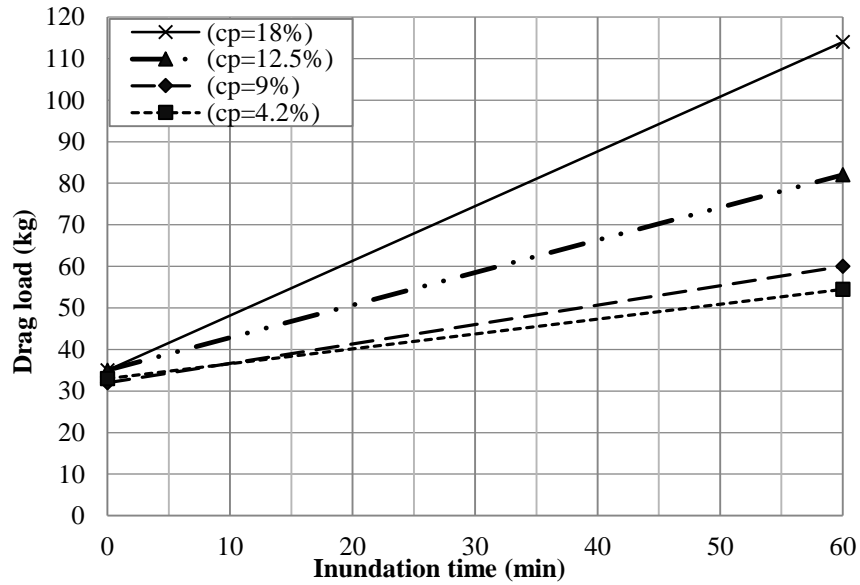
Figure 6.5 Drag load VS time of inundation, for IR=0.5m/hr & σ =80kPa
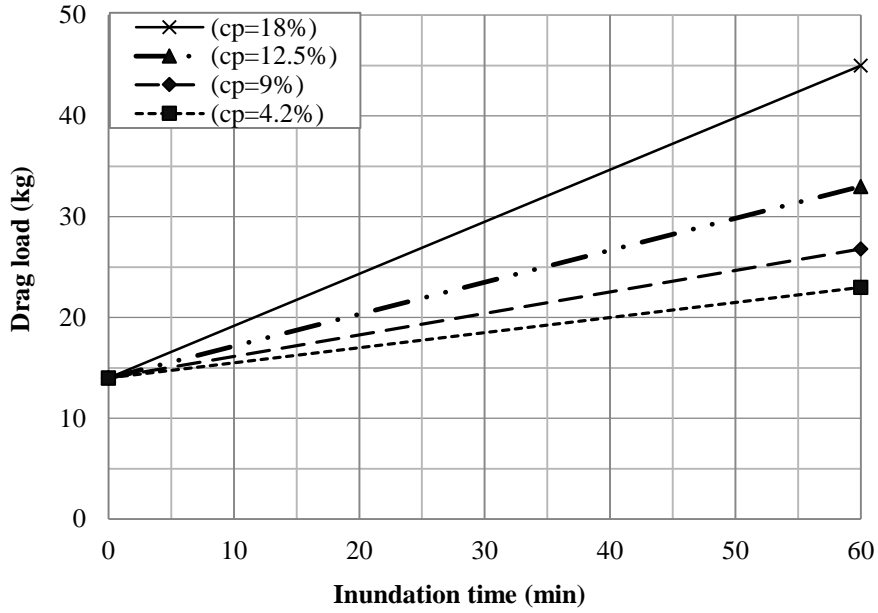
Figure 6.6 Drag load VS time of inundation, for IR=0.5m/hr & σ =40kPa
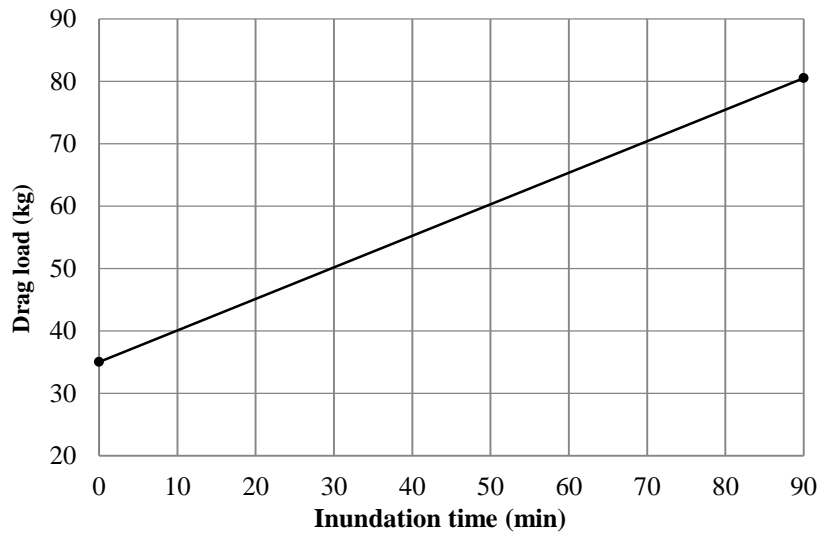
Figure 6.7 Drag load VS time of inundation, for IR=0.33m/hr, C_p=12.5% and σ =80kPa

For inundation rates 0.33, 0.5 and 1m/hr, the average rate of increase in drag load with respect to

time can be deduced from the slope of the straight lines in Figures 6.1 through 6.7, and the values

were found to be as follows from Equation [6.2] and Table 6.1:

$$\Delta Q'_n = \Delta t * k_{(t)} \dots \dots \quad [6.2]$$

$$const: k_{(t)} = \frac{\Delta Qn(\text{kg})}{\Delta t(\text{min})}$$

Table 6.1 Rate of increase in drag load with respect to time

C_p (%)	For σ =40kPa			For σ =80kPa			For σ =120kPa		
	$k_{(t)}$ for IR: 1m/hr	$k_{(t)}$ for IR: 0.5m/hr	$k_{(t)}$ for IR: 0.33m/hr	$k_{(t)}$ for IR:1m/hr	$k_{(t)}$ for IR: 0.5m/hr	$k_{(t)}$ for IR: 0.33m/hr	$k_{(t)}$ for IR: 1m/hr	$k_{(t)}$ for IR: 0.5m/hr	$k_{(t)}$ for IR: 0.33m/hr
4.2	0.3167	0.15	0.05	0.767	0.358	0.23	1.5	0.6667	0.32
9	0.433	0.2133	0.14	1	0.4667	0.32	2	0.9167	0.73
12.5	0.667	0.3167	0.26	1.8	0.7833	0.506	3.1	1.4167	1.12
18	1.133	0.5167	0.45	3	1.3167	1.1	4.67	2.0833	1.25

The relationships presented in these figures were used for establishing the values of constant $k_{(t)}$ in Equation [6.3] for estimating the drag load at any time *t* after inundation, knowing the rate of inundation.

$$Q'_{n(t)} = k_{(t)} * t \dots \dots \dots \dots \dots \quad [6.3]$$

6.2.2 Maximum Drag Load

In this section, an analytical model is introduced for calculating the maximum drag load acting on end bearing piles due to the inundation of collapsible soils from the bottom $Q'_{n(max)}$, based on the current experimental study tests results. The maximum drag load before inundation $Q_{n(max)}$ can be calculated using the beta method:

$$q_n = \Sigma \sigma K \tan \delta' \dots \dots \dots \dots \dots \quad [6.4]$$
$$\beta = K \tan \delta' \dots \dots \dots \dots \dots \dots \dots \quad [6.5]$$

$$q_n = \Sigma \sigma \, \beta \,\ldots\ldots\ldots\ldots\ldots\ldots\ldots \quad [6.6]$$

$$K_s = 1 - \sin \varphi' \,\ldots\ldots\ldots\ldots\ldots \quad [6.7]$$

$$Q_{n(max)} = \int_{0}^{L} \beta(\pi D)\,(\gamma'Z + \sigma)\,dz \,\ldots \quad [6.8]$$

The maximum drag load acting on piles due to the full inundation of collapsible soils from the bottom $Q'_{n(max)}$ can be calculated by integrating the NSF (f_n) along the pile length using the negative skin friction factor $\bar{\beta}$ introduced by Mashhour (2009) as shown in Equation [6.9].

$$Q'_{n(max)} = \int_{0}^{L} \bar{\beta}(\pi D)\,(\gamma'Z + \sigma)\,dz \,\ldots \, [6.9]$$

The neutral plane is located at the pile tip for all the cases analyzed in this research, and the distribution of f_n along the pile is presented in Figures 6.8 and 6.9. These distribution profiles were deduced based on the numerical model postulated by Kakoli (2011) and Noor et al., (2013), which showed agreement with the field data obtained in the literature (Lee et., al 2002; Chen et., al 2008; Ma et., al 2009 and Weiping et al., 2014).

(a) σ = 40 kPa   **(b) σ = 80 kPa**   **(c) σ = 120 kPa**
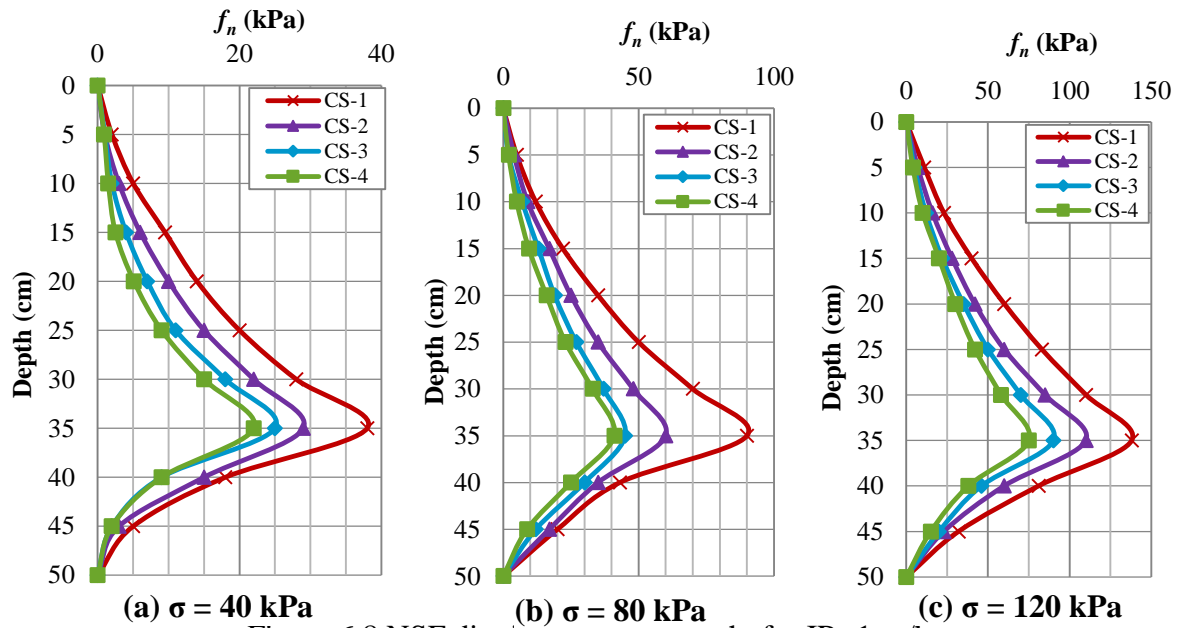
Figure 6.8 NSF distribution with depth, for IR=1 m/hr

(a) σ = 40 kPa   **(b) σ = 80 kPa**   **(c) σ = 120 kPa**
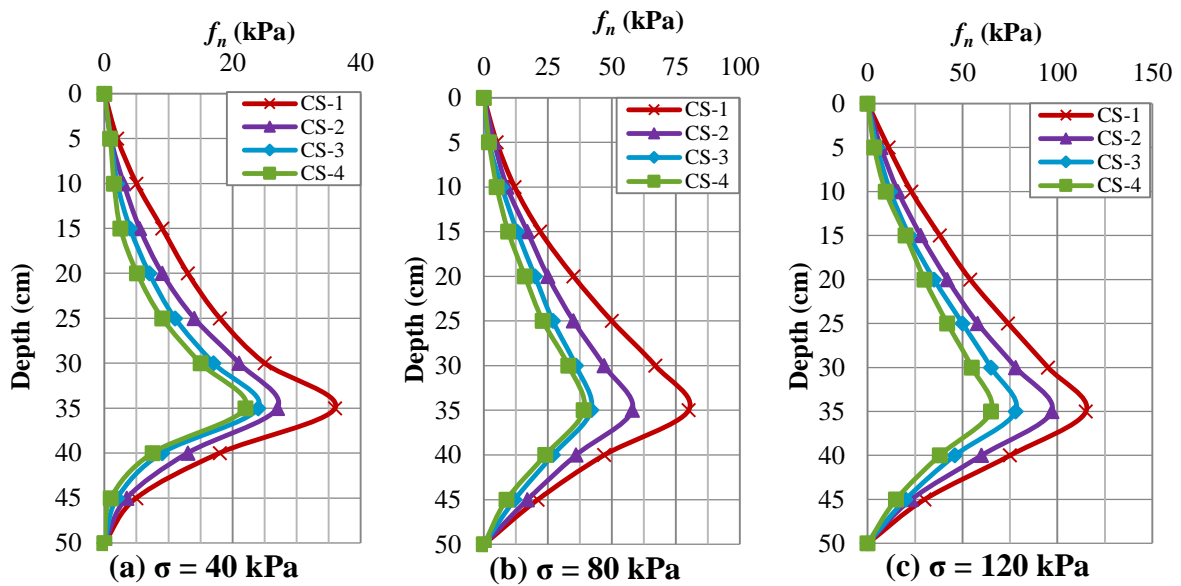
Figure 6.9 NSF distribution with depth, for IR=0.5 m/hr

The average skin friction f_n values were used in the analysis, acting on the entire pile length since the neutral plane is located at the pile tip.

The values of the negative skin friction coefficient in collapsible soils $\bar{\beta}$ proposed in this section, are based on the experimental results obtained in the current study. Equation [6.10] was applied to obtain the values of $\bar{\beta}$, as all the other parameters were obtained by measurements.

$$\bar{\beta} = \frac{Q'_{n(max)}}{\int_0^L (\pi D)\,(\gamma'Z\,+\,\sigma)\,dz} \quad \text{...} \text{...} \text{...} \text{...} \text{...} \; [6.10]$$

Figures 6.10 through 6.13 present the relationships between $\bar{\beta}$, inundation pressure and collapse potential for the different inundation rates applied in the experiments.
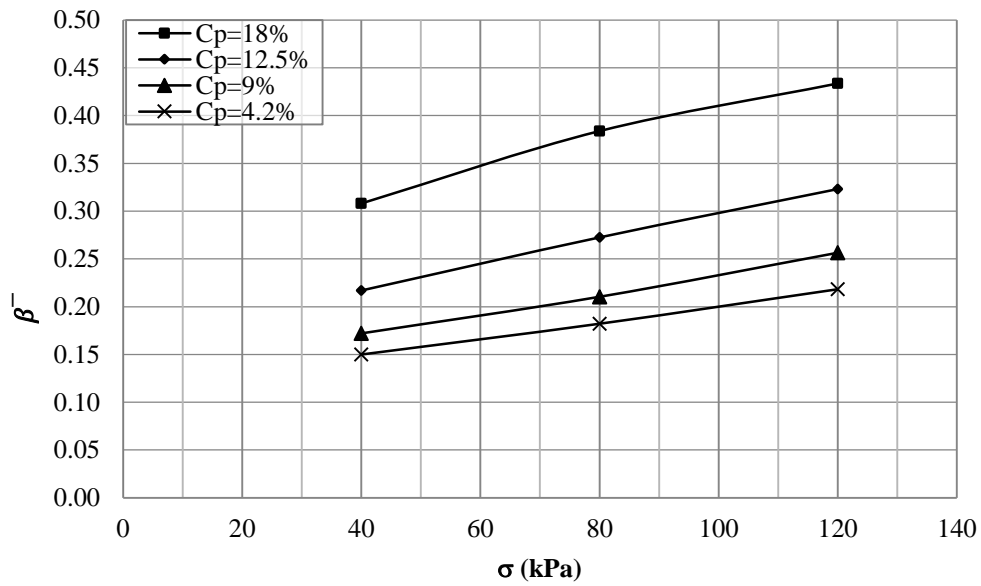
Figure 6.10 $\bar{\beta}$ VS inundation pressure for different soils for IR: 1m/hr
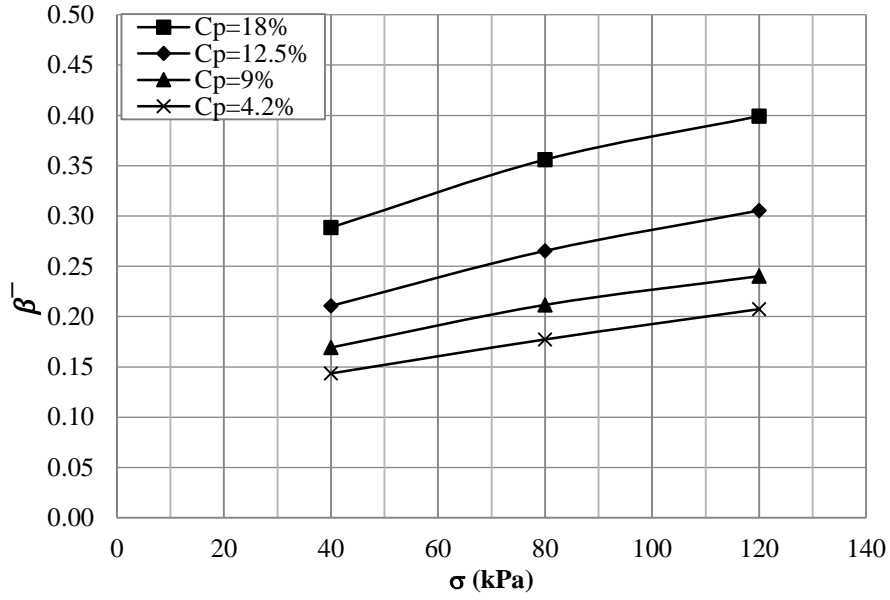
Figure 6.11 $\bar{\beta}$ VS inundation pressure for IR: 0.5m/hr
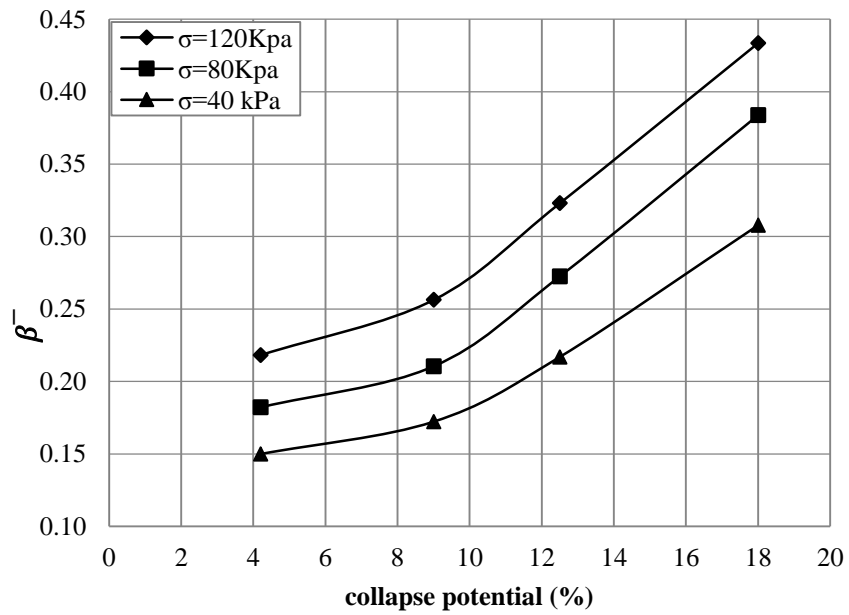
Figure 6.12 $\bar{\beta}$ VS collapse potential for inundation IR: 1m/hr
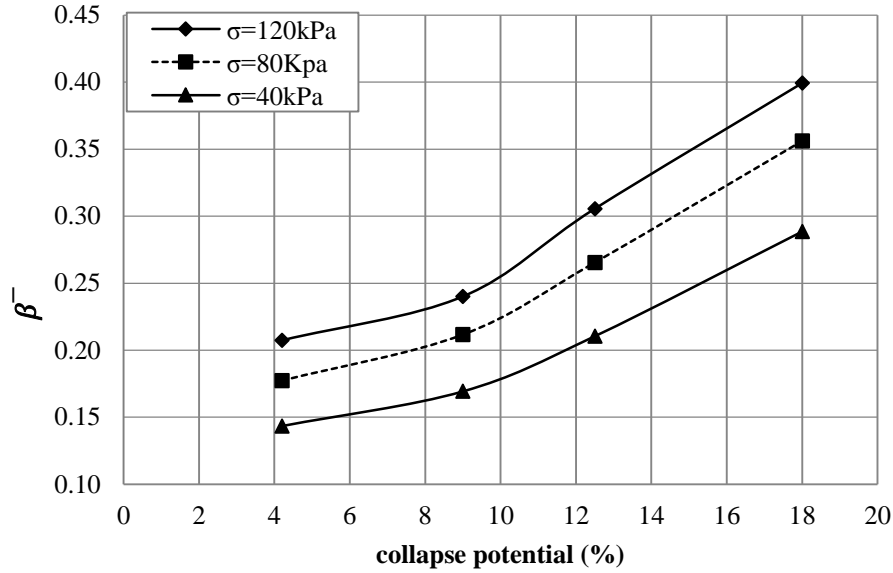
Figure 6.13 $\bar{\beta}$ VS collapse potential for IR: 0.5m/hr

The following equation is introduced to calculate $\bar{\beta}$, taking into account the inundation pressure, collapse potential and inundation rate:

$$\bar{\beta} = k_1 C_P + k_2 \dots\dots\dots\dots \quad [6.11]$$

where the values of constants k_1 and k_2 were calculated from relationships and summarized in Tables 6.2 and 6.3 as functions of the soil collapse potential, inundation pressure and inundation rate.

Table 6.2 Values of constants k_1 and k_2 for inundation rate 0.5m/hr

σ (kPa)	C_p (%)	k_1	k_2
40	0-9	0.0051	0.1254
80		0.0072	0.1471
120		0.0068	0.1787
40	9-18	0.0133	0.0472
80		0.0161	0.0658
120		0.0176	0.0828

Table 6.3 Values of constants k_1 and k_2 for inundation rate 1m/hr

σ (kPa)	C_p (%)	k_1	k_2
40		0.0047	0.1303
80	0-9	0.0059	0.1573
120		0.0079	0.1849
40		0.0152	0.0321
80	9-18	0.0193	0.0342
120		0.0197	0.0779

Correction factor Rc introduced by Mashhour (2009), accounts for the effect of collapsible soil, as given in Equation [6.12], and thus $Q'_{n(max)}$ can be calculated from Equation [6.13], so that:

$$R_c = \frac{\bar{\beta}}{\beta} = \frac{k_1 C_P + k_2}{(1 - sin\varphi')\tan\delta} \geq 1.0 \dots \text{ [6.12]}$$

$$Q'_{n(max)} = R_C\, Q_{n(max)} \dots\dots\dots\dots\dots\dots \text{ [6.13]}$$

The values of $\bar{\beta}$ and R_c are deduced based on experimental results summarized in Table 6.4.

Table 6.4 Negative skin friction coefficient $\bar{\beta}$ from the experimental tests

Soil Type	C_p (%)	σ (kPa)	IR (m/hr)	φ' (°)	γ (kN/m³)	$Q_{n(max)}$ (kg)	β	$Q'_{n(max)}$ (kg)	$\bar{\beta}$	Rc
CS-1	18	40	1	31	15.3	14	0.093	48	0.31	3.31
CS-1	18	40	0.5	31	15.3	14	0.093	45	0.29	3.11
CS-1	18	80	1	31	15.3	35	0.116	125	0.38	3.51
CS-1	18	80	0.5	31	15.3	35	0.116	116	0.36	3.26
CS-1	18	120	1	31	15.3	50	0.111	190	0.43	3.76
CS-1	18	120	0.5	31	15.3	50	0.111	175	0.4	3.46
CS-2	12.5	40	1	35	16.2	14	0.093	34	0.22	2.34
CS-2	12.5	40	0.5	35	16.2	14	0.093	33	0.21	2.27
CS-2	12.5	80	1	35	16.2	35	0.116	89	0.27	2.49
CS-2	12.5	80	0.5	35	16.2	35	0.116	85	0.27	2.38
CS-2	12.5	120	1	35	16.2	55	0.122	148	0.32	2.66
CS-2	12.5	120	0.5	35	16.2	55	0.122	140	0.31	2.51
CS-3	9	40	1	38.5	16.25	14	0.092	27	0.172	1.85
CS-3	9	40	0.5	38.5	16.25	14	0.092	26	0.17	1.79
CS-3	9	80	1	38.5	16.25	32	0.106	62	0.21	1.90
CS-3	9	80	0.5	38.5	16.25	32	0.106	61	0.21	1.87
CS-3	9	120	1	38.5	16.25	55	0.122	115	0.26	2.06
CS-3	9	120	0.5	38.5	16.25	55	0.122	110	0.24	1.91
CS-4	4.2	40	1	40	16.28	14	0.092	23.5	0.15	1.61
CS-4	4.2	40	0.5	40	16.28	14	0.092	22.5	0.14	1.54
CS-4	4.2	80	1	40	16.28	33	0.109	56	0.18	1.66
CS-4	4.2	80	0.5	40	16.28	33	0.109	54.5	0.18	1.62
CS-4	4.2	120	1	40	16.28	55	0.122	100	0.22	1.79
CS-4	4.2	120	0.5	40	16.28	55	0.122	95	0.21	1.70

Numerical results were used to extend the results obtained from the experimental study for a wider range of parameters. Figures 6.14 and 6.15 show the variation of *Rc* with respect to the collapse potential and inundation pressure based on the experimental and numerical results. It can be observed from the previous tables and figures based on experimental results that the effect of inundation rate was very minimal (up to a maximum of 8%) and can be ignored
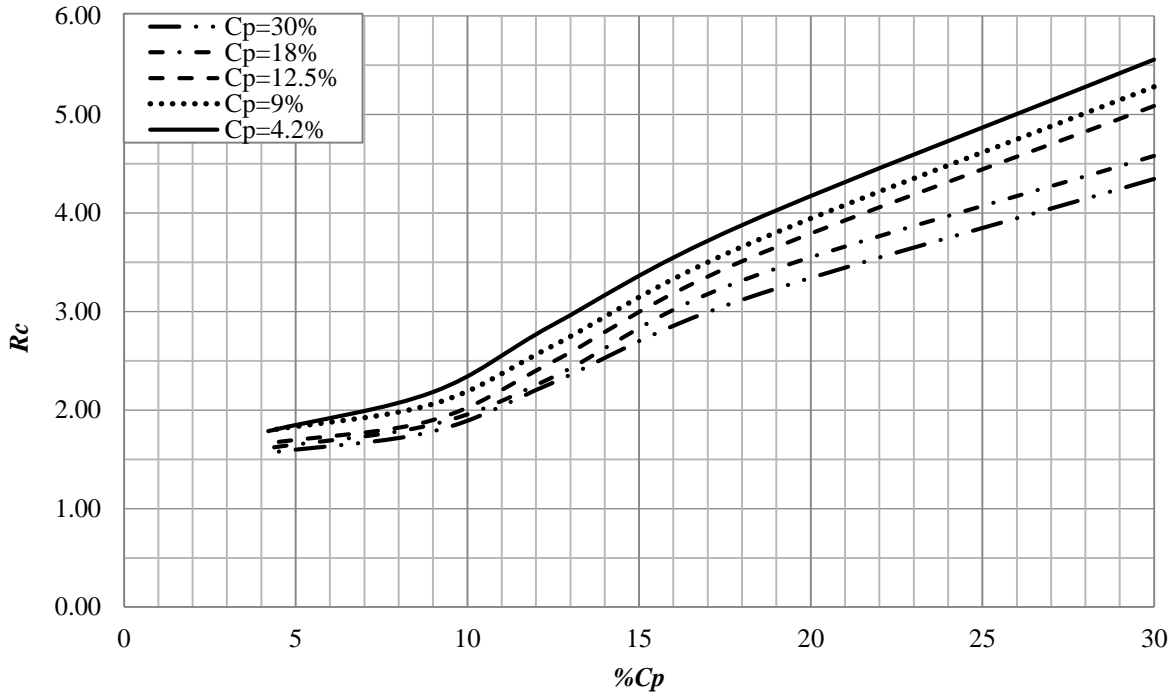
Figure 6.14 Correction factor Rc versus C_p
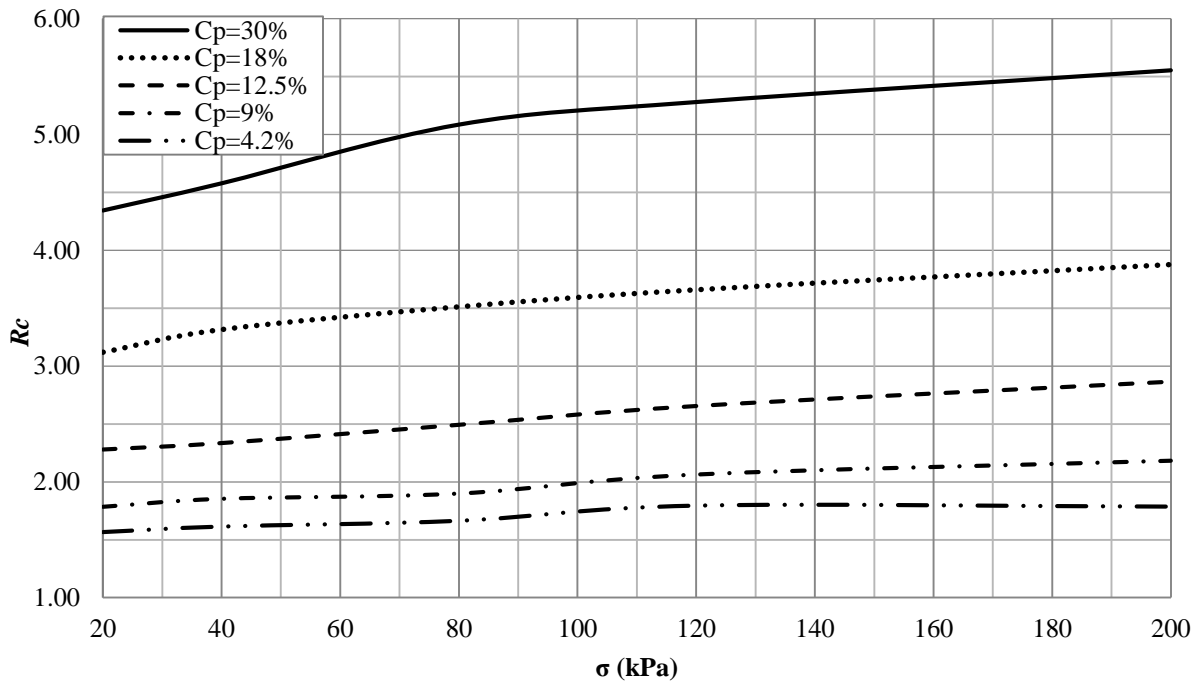
Figure 6.15 Correction factor Rc versus C_p

The negative skin friction coefficient in collapsible soils $\bar{\beta}$ and correction factor Rc from these figures can be obtained from Equations [6.14] and [6.15]

$$\bar{\beta} = 0.001\sigma + 0.015C_P \;............\; [6.14]$$

$$R_c = \frac{\bar{\beta}}{\beta} = \frac{0.001\sigma + 0.015C_P}{(1 - sin\varphi')\tan\delta'} \geq 1.0 \;...\; [6.15]$$

6.3 Analytical Model for Partial Inundation

Full collapse occurs due to full inundation, ie 100% saturation, and so inundation caused by rise in the groundwater table is considered to be the critical wetting scheme responsible for soil collapse and accordingly for the development of high negative skin friction on piles. In reality however, many other sources of wetting can cause partial inundation (and the associated risk of collapse) reaching degrees of saturation much less than 100%. It is therefore imperative to take into account the effect of the degree of wetting ($\%D_W$) on drag load. The effects of Cp, σ, δ', ϕ' and $\%S$ on drag load are demonstrated in the experimental results presented in Figures 4.46 through Figure 4.51 and also in Figures 4.55, 4.56 and 4.57.

Since partial collapse takes place due to partial saturation, better understanding of unsaturated soil parameters is necessary in order to analyze the complex interaction between soils and pile surface under wetting conditions. The saturation water characteristic curves SWCC is one of the most important relationships to determine unsaturated soils behaviour, as it relates the degree of saturation of soil to soil suction, and thus the change in effective pressure as explained in the previous introductory chapters. In this section the SWCC of the soil mixtures used in the current experimental study was used to relate the rate of increase in degree of saturation (upon partial inundation) to the increase in drag load. The development of such a relationship should enable designers to predict the drag load at different stages of wetting, by knowing the SWCC of the soil.

An SWCC based on the GSD and soil index properties suggested by Zapata et al., (2000) was used in this investigation to generate the SWCC for the soil mixtures used in this study as shown in Figure 6.18.
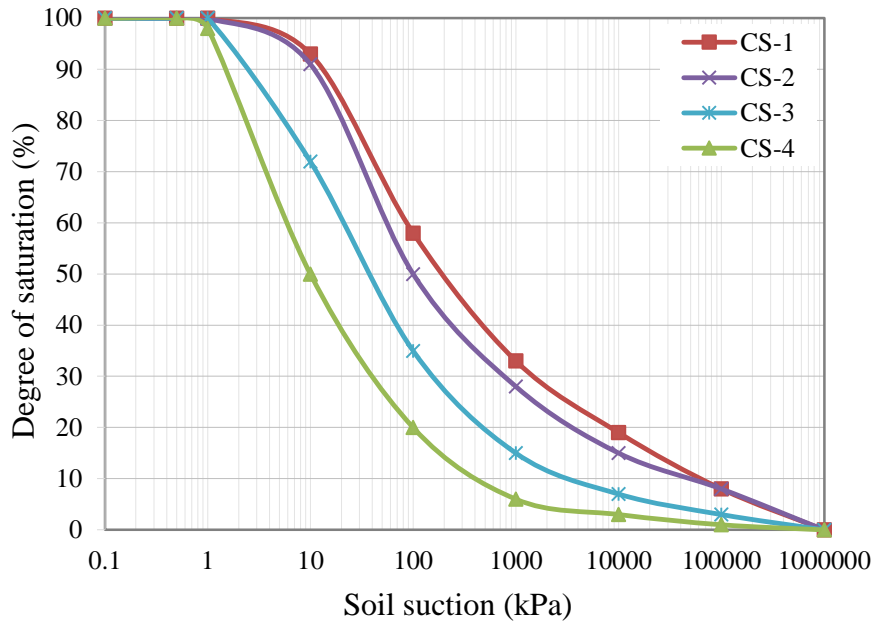
Figure 6.18 SWCC for collapsible soil mixtures

Volumetric water content can be written as a function of the instantaneous overall volume of a soil specimen, $(1 + e)$; and the gravimetric water content, w. Since gravimetric water content can be expressed as a function of soil suction, it is likewise possible to write the volumetric water content as a function of the soil suction as expressed in Equations [6.16, 6.17 and 6.18].

$$\theta(w) \frac{w(\psi)G_s}{1 + e(w)} \dots\dots\dots\dots\dots. \quad [6.16]$$

$$\theta = \frac{w(\psi)G_s}{1 + e} \dots\dots\dots\dots\dots. \quad [6.17]$$

$$\theta = \frac{w(S)G_s}{1 + e} \dots\dots\dots\dots\dots\dots. \quad [6.18]$$

The volumetric water content of the soil mixtures used in this study was determined from the equations above based on the response-to-wetting test measurements, and the values are summarized in Table 6.5, where:

θ_s = Saturated volumetric water content; and

θ_r = Residual volumetric water content

The coefficient of permeability in the unsaturated phase (k_w) can be determined from the SWCC, as it is directly proportional to the water content and inversely proportional to the matric suction. The relationship suggested by Brooks and Corey (1964) is presented in Equation [6.19]

$$k_w = k_s(S_e)^\delta \;................ \;[6.19]$$

where:

Se = Effective degree of saturation, determined from SWCC;

k_s = Coeffecient of permeability in the saturated phase;

k_a = Coeffecient of permeability in the unsaturated phase; and

δ = an empirical constant determined from the pore size distribution index (λ)

$$\delta = \frac{2 + 3\lambda}{\lambda} \;............ \;[6.20]$$

Table 6.5 Unsaturated soil parameters for collapsible soil mixtures

Soil Mix	Unsaturated phase			Saturated phase		
	k_a (cm/sec)	(%) S_o	(%) θ_r	(%) w_{sat}	k_{sat} (cm/sec)	(%) θ_s
CS-1	$3.73*10^{-05}$	16.75	7.44	17.76	$1.33*10^{-03}$	32.25
CS-2	$1.75*10^{-04}$	19.05	7.85	18.26	$4.83*10^{-03}$	32.78
CS-3	$2.43*10^{-04}$	19.35	7.89	20.15	$6.50*10^{-03}$	34.97
CS-4	$3.26*10^{-04}$	19.77	7.96	22.55	$8.33*10^{-03}$	37.49

The relationships between volumetric water content (θ) and soil suction (ψ) for collapsible soil mixtures were established based on the SWCC, are presented in Figure 6.19.
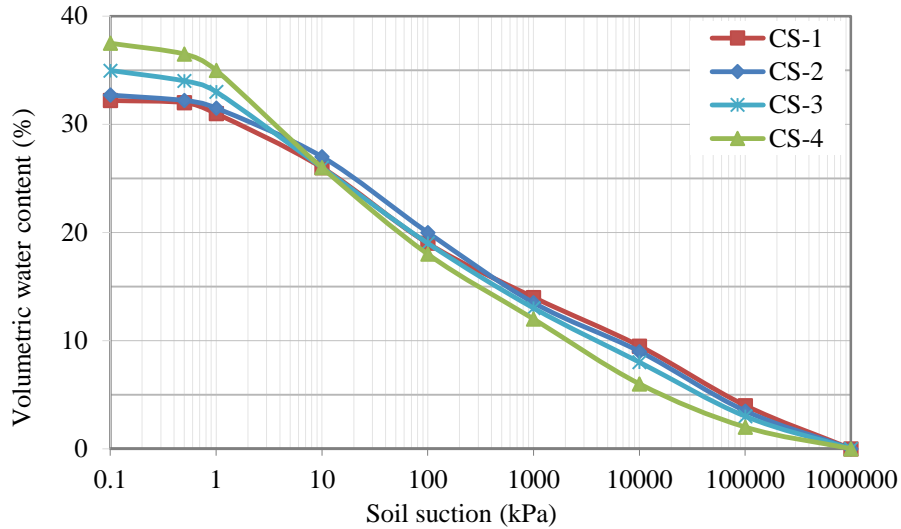
Figure 6.19 Matric suction VS Volumetric water content for collapsible soil mixtures

The analytical models presented here for calculating the maximum drag load, are based on the assumption that at this state where $Q'_{n\,(max)}$ was reached, the neutral plane was at the pile tip for all tests. This assumption had to be validated, especially for lower degrees of wetting. To insure the validity of this assumption, the infiltration of water in unsaturated soil mixtures is presented next. Equations 6.21, 6.22 and 6.23 can be used for calculating the infiltration rate (f), cumulative infiltration (F) and the flux water in soil respectively.

$$f = K\left(1 + \frac{\psi_f}{L}\right) \ldots\ldots\ldots\ldots\ldots\ldots\ldots\ldots \quad [6.21]$$

where

ψ_f: Pressure head (cm), negative for unsaturated soils, and positive for saturated soils; and

K : Unsaturated hydraulic conductivity (cm/min)

139

$$F = K_t + \Delta\theta\psi_f \ln\left(1 + \frac{F}{\Delta\theta\psi_f}\right) \dots\dots\dots\dots \; [6.22]$$

$$q = -K(\psi)\left(\frac{dh}{dz}\right) = -K(\psi)\left(\frac{h_2 - h_1}{z_2 - z_1}\right)\dots\dots \; [6.23]$$

where q : is the flux water in soil (cm/min)

Figure 6.20 illustrates the water infiltration distribution along the soil profile for different degrees of wetting, for soil mixture CS-1. Each relationship in the figure presents the distribution of the degree of saturation at the end of infiltration for each wetting increment.
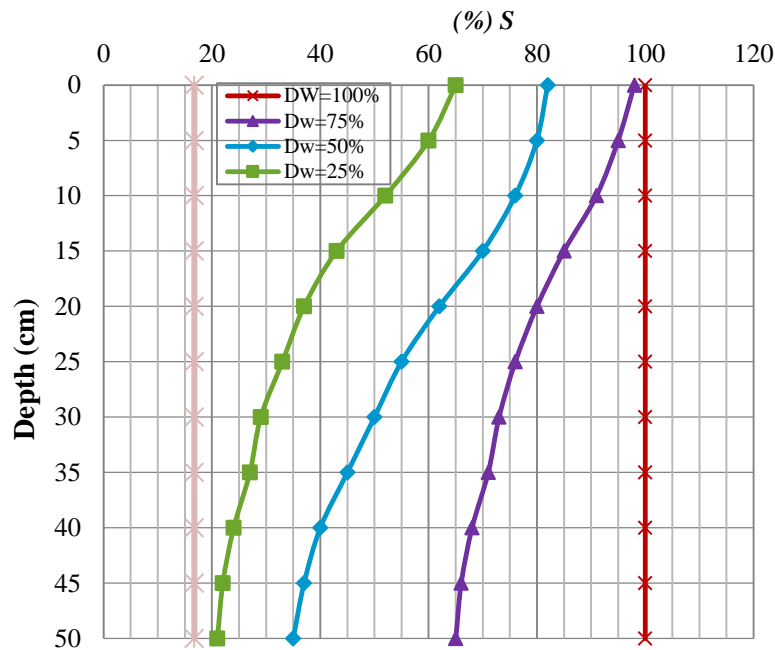
Figure 6.20 Degree of saturation VS soil depth for CS-1

It can be observed from Figure 6.20 that at an average degree of wetting of 25%, water infiltration covers the entire length of the soil, causing partial wetting along the entire length of the pile, sufficient to generate NSF along the entire length of the pile.

The distribution of f_n along the pile for different degrees of wetting is presented in Figure 6.21, where these distribution profiles were deduced based on data obtained in the literature.

(a) $C_p = 18\%$

(b) $C_p = 12.5\%$

(c) $C_p = 9\%$

(d) $C_p = 4.2\%$
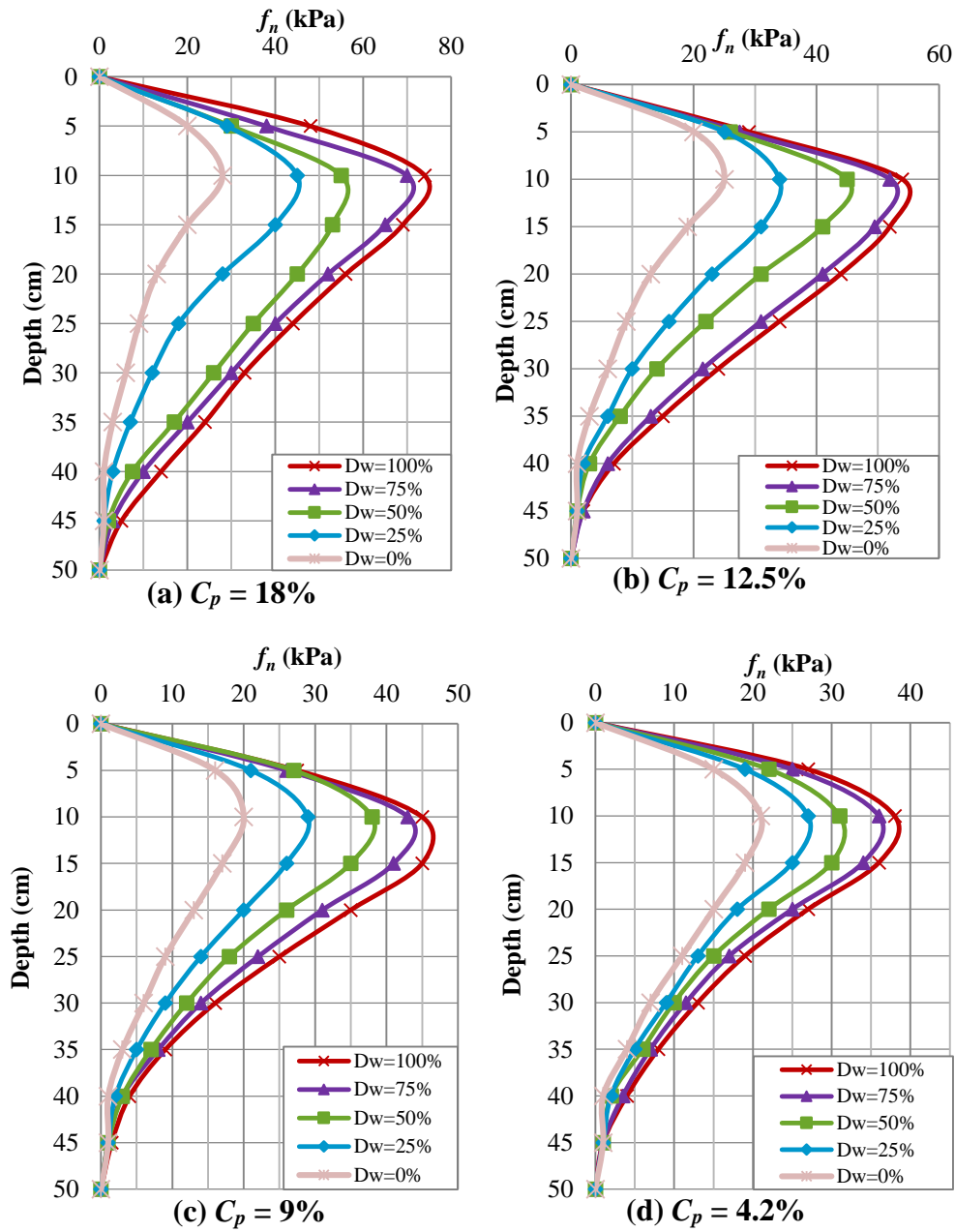
Figure 6.21 NSF distribution with depth for $\sigma = 80$ kPa

Figures 6.22 through 6.25 present the relationship between the degree of saturation with respect to the matric suction and the negative skin friction.
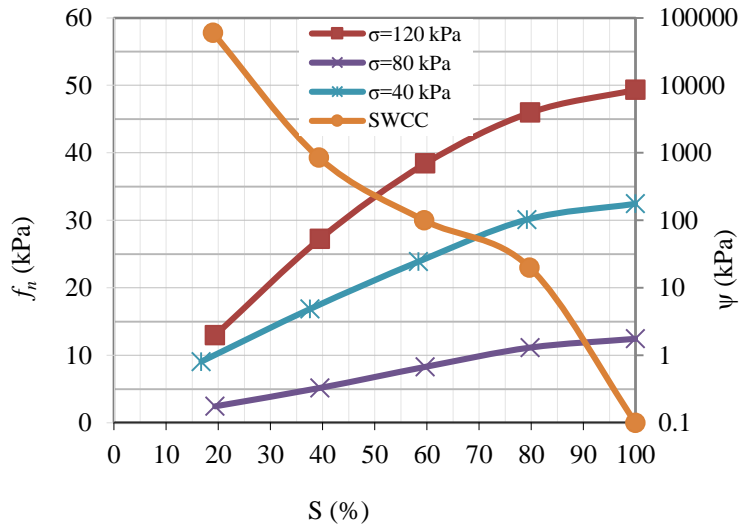
Figure 6.22 Degree of saturation VS NSF (f_n) and matric suction (ψ) for CS-1
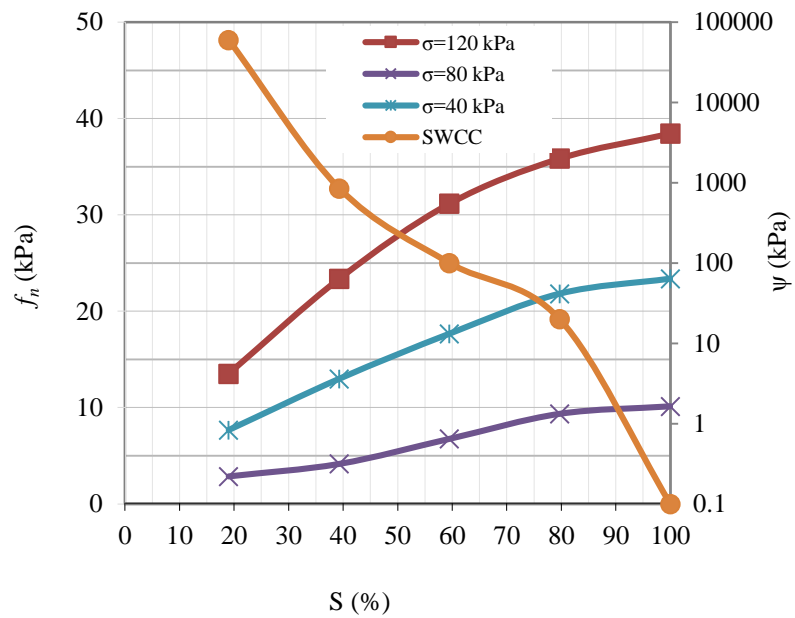
Figure 6.23 Degree of saturation VS NSF (f_n) and matric suction (ψ) for CS-2
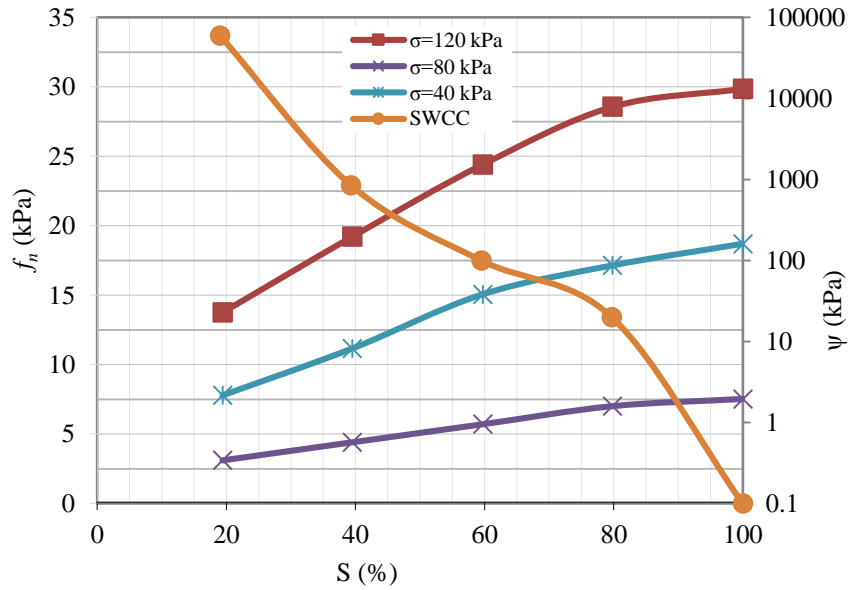
Figure 6.24 Degree of saturation VS NSF (f_n) and matric suction (ψ) for CS-3
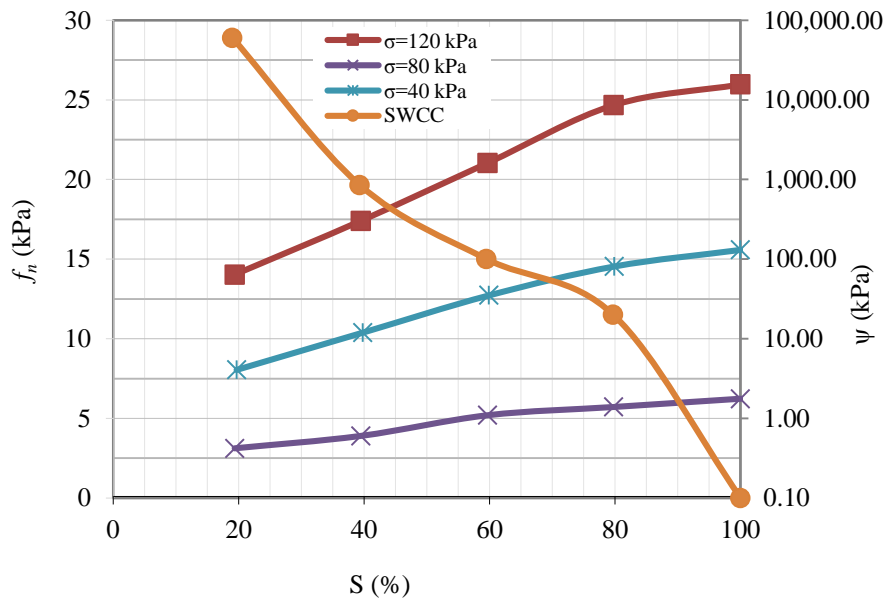
Figure 6.25 Degree of saturation VS NSF (f_n) and matric suction (ψ) for CS-3

In order to establish the analytical model for estimating drag load at different degrees of saturation for different C_p values and different inundation pressures, the values of $\bar{\beta}$ were obtained based on the experimental measurements for different degrees of saturation by back calculation as shown in Equation [6.24]. Equation [6.25] is introduced to calculate $\bar{\beta}$, knowing the collapse potential,

inundation pressure and the percentage of inundation; the values of constants in Equation [6.25] can be obtained from Table 6.6.

$$\bar{\beta} = \frac{Q'_{n(max)}}{\int_0^{L_{NP}} (\pi D) \, (\gamma' Z + \sigma) \, dz} \quad \text{... ...} \quad [6.24]$$

$$\bar{\beta} = k_3(k_1 C_P + k_2) \quad \text{... ... ...} \quad [6.25]$$

Table 6.6 Values of constants k_1 k_2 and k_3

C_p (%)	σ (kPa)	D_W (%)	k_3	k_1	k_2
0-9	40	0	0.00	0.0051	0.125
		25	0.51		
		50	0.81		
		75	0.95		
		100	1.00		
	80	0	0.00	0.0072	0.147
		25	0.67		
		50	0.82		
		75	0.93		
		100	1.00		
	120	0	0.00	0.0068	0.178
		25	0.62		
		50	0.81		
		75	0.94		
		100	1.00		
9-18	40	0	0.00	0.0133	0.047
		25	0.49		
		50	0.76		
		75	0.94		
		100	1.00		
	80	0	0.00	0.0161	0.065
		25	0.52		
		50	0.74		
		75	0.93		
		100	1.00		
	120	0	0.00	0.0176	0.082
		25	0.57		
		50	0.76		
		75	0.93		
		100	1.00		

Figures 6.26 to 6.29 present the relationships between the $\bar{\beta}$ value and the degree of wetting; the inundation pressure and the collapse potential.
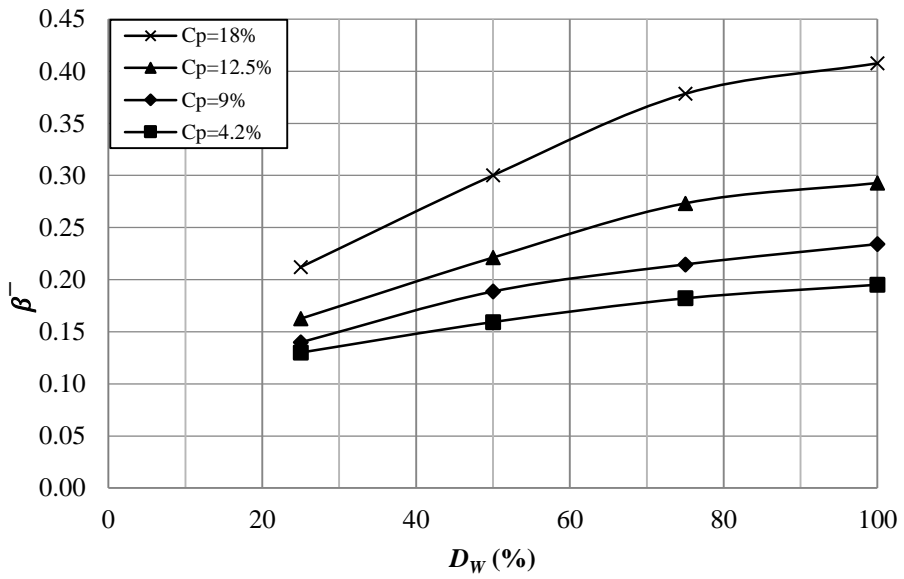
Figure 6.26 $\bar{\beta}$ versus degree of wetting for inundation pressure 80kPa
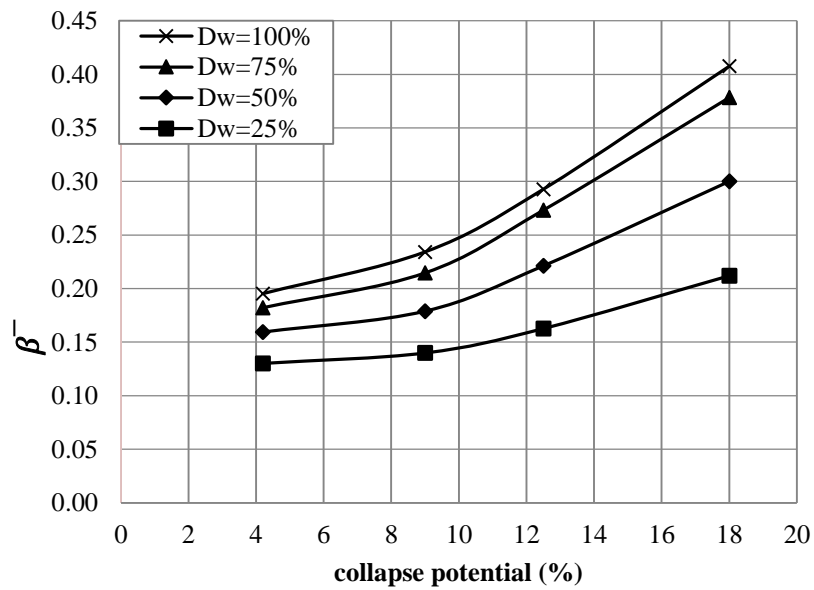
Figure 6.27 $\bar{\beta}$ versus collapse potential for inundation pressure 80kPa
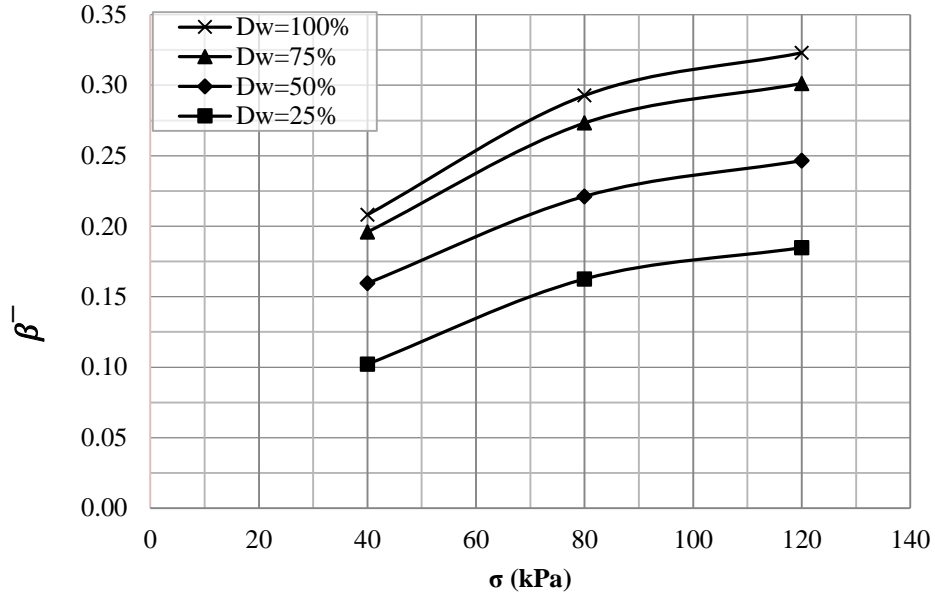
Figure 6.28 $\bar{\beta}$ versus inundation pressure for C_p=12.5%
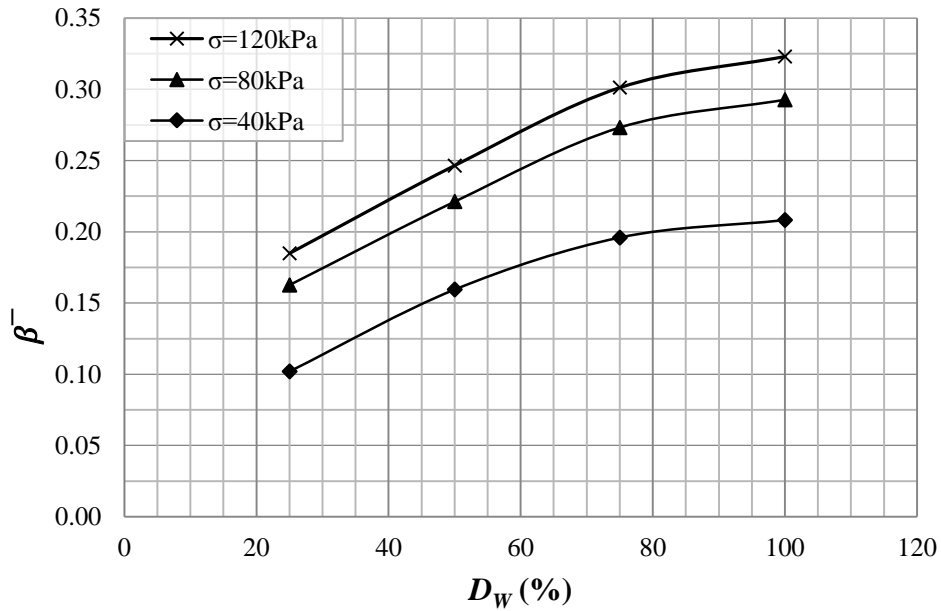
Figure 6.29 $\bar{\beta}$ versus degree of wetting for C_p=12.5%

Correction factor R_c can be calculated from Equation [6.26], and thus $Q'_{n(max)}$ can be calculated from Equation [6.27].

$$R_c = \frac{\bar{\beta}}{\beta} = \frac{(k_1 C_P + k_2)k_3}{(1 - sin\varphi')\, tan\,\delta'} \geq 1.0 \ldots [6.26]$$

$$Q'_{n(max)} = R_C\, Q_{n(max)} \ldots \ldots \ldots \ldots \ldots [6.27]$$

The values of $\bar{\beta}$ and R_c deduced based on experimental results are summarized in Table 6.7.

Table 6.7 Negative skin friction coefficient $\overline{\boldsymbol{\beta}}$ from the experimental tests

Soil Type	C_p (%)	σ (kPa)	% D_W	% θ	φ'	γ (kN/m³)	β	$Q'_{n(max)}$ (kg)	$\overline{\beta}$	R_c
CS-1	18	80	25	12.2	31	15.3	0.116	65	0.21	1.83
CS-1	18	80	50	18.1	31	15.3	0.116	92	0.30	2.58
CS-1	18	80	75	20.2	31	15.3	0.116	116	0.38	3.26
CS-1	18	80	100	32.2	31	15.3	0.116	125	0.41	3.51
CS-2	12.5	40	25	12.5	35	16.2	0.093	16	0.10	1.10
CS-2	12.5	40	50	19.8	35	16.2	0.093	25	0.16	1.72
CS-2	12.5	40	75	24.1	35	16.2	0.093	32	0.20	2.20
CS-2	12.5	40	100	32.4	35	16.2	0.093	34	0.21	2.34
CS-2	12.5	80	25	12.9	35	16.2	0.116	50	0.16	1.40
CS-2	12.5	80	50	20.0	35	16.2	0.116	68	0.22	1.90
CS-2	12.5	80	75	24.2	35	16.2	0.116	84	0.27	2.35
CS-2	12.5	80	100	32.7	35	16.2	0.116	90	0.29	2.52
CS-2	12.5	120	25	13.1	35	16.2	0.122	79	0.18	1.61
CS-2	12.5	120	50	20.3	35	16.2	0.122	95	0.25	2.15
CS-2	12.5	120	75	24.5	35	16.2	0.122	111	0.30	2.48
CS-2	12.5	120	100	33.0	35	16.2	0.122	120	0.32	2.66
CS-3	9	80	25	15.4	38.5	16.25	0.106	43	0.14	1.32
CS-3	9	80	50	23.2	38.5	16.25	0.106	55	0.18	1.68
CS-3	9	80	75	27.2	38.5	16.25	0.106	66	0.21	2.02
CS-4	9	80	100	34.97	40	16.28	0.106	72	0.23	2.21
CS-4	4.2	80	25	19.1	40	16.28	0.109	40	0.13	1.19
CS-4	4.2	80	50	26.0	40	16.28	0.109	49	0.16	1.46
CS-4	4.2	80	75	29.2	40	16.28	0.109	56	0.18	1.66
CS-4	4.2	80	100	37.5	40	16.28	0.109	60	0.20	1.78

Figures 6.30 through 6.32 show the variation of R_c with respect to the degree of wetting, collapse potential and inundation pressure.
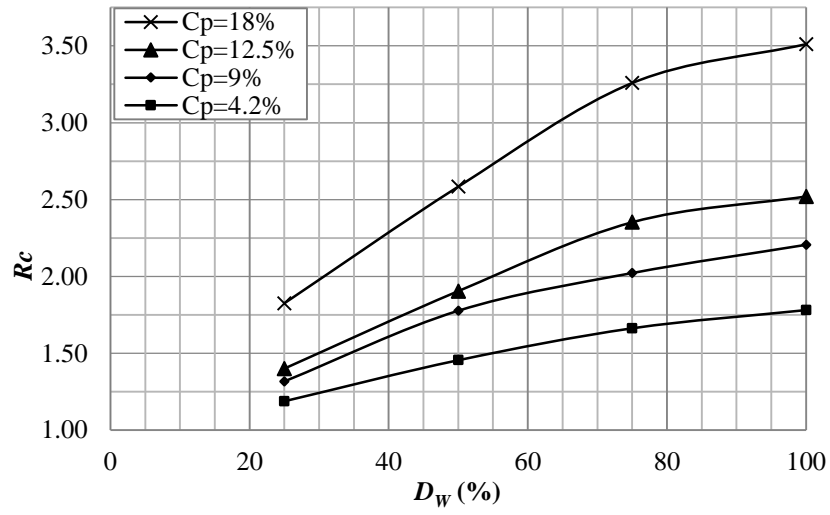
Figure 6.30 *Rc* versus degree of wetting for σ=80kPa
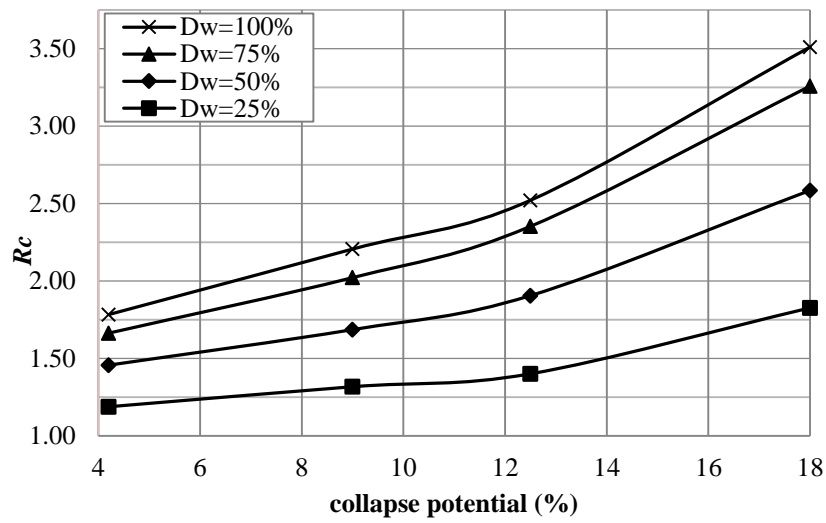
Figure 6.31 *Rc* versus collapse potential for inundation pressure 80kPa
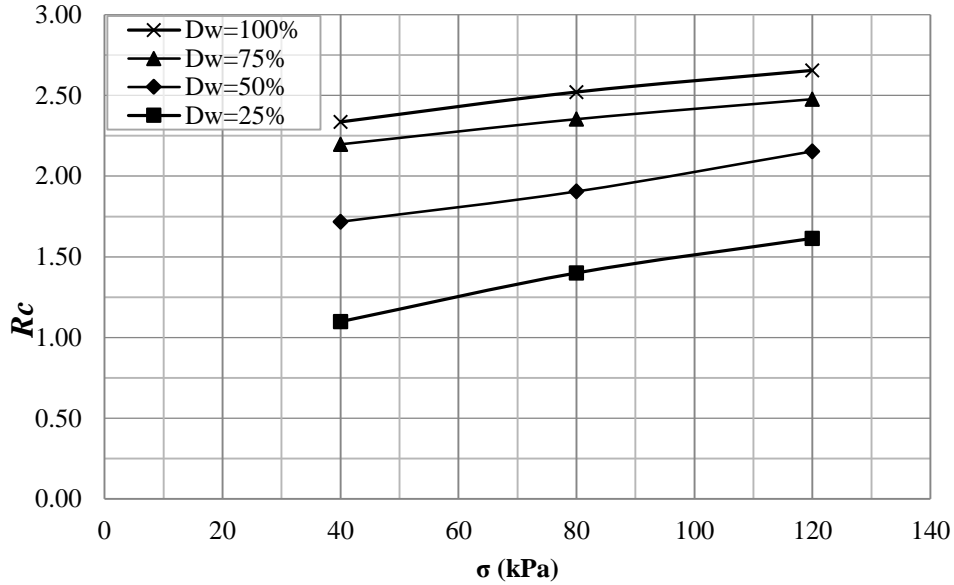
Figure 6.32 *Rc* inundation pressure for C_p=12.5%

Since the volumetric water content is one of the most important parameters governing unsaturated soil behaviour, the relationship between volumetric water content (%θ) versus $\bar{\beta}$ and R_c are presented in Figures 6.33 and 6.34, respectively.
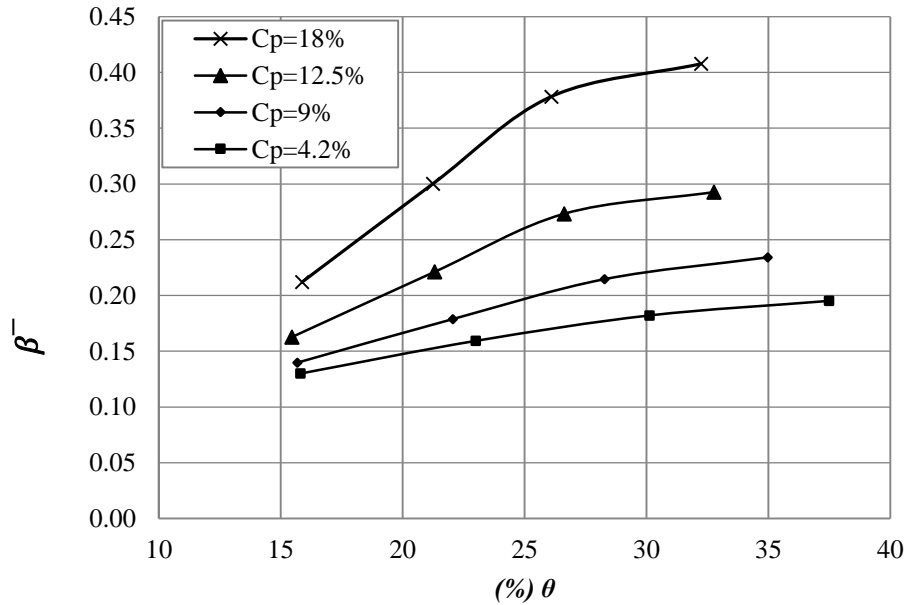
Figure 6.33 $\bar{\beta}$ versus collapse potential for inundation pressure 80kPa
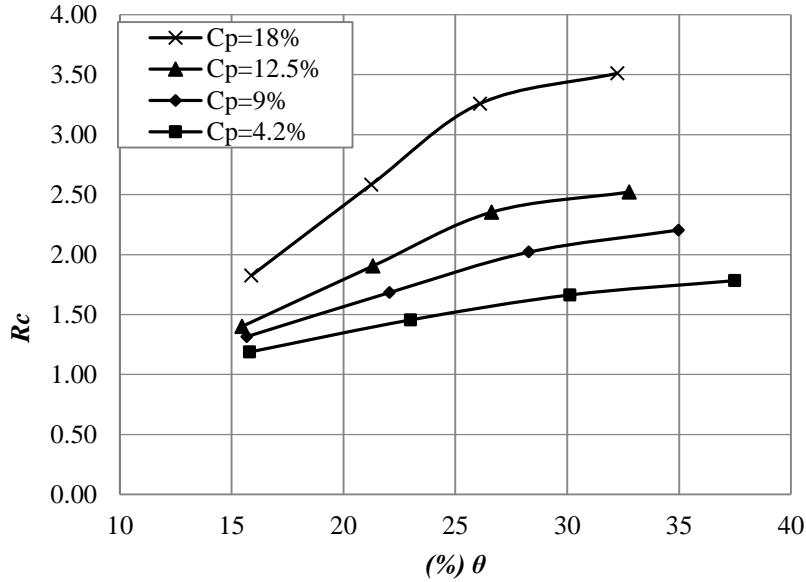
Figure 6.34 *Rc* versus volumetric water content for σ=80kPa

6.4 Empirical Method for Estimating NSF

An empirical method based on the tests results is presented herein, introducing an equation for obtaining the negative skin friction stresses developed on the pile shaft due to the full inundation of the collapsible soil.

Figure 6.35 presents the relationship between the average negative skin friction stress after inundation; and the inundation pressure obtained from experiments, for different collapsible soil mixtures.

The values of the skin friction after inundation $f'_{n(avg.)}$ were obtained directly from Equation [6.28], knowing the maximum drag load after inundation $Q'_{n(max)}$.

$$f'_{n(avg.)} = \frac{Q'_{n(max)}}{\int_0^L (\pi D)\ dz} \dots \dots\ [6.28]$$

150
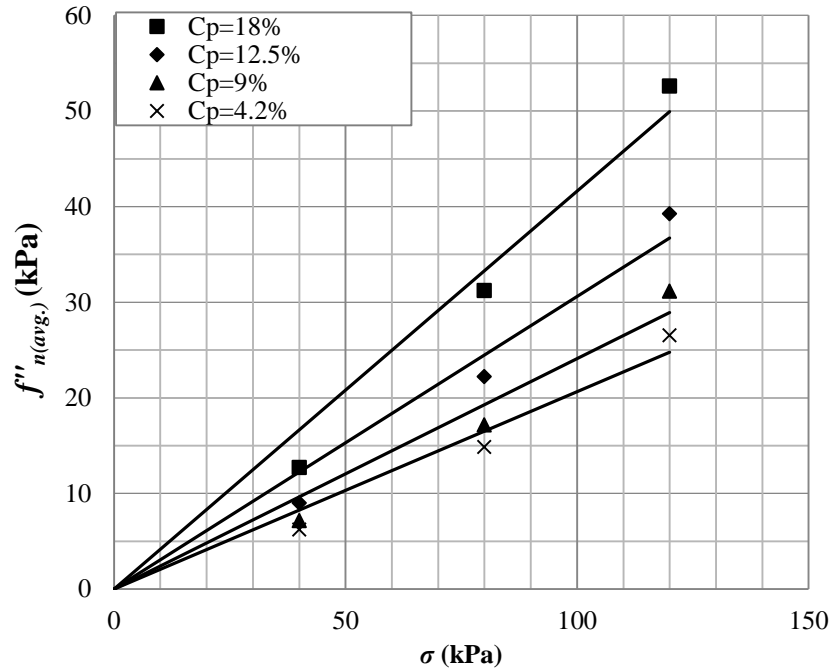
Figure 6.35 Average NSF after inundation $f'_{n(avg.)}$ vs inundation pressure σ

Figure 6.35 shows that the relationship between $f'_{n(avg.)}$ and σ is linear for each of the soil mixtures, where all the lines pass through the origin. The negative skin friction can thus be determined from Equation [6.29].

$$f'_n = \sigma \tan \alpha \ \dots \dots \dots \ [6.29]$$

The linear relationships presented in Figure 6.36 make it possible to determine the values of α; these values are summarized with respect to collapse potential in Table 6.8.
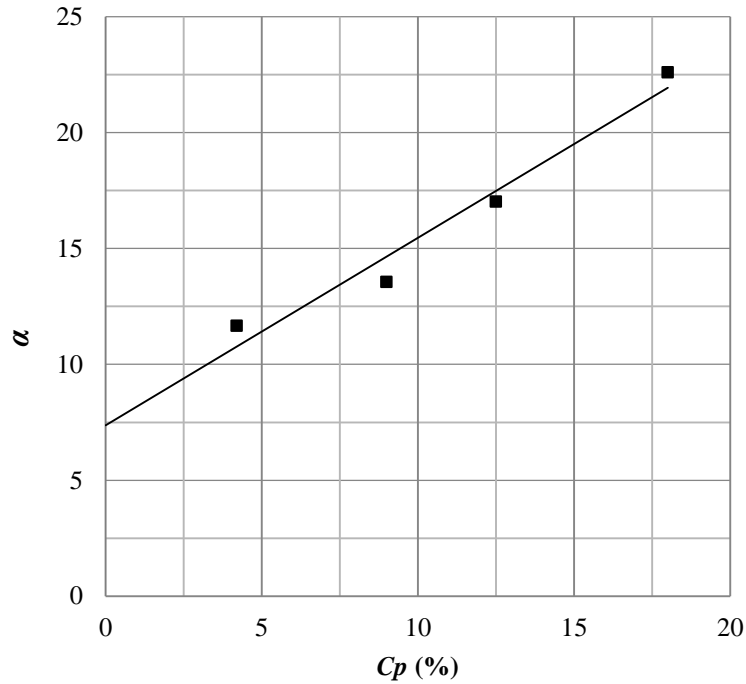
Figure 6.36 α versus collapse potential C_p

Table 6.8 Variation of tan α for different collapse potential values

C_p (%)	tan α	α
18	0.416	22.59
12.5	0.3059	17.02
9	0.241	13.55
4.2	0.2064	11.67

6.5 Validation of Analytical Model

Field tests results reported in the literature (Li et al. 1994; Grigorian 1997; Chen et al. 2008; and Ma et al. 2009); were used to validate the present analytical model. Table 6.9 summarizes some of the soil properties for field tests reported by Grigorian (1997).

Table 6.9 Soil properties after Grigoryan (1997)

Region	Collapsible layer depth from the ground level (m)	Collapsible layer thickness (m)	e_o	w_n (%)	c (kPa)	G_s	φ (°)	C_p	γ_{bulk} (kPa)
Volgodon	11	4	0.73	14	24	2.68	17	8	17
Nikopol	0	6	0.91	7	5	2.8	20	7	14.3

In China loess soils cover substantial areas, forming almost 6.6% of the total land area (Lin and Liang 1982; and Lin and Xu 2008). The collapsible soil properties of China's loess soils have been studied by many researchers, providing ranges for a number of parameters for different zones as demonstrated in Table 6.10; (suggested by Lin and Liang (1982)). For field tests reported by Li et al. (1994); Chen et al. (2008); and Ma et al. (2009), some missing parameters were reasonably assumed based on loess soil properties for zones in China provided by Lin and Liang (1982) and Lin and Xu (2008).

Table 6.10 Soil Properties after Lin and Liang (1982)

Region	Category of collapsibility	Unit Collapse δ_s	Initial Pressure P_{sh} (Mpa)	Subsidence under own weight on wetting	Unit Weight γ (kN/m³)	Void Ratio e	C (Mpa)	ϕ (°)
Lanzhou	III	0.05-0.12	0.02-0.05	Serious	14	1.16	0.025	20
Yanan	II-III	0.06 (mean)	0.03-0.06	Serious or Mild	14.5	1.05	0.025	25
Xian	II-III	0.04-0.08	0.06-0.12	Non-existent or Mild	15	1.1	0.025	21.5

Table 6.11 shows a summary of the data collected from field tests reported by Li et al. (1994); Grigorian (1997); Chen et al. (2008); and Ma et al. (2009).

Table 6.11 Validation of analytical model using field tests results

Researcher	Max NSF measured (kPa)		Pile Length (m)	Pile Diameter (m)	Neutral Plane (m)	NSF(calc) $f=(Rc)\beta\gamma z$ (kPa)	ERROR (%)
Li et al. (1994)	A_1	27.4	40	1.2	17.5	26.60	-2.92
	B_1	27.3	32	1	12	28.06	2.79
	A_2	43.6	40	1.2	25	43.85	0.57
	B_2	44.9	32	1	21	44.20	-1.56
Grigorian (1997)	Volgodon	43.6	18	1	4	43.06	3.18
	Nikopol	19.7	22	0.5	6	18.75	-4.81
Chen et al. (2008)	33.1		40	0.8	19	32.30	-2.42
Ma et al. (2009)	44		60	0.8	16	44.55	1.24

It can be observed that the values of negative skin friction calculated using the proposed analytical model, are in a good agreement with these recorded in the field, with a maximum error of less than 5%.

6.6 Design Procedure

Inundation from the bottom due to a rise in the groundwater table can cause soil to become fully inundated, increasing the degree of saturation of collapsible soil all the way to 100%. In this case full collapse settlement is expected under the existing surcharge load acting on the soil, inducing NSF on the piles. Wetting from the top however, due to pipe leakage, heavy rain and/or; surface run off, can only cause partial soil inundation, increasing the degree of saturation of collapsible soil to a certain limit that does not reach 100%, causing partial collapse settlement, and inducing a corresponding amount of NSF on the piles.

A new procedure for designing a single end-bearing pile subjected to drag loads due to the settlement of collapsible soils caused by full and partial inundation is proposed here, taking into account the rate of inundation in the case of inundation from the bottom and the degree of saturation in the case of partial inundation from the top. The design procedure suggests a correction factor extending the theory proposed by Hanna and Sharif (2006) to incorporate the effect of collapsible soil. This correction factor (R_c) can be obtained from some figures presented in this chapter, taking into account the different factors that govern the development of negative skin friction in collapsible soil upon inundation.

The following steps make it possible to calculate the maximum drag load due to the inundation of collapsible soil:

1. Calculate the maximum drag force acting on piles before inundation using Equations [6.5-6.8], with the following parameters known: soil properties including: the bulk unit weight (γ), angle of internal friction (ϕ), the surcharge acting on soil (σ), and the angle of friction between soil and pile surface (δ'); pile dimensions: length subjected to NSF: (L) and pile diameter: (D).

2. Calculate the maximum drag force acting on piles after the surrounding collapsible soil is inundated with water, for the following two cases:

    A- <u>Full inundation from the bottom:</u>

        Obtain the correction factor (Rc) from Figures 6.14 or 6.15, knowing the values of: σ and C_p.

B-   Partial inundation from the top:

Knowing the values of σ and C_p, the average degree of wetting and the average volumetric water content, obtain the correction factor (Rc) from Figures 6.30-6.34. After obtaining the correction factor, substitute it in Equation [6.13] to get the maximum drag load after inundation, $Q'_{n(max)}$.

3. To calculate the allowable bearing load of the pile Q_a, use Equation [2.16] proposed by Hanna and Sharif (2006), substituting by $Q'_{n(max)}$ as shown in Equation [6.28].

$$Q_a = \left[\frac{Q_t + Q_s}{FS} - Q'_{n(max)} \right] \dots \dots [6.28]$$

CHAPTER 7

CONCLUSIONS AND RECOMMENDATIONS

7.1 General

The experimental and numerical investigations presented here cover a wide range of soil/pile conditions and, consider the effect of wetting schemes, collapsible soil type and loading conditions on NSF over time. The results were used to develop qualitative and quantitative analyses to provide a better understanding of soil/pile interaction upon the inundation of collapsible soil with water.

The main conclusions obtained from this study are summarized here and recommendations for future work are provided in this chapter.

7.2 Conclusions

Based on the experimental and numerical results, the following conclusions were drawn:

1. The experimental results showed that drag load increased linearly with the increase of inundation pressure acting on the soil and with the increase of collapse potential. The range of inundation pressure applied in this study was between 40 and 120 kPa, while the collapse potential for different soil mixtures varied between 4.2 to 18%, which believed to cover a wide range of practical cases.

2. The effect of the rate of inundation (full inundation from the bottom) was studied in this research. Inundation rates between 0.34 to 1.0 m/hr were applied, where the change in the maximum drag load with respect to the rate of inundation did not exceed 8%. This effect was more pronounced for highly collapsible soils subjected to high values of inundation

pressure, and it became less significant when the hydraulic gradient was much less than the critical value.

3. The test results for staged inundation from the top, identified the relationships between the degree of wetting and the maximum drag load. The NSF was shown to increase significantly with the increase in the degree of wetting up to nearly 75%, where the maximum drag load is reached only when the soil is fully saturated (at 100% saturation).

4. Numerical analysis was carried out to extend the range of parameters used in the experimental program. Analytical models were established, providing relationships for predicting negative skin friction stresses on piles in collapsible soil. These relationships were obtained by analyzing experimental and numerical results, and were validated by field data reported in the literature.

5. A new design procedure has been postulated for designing piles in collapsible soil. This design procedure accounts for the effects of the inundation rate, the wetting scheme and different soil and loading conditions, providing solutions for various conditions that can arise for a wide range of parameters.

6. Estimating the efficiency of pre-wetting for reducing/eliminating the NSF can be obtained based on the relationships provided in this study.

7.3 Recommendations for Future Work

In this research, a small-scale experimental setup was used to obtain analytical models. The effects of various parameters were studied for a wide range of values however, the experiments were limited for specific loading conditions, pile type, soil conditions and wetting schemes as indicated in the previous chapters. The following recommendations are therefore suggested for future work:

1. This study was limited to end-bearing piles, where the neutral plane was assumed to be at the pile tip for all cases. Studying other cases including floating piles is recommended, where measurements along the pile length are recorded in order to plot the stress distribution and to observe the change in the neutral plane location under different wetting schemes and for different pile length/diameter ratios.

2. The prototype model used in this study was limited to driven piles; however, considering the effect of pile installation technique is recommended.

3. The inundation pressure applied in the experimental and numerical investigations was limited to 120 kPa and 200 kPa respectively. The effects of higher inundation pressures could be investigated.

4. Global wetting of collapsible soil was investigated in this study, where soil tank was inundated uniformly. It would be worthwhile to study the effect of local wetting.

5. The collapsible soil used in this study was a mixture of sand and kaolin clay at different clay contents, covering a wide range of collapse potential values. Different collapsible soil types could be investigated.

REFERENCES

1. Abdrabbo, F.M., and Abdelaziz, T.M. (2006). "Study of the infiltration of water through collapsible soil". Geotechnical Special Publication. No. 147, in Proceedings of the Fourth International Conference on Unsaturated Soils, pp. 1049–1060.

2. Adnan, B., A., and Erdil, T., R. (1992). "Evaluation and control of collapsible soils." Journal of Geotechnical Engineering, ASCE 118 (10) pp. 1491-1504.

3. Alwail, T., A., Ho, C. L. and Fragaszy, R. J. (1994). "Collapse mechanism of compacted clayey and silty sands." Conf. Vertical and Horizontal Deformations of Foundations and Embankments, ASCE, Jun 16-18, (2), College Station, TX, USA, pp. 1435-1446.

4. Auvinet, G. and Hanel, J. J. (1981). " Negative skin friction on piles in Mexico City clay". Proceedings, 10th International Conference on Soil Mechanics and Foundation Engineering, Stockholm, Sweden, pp. 599-604.

5. Ayadat, T. and Hanna, A.M. (2007). "Identification of collapsible soil using the fall cone apparatus." ASTM, Journal of Geotechnical Engineering, 30(4), pp. 312-323

6. Ayadat, T. and Hanna, A., (2008). "Effects of hydraulic shear stress and rate of erosion on the magnitude, degree, and rate of collapse" Geomechanics and Geoengineering Journal, Vol. 3, Iss. 1, pp 59-69.

7. Barden, L., McGown, A. and Collins, K., (1973). "The collapse Mechanism in Partly Saturated Soil", Engineering Geology, Vol. 7, 49-60.

8. Bjerrum L. Johannessen, I.J., and Eide, O., (1969). "Reduction of negative skin friction on steel piles to rock". Proceedings 7th International Conference on Soil Mechanics and Foundation Engineering, Mexico City, August 25 - 29, Vol. 2, pp. 27 - 34.

9. Bond A.J. and Jardine R.J., (1995). "Shaft capacity of displacement piles in a high OCR clay", GEOTECHNIQUE, Vol: 45, pp. 3-23.

10. Bozozuk, M., (1972). "Downdrag measurement on 160-ft floating pipe test pile in marine clay". Canadian Geotechnical Journal, Vol. 9, No. 2, pp. 127-136.

11. Briaud, J.L., (1997). "Bitumen Selection for Downdrag on Piles," Journal of Geotechnical and Geoenvironmental Engineering, Vol. 123, No. 12, ASCE, New York, December.

12. Burland, J. B. (1973). "Shaft Friction of Piles in Clay –A Simple Fundamental Approach." Ground Engineering, Vol. 6(3), pp. 30-42.

13. Burland, J.B. and Starke, W. (1994). "Review of measured negative pile friction in terms of effective stress". Proc. of 13th International Conference on Soil Mechanics and Foundation Engineering, New Delhi, pp 493 – 496.

14. Chen, P., Wei, C., and Ma, T. (2014). "Analytical Model of Soil-Water Characteristics Considering the Effect of Air Entrapment." International Journal of Geo-mechanics, ASCE, 04014102.

15. Chen, Z.H., Huang, X.F., Qin, B., Fang, X.W., and Guo, J.F. (2008). "Negative skin friction for cast-in-place piles in thick collapsible loess". Unsaturated Soils. Advances in Geo-Engineering, D.G. Toll, C.E. Augrade, D. Gallipoli, and S.J. Wheeler, Taylor and Fracis 2008, pp. 979–985.

16. Chow, Y. K., Chin, J. T., and Lee, S. L. (1990). "Negative skin friction on pile groups." International Journal for Numerical and Analytical Methods in Geomechanics, 14(2), pp. 75–91.

17. Chung, S.H., and Yang, S.R. (2014). "Loading behaviour of small scale single pile in unsaturated clayey soil". Materials Research Innovations; 18(S2), pp. 177-181.

18. Clemence, S.P., Finbarr, A.O., (1981). "Design consideration for collapsible soils". Journal of Geotechnical Engineering, ASCE 107 (3), pp. 305– 317.

19. Clemente, F. M., (1981). "Downdrag on bitumen coated piles in a warm climate". Proceedings of the 10th International Conference on Soil Mechanics and Foundation Engineering, Stockholm, Vol. 2, pp. 673 - 676.

20. Costa L. M., Pontes I. D. S., Guimarães L. J. N., and Ferreira S. R. M. (2007). "Numerical modelling of hydro-mechanical behaviour of collapsible soils" Communications in Numerical Methods in Engineering Volume 24, Issue 12, pp 1839–1852.

21. Delage, P., Cui Y.J. and Antoine, P. (2005). "Geotechnical problems related with loess deposits in Northern France" Proceedings of International Conference on Problematic Soils, pp. 517-540.

22. Evans, R.D., Jefferson, I., Northmore, K.J., Synac, O., and Serridge, C.J. (2004). "Geophysical investigation and in-situ treatment of collapsible soils". Geotechnical Special Publication, n 126 II, Geotechnical Engineering for Transportation Projects: Proceedings of Geo-Trans, pp. 1848–1857.

23. Evstatiev, D. (1995). "Design and treatment as loess bases in Bulgaria". In Genesis and properties of collapsible soils. Edited by Ed. Derbyshire, T. Dijkastra, J. Smalley, NATO ASI Series C: Matematical and Physical Sciences vol. 468, Kluwer Akad. Publishers, pp. 375–382.

24. El-Ehwany, M., and Houston, S. L. (1990). "Settlement and moisture movement in collapsible soils." Journal of Geotechnical Engineering, ASCE. Vol, 116, No 10, pp. 1521– 1535.

25. Elkady, T. Y. (2002). "Static and Dynamic Behavior of Collapsible Soils." Ph.D. Dissertation, Arizona State University, Tempe.

26. Endo M., Minou, A., Kawasaki T. and Shibata, T. (1969). "Negative skin friction acting on steel piles in clay". Proc. 7th International Conference on Soil Mechanics and Foundation Engineering, Mexico City, August 25 - 29, Vol. 2, pp. 85 - 92.

27. Fellenius, B. H. and Broms, B. B. (1969). "Negative skin friction for long piles driven in clay". Proc. 7th ICSMFE, Mexico City, Vol. 2, pp. 93-98.

28. Fellenius, B.H., (1972). "Downdrag on piles in clay due to negative skin friction". Canadian Geotechnical Journal, 9(4): 323–337.

29. Fellenius, B. H., (1989). "Unified design of piles and pile groups". Transportation Research Board, Washington, TRB Record 1169, pp. 75 - 82.

30. Fellenius, B.H., (2008). "Effective stress analysis and set-up for shaft capacity of piles in clay." The Geo-Institute, ASCE Geotechnical Special Publication, GSP 180, pp. 384 - 406.

31. Fellenius, B.H., (2014). "Piled foundation design as reflected in codes and standards". Proceedings of the DFI-EFFC International Conference on Piling and Deep Foundations, Stockholm, May 21-23, pp. 1013-1030.

32. Fredlund, D. G. and Gan, J. K-M. (1995). "The collapse mechanism of a soil subjected to one-dimensional loading and wetting". Genesis and Properties of Collapsible Soils. Edited by E. Derbyshire, T. Dijkstra and I. J. Smalley, NATO ASI Series, Vol. 468, Kluwer Academic Publishers, pp. 173-205.

33. Fredlund, D.G., and Houston, S.L. (2009). "Protocol for the assessment of unsaturated soil properties in geotechnical engineering practice". Canadian Geotechnical Journal, 46(6): 694–707.

34. Fredlund, D. G., and Houston, S. L. (2013). "Interpretation of soil-water characteristic curves when volume change occurs as soil suction is changed". Advances in Unsaturated Soils, (Caicedo et al. eds), pp. 15-31.

35. Fredlund, D. G. (2006). "Unsaturated Soil Mechanics in Engineering Practice," Journal of Geotechnical and Geoenvironmental Engineering, Vol. 132, No. 3, pp. 286–321.

36. Garlanger, J. E. (1974). "Measurement of Pile Downdrag beneath an existing Bridge Abutment," Highway Research Board, Transport Research Record No. 517, pp. 61-69.

37. GAO, X. J., WANG, J.C., ZHU, X.R., (2007). "Static load test and load transfer mechanism study of squeezed branch and plate pile in collapsible loess foundation," Journal of Zhejiang University - Science A, 8(7): 1110-1117.

38. Grigoryan, A.A., and. Grigoryan, R. G (1975). "Experimental investigation of "negative-friction" forces along the lateral surface of piles as the soils experience slum-type settlement under their own weight," Osn., Fundam. Mekh. Gruntov, No. 5, 10-13.

39. Grigoryan, A.A., and Yushube, S.V. (1986). "Interaction between bored-cast-in-place piles and soils under Type II collapsibility conditions," Osn.,Fundam. Mekh. Gruntov, No. 2, 14-17.

40. Grigoryan, A. A. and Chinenkov, Yu. A. (1990). "Experience gained with construction on long piles with broadened heels in soils prone to slump-type settlement," Osn.,Fundam. Mekh. Gruntov, No. 4, 2–5.

41. Grigoryan, A. A. (1991). "Construction on loess soils," Osn.,Fundam. Mekh. Gruntov, No. 1, 24–27

42. Grigoryan, A., A., (1997). "Pile foundations for buildings and structures in collapsible soils" Publisher Rotterdam; Brookfield, VT: A.A. Balkema, , ISBN 9054107634.

43. Grigoryan, A. A. (1991). "Construction on loess soils", Osn. Fundam. Mekh. Gruntov, No. 1, pp. 24–27

44. Grigoryan, A. A. (2005). " On certain characteristic design features of pile foundations in soils classed as type II in terms of proneness to slump-type settlement," Osn., Fundam. Mekh. Gruntov, No. 1, 21-25.

45. Hanna, A.M., and Sharif A. (2006). "Drag force on a single pile in clay subjected to surcharge loading". International Journal of Geo-mechanics, ASCE, 6 (2), pp. 89-9.

46. Hepworth, R.C. (1993). "Negative Skin Friction due to Wetting of Unsaturated Soil." Unsaturated Soils. Geotechnical Special Publication No. 39 (ed. S.L. Houston and W.K. Wray), New York: ASCE, pp. 44-53.

47. Ho, D. Y. F., and Fredlund, D. G. (1982). "A multistage triaxial tests for unsaturated soils". ASTM, Geotechnical Testing Journal, 5(1/2), pp. 18-25.

48. Ho, C., Steadman, L. L. and Fragaszy, R. (1988). "Influence of fines on the collapse potential of compacted sandy soil." Proceedings, 24th Symposium on Engineering geology and soils Engineering, Washington state University, Pullman, Washington, pp. 57-72.

49. Houston, W. N. and Houston, S, L. (1989). "State-of-the practice mitigation measures for collapsible soils sites." Proceedings of the Foundation Engineering Congress, ASCE, Evanston, Il. p 161-175

50. Houston, W.N., Mahmoud, H.H., and Houston, S.L. (1993). "Laboratory procedure for partial-wetting collapse determination" Unsaturated Soils, Geotechnical Special Publication No. 39 (ed. S.L. Houston and W.K. Wray), New York: ASCE, pp. 54-63.

51. Houston, S.L. and Houston, W.N. (1997). "Collapsible Soil Engineering". Unsaturated Soil Engineering Practice, Geotechnical Special Publication No. 68, ASCE, (Houston and Fredlund, eds.). pp. 199-232.

52. Houston, S., (2014). "Characterization of Unsaturated Soils: The Importance of Response to Wetting." Geo-Congress 2014 Keynote Lectures: pp. 77-96.

53. Jennings, J. E., and Knight, K. (1975). "A guide to construction on or with material exhibiting additional settlement due to collapse of grain structure." Proc., 6th Regional Conf. of Africa on SMFE, pp. 99-105.

54. Johannessen, I.J., and Bjerrum, L. (1965). "Measurement of the compression of a steel pile to rock due to settlement of the surrounding clay". In Proceedings of the 6th International Conference on Soil Mechanics and Foundation Engineering, Montréal, Que., 8–15 September 1965. Pergamon Press, Oxford, UK. pp. 261–264.

55. Kakoli, S.T.N. (2011). "Negative skin friction induced on piles in collapsible soils due to inundation". Ph.D thesis, Concordia University, Montreal, Quebec.

56. Kalashnikova, O. P. (1976). "Investigation of the behavior of piles in a collapsible soil stabilized through a leading hole." Soil Mechanics and Foundation Engineering journal, Vol. 13, No. 1, pp. 16-19.

57. Kakoli S.T.N., Hanna A.M. and Ayadat T. (2011). "Simulation of Collapsible Soils Subjected to Inundation". Proceedings of the 17th International Conference on Soil Mechanics and Geotechnical Engineering pp., 3431 – 3434.

58. Keenan, G.H., and Bozozuk, M., (1985). "Downdrag on three-pile group of pipe piles". In: (2nd edn. ed.), Proc. 11th Int. Conf. Mech. & Found. Engng. Vol. 3 pp. 1407–1412.

59. Kezdi, A. (1974). "Handbook of soil mechanics" Soil Physics, (1), Elsevier, Amesterdam, Netherlands.

60. Knight, K. (1963). "The Origin and Occurrence of Collapsing soils." Proc. of 3rd Regional Conf. for Africa on Soil Mech. and Found. Eng., 1: pp. 127-130.

61. Konrad, J.M. & Roy, M. (1987). "Bearing capacity of friction piles in marine clay." Geotechnique, 37(2): 163-175.

62. Krutov, V. I. (2003). "Consideration of additional loading on piles due to forces of loading friction in soils prone to slump-type settlement,". Osn., Fundam. Mekh. Gruntov, No. 6, pp. 23-27.

63. Lawton, E. C., Fragaszy, R. J., and Hetherington, M. D. (1992). ''Review of Wetting-Induced Collapse in Compacted Soil.'' Journal of Geotechnical Engineering, 118(9), pp. 1376–1394

64. Lee, C. Y. (1993). "Pile group settlement analysis by hybrid layer approach." Journal of Geotechnical Engineering, ASCE, 119(6), pp. 984-997.

65. Lee, C.J., Bolton, M.D., and Al-Tabaa, A. (2001). "Recent findings on negative skin friction in piles and pile groups in consolidating ground" 5th International Conference on Deep Foundation Practice, Singapore, April, pp. 273-280.

66. Lee, C.J., Bolton, M.D., and Al-Tabbaa, A., (2002). "Numerical modelling of group effects on the distribution of dragloads in pile foundations". Geotechnique 52 (5), pp. 325–335.

67. Leung, C.F., Radhakrishnan, R., and Tan, S.A., (1991). "Performance of precast driven piles in marine clay". American Society of Civil Engineers, ASCE Journal of Geotechnical Engineering, Vol. 117, No. 4, pp. 637 - 657.

68. Li Dazhan, Teng Yanjing, He Yihua, and Sui Guoxiu. (1994). "Vertical bearing behavior of large diameter belled pile in collapsible loess." Chinese Journal of Geotechnical Engineering 16(2), pp. 11-21.

69. Zaiguan Lin snd Weimingl Liang (1982). "Engineering properties and zoning of loess and loess-like soils in China". Canadian Geotechnical Journal, (19), pp. 76-91.

70. Z.G. Lin & Z.J. Xu (2008). "Loess in China and landslides in loess slopes". Landslides and Engineered Slopes – Chen et al. (eds), 2008 Taylor & Francis Group, London, ISBN 978-0-415-41196-7. pp. 129-144.

71. Lommler, J., and Bandini, P., (2015). "Characterization of Collapsible Soils." IFCEE, pp. 1834-1841.

72. Ma Kanyan, Zhang Jiwen , Wang Donghong. (2009). "Negative Skin Friction of pile in Self-weight Collapse Loess Site." Geotechnical Engineering Technique, Issue 4, pp. 163-166.

73. Mashhour, I. (2009). "Negative skin friction on single piles in collapsible soils". MA.Sc thesis, Concordia University, Montreal, Quebec.

74. Meyerhof, G.G. (1976). "Bearing Capacity and settlement of pile foundations". The Eleventh Terzaghi Lecture (1975) November 5, Journal of the Geotechnical Engineering Division, ASCE, 102 (GT3), pp. 195-228.

75. Mihalache, C. and Buscarnera, G. (2015). "Is Wetting Collapse an Unstable Compaction Process?" Journal of Geotechnecial and Geoenvironmental Engineering, 141(2), 04014098.

76. Miller, H., Djerbib, Y, Jefferson, I.F., and Smalley, I.J. (1998). "Modeling the collapse of metastable loess soils." Proceedings of the 3rd International Conference on Geo-Computation, University of Bristol, United Kingdom, pp. 17-19.

77. Noor, S. T., Hanna, A., and Mashhour, I. (2013). "Numerical modeling of piles in collapsible soil subjected to inundation." International Journal of Geomechanics 13 (5), pp. 514–526.

78. Pengelly, A., Boehm, D., Rector, E. and Welsh, J. (1997). "Engineering Experience with in Situ Modification of Collapsible and Expansive Soils. Unsaturated Soil Engineering", ASCE, Special Geotechnical Publication.

79. Pereira, J. H. F., and Fredlund, D. G. (2000). "Volume change behaviour of collapsible compacted gneiss soil". ASCE Journal of Geotechnical and Geoenvironmental Engineering, 126, pp. 907-916.

80. "PLAXIS 2D 2010 Material Models Manual" (2010). Delft University of Technology & PLAXIS B.V.

81. Poorooshasb, H. B., Alamgir, M., and Miura, N. (1996). "Negative skin friction on rigid and deformable piles." Computers and Geotechnics, 18(2), 109–126.

82. Poulos, H.G. (1997). "Piles subjected to negative friction: A procedure for design". Geotechnical Engineering (Southeast Asian Geotechnical Society), 28(1), pp. 23–44.

83. Poulos, H. G., and Davis, E. H. (1980). "Pile foundation analysis and design". Wiley, New York.

84. Proctor, R. R. (1933). "The design and construction of rolled-earth dams". Engineering News Record, Vol.3.

85. Rogers, C. D. F., (1995). "Types and distribution of collapsible soils." In Derbyshire, E., Dijkstra, T., and Smalley, I. J. (eds.), Genesis and Properties of Collapsible Soils. Kluwer Academic Publishers, pp. 1–17

86. Rollins, K. and Rogers, G.W. (1994). "Mitigation Measures for Small Structures on Collapsible Alluvial Soils." J. Geot. Engr., ASCE, 120(9).

87. Sedran, G., Stolle, D.F.E., and Horvath, R.G. (2001). "An investigation of scaling and dimensional analysis of axially loaded piles." Canadian Geotech. Journal, 38(3): 530–541.

88. Tadepalli, R., and Fredlund, D. G. (1991). "The collapse behavior of a compacted soil during inundation". Canadian Geotechnical Journal, 28(4), pp. 477-488.

89. Teh, C. I., and Wong, K. S. (1995). "Analysis of downdrag on pile groups." Geotechnique, 45(2), pp. 191–207

90. Terzaghi, K., and Ralph B. Peck, (1948). "Soil Mechanics in Engineering Practice", 1st Edition, John Wiley and Sons, New York, pp. 456-483.

91. Vanapalli, S.K. and Taylan, Z.N., (2012). "Design of single piles using the mechanics of unsaturated soils." International Journal of GEOMATE, 2(1): 197-204.

92. Walker, L. K. and Darwall, P., (1973). "Drag-Down on coated and uncoated piles". Proceedings of the 8th International Conference on Soil Mechanics and Foundation Engineering, Moscow, Vol. 2.2, pp. 257 - 262.

93. Walsh, K., Houston, W., and Houston, S. (1993). "Evaluation of In-Place Wetting Using Soil Suction Measurements." Journal of Geotechnical Engineering 119(5), pp. 862–873.

94. Weiping C., Yunmin C., and Wolfe W. E. (2014) "New Load Transfer Hyperbolic Model for Pile-Soil Interface and Negative Skin Friction on Single Piles Embedded in Soft Soils" International Journal of Geomechanics, 14(1) pp. 92-100.

95. Zapata, C.E., Houstan, W.N., Houstan, S., and Walsh, K.D. (2000). "Soil-water characteristic curve variability". Advances in unsaturated Geotechnics" (GSP 99), In Proceedings of Geodenver Conference, Denver, Colo., 5-8 August, pp. 84–124.